The Astrophysical Journal, 798:73 (33pp), 2015 January 10 doi:10.1088/0004-637X/798/2/73

BANYAN. V. A SYSTEMATIC ALL-SKY SURVEY FOR NEW VERY LATE-TYPE LOW-MASS STARS AND BROWN DWARFS IN NEARBY YOUNG MOVING GROUPS

Jonathan Gagné[1], David Lafrenière[1], René Doyon[1], Lison Malo[1,2], and Étienne Artigau[1]
[1] Département de Physique, Université de Montréal, C.P. 6128 Succ. Centre-ville, Montréal, QC H3C 3J7, Canada
[2] Canada-France-Hawaii Telescope, 65-1238 Mamalahoa Hwy, Kamuela, HI 96743, USA
Received 2014 June 28; accepted 2014 October 16; published 2014 December 23

ABSTRACT

We present the BANYAN All-Sky Survey (BASS) catalog, consisting of 228 new late-type (M4–L6) candidate members of nearby young moving groups (YMGs) with an expected false-positive rate of ∼13%. This sample includes 79 new candidate young brown dwarfs and 22 planetary-mass objects. These candidates were identified through the first systematic all-sky survey for late-type low-mass stars and brown dwarfs in YMGs. We cross-matched the Two Micron All Sky Survey and AllWISE catalogs outside of the galactic plane to build a sample of 98,970 potential ⩾M5 dwarfs in the solar neighborhood and calculated their proper motions with typical precisions of 5–15 mas yr^{-1}. We selected highly probable candidate members of several YMGs from this sample using the Bayesian Analysis for Nearby Young AssociatioNs II tool (BANYAN II). We used the most probable statistical distances inferred from BANYAN II to estimate the spectral type and mass of these candidate YMG members. We used this unique sample to show tentative signs of mass segregation in the AB Doradus moving group and the Tucana-Horologium and Columba associations. The BASS sample has already been successful in identifying several new young brown dwarfs in earlier publications, and will be of great interest in studying the initial mass function of YMGs and for the search of exoplanets by direct imaging; the input sample of potential close-by ⩾M5 dwarfs will be useful to study the kinematics of low-mass stars and brown dwarfs and search for new proper motion pairs.

Key words: brown dwarfs – methods: data analysis – proper motions – stars: kinematics and dynamics – stars: low-mass

1. INTRODUCTION

A few decades ago, several groups of stars sharing similar Galactic space velocities have been identified in the solar neighborhood. These similar kinematics are a consequence of the young age (typically 10–200 Myr) of these groups (i.e., young moving groups; YMGs), which formed from a common origin. The closest and youngest YMGs include the TW Hydrae association (TWA; de La Reza et al. 1989; Kastner et al. 1997; Zuckerman & Song 2004; 5–15 Myr; Weinberger et al. 2013), β Pictoris (βPMG; Zuckerman et al. 2001; 20–26 Myr; Mamajek & Bell 2014; Malo et al. 2014b; Binks & Jeffries 2014), Tucana-Horologium (THA; Torres et al. 2000; Zuckerman & Webb 2000; 20–40 Myr; Kraus et al. 2014), Carina (CAR; 20–40 Myr; Torres et al. 2008), Columba (COL; 20–40 Myr; Torres et al. 2008), Argus (ARG; 30–50 Myr; Makarov & Urban 2000), and AB Doradus (ABDMG; Zuckerman et al. 2004; 110–130 Myr; Luhman et al. 2005; Barenfeld et al. 2013). Identifying these YMGs was made possible with the advent of the HIPPARCOS survey (Perryman et al. 1997), which provided parallax measurements for ∼120,000 bright stars. Because of its limited sensitivity and the fact that it operated at visible wavelengths, this survey mainly studied stars with spectral types earlier than ∼K0. Identifying the missing later-type, low-mass members of YMGs is of great interest for multiple reasons: it would provide constraints on the low-mass end of their initial mass function and accessible benchmarks for cool, low-pressure atmospheres, similar to those of directly imaged giant planets (e.g., Delorme et al. 2012; Faherty et al. 2013; Liu et al. 2013b). Furthermore, direct imaging of exoplanets around these low-mass members would be facilitated by their proximity and the fact that younger planets are hotter, and thus brighter (e.g., see Bowler et al. 2012a, 2012b, 2013; Delorme et al. 2013; Naud et al. 2014). For these reasons, a large number of studies were aimed at finding these missing low-mass members and refine our understanding of YMGs (see Torres et al. 2003, 2006; Weinberger et al. 2004; Looper et al. 2007, 2010a, 2010b; Shkolnik et al. 2009, 2012; Bonnefoy et al. 2009, 2014; Lépine & Simon 2009; Schlieder et al. 2010, 2012a, 2012b; Rice et al. 2010; Rodriguez et al. 2011, 2013; Kiss et al. 2011; Schneider et al. 2012a, 2014; Faherty et al. 2012, 2013; Delorme et al. 2012; Malo et al. 2013, 2014a, 2014b; Weinberger et al. 2013; Moór et al. 2013; Liu et al. 2013b; Hinkley et al. 2013; Kraus et al. 2014; Gagné et al. 2014a, 2014b, 2014c; Riedel et al. 2014; Manjavacas et al. 2014; Zapatero Osorio et al. 2014; Mamajek & Bell 2014).

The identification of later-type members of nearby YMGs is a challenging task in the absence of reliable parallax and radial velocity (RV) measurements since their members are spread on large regions of the celestial sphere. Furthermore, obtaining parallax and RV measurements for such faint targets is time-consuming. Careful pre-selection of candidates is thus essential to keep the follow-up effort to a manageable size. Efforts have already been made in identifying late-type members in YMGs, notably by selecting X-ray or UV-bright stars (Torres et al. 2008; Rodriguez et al. 2011; Shkolnik et al. 2012) and by comparing their proper motions to those of known members with the convergent point proper motion analysis (Montes et al. 2001; Rodriguez et al. 2013). However, this method does not use all available measurements (e.g., photometry, magnitude of proper motion, RV, and parallax), therefore it generally suffers from a large contamination of field stars that have proper motions similar to those of YMG members by pure chance, as well as cross-contamination between different YMG candidates. In particular, some YMGs such as COL, βPMG, and TWA happen to share similar proper motion distributions as viewed from the

Earth, which makes it difficult to differentiate their members using only sky position and the direction of proper motion without RV measurements.

To address these problems, Malo et al. (2013) developed the Bayesian Analysis for Nearby Young AssociatioNs (BANYAN[3]), a statistical tool based on Bayesian inference, to identify strong K5–M5 candidate members of YMGs primarily from a sample of X-ray bright sources. In addition to proper motion and sky position, this tool takes advantage of I_C and J photometry measurements to ensure that candidate members fall in a region of the color–magnitude diagram (CMD) consistent with other YMG members; younger low-mass stars (LMSs) and brown dwarfs (BDs) are inflated and thus brighter than field stars as they are still undergoing gravitational contraction. This approach provides a more robust set of candidates, as well as most probable distance and RV predictions. However, this study is still limited to detecting candidates with spectral types earlier than ∼M5, and photometric measurements in the I_C band are required to take CMD information into account. In parallel, Gagné et al. (2014b) presented BANYAN II,[4] a new selection tool based on BANYAN that includes several improvements (e.g., a better modeling of YMGs spatial and kinematic properties and an extensive treatment of contamination and completeness), and is specifically designed to identify >M5 YMG candidates by relying on two different CMDs constructed with photometry from the Two Micron All-Sky Survey (2MASS; Skrutskie et al. 2006) and the *WISE* survey (Wright et al. 2010). This tool was used in Gagné et al. (2014b) to identify 39 new M5–L4 candidate members among known young field LMSs and BDs. Recently, Kraus et al. (2014) identified 129 new K3–M6 strong candidate members of THA by carrying extensive RV measurements of targets selected for having proper motion and CMD positions similar to those of other THA members. Their results indicate that samples based on *Galaxy Evolution Explorer* (Martin et al. 2005) or *ROSAT* (Voges et al. 1999) miss candidates later than ∼ M2 at distances beyond $\gtrsim$40 pc.

We present here the BANYAN All-sky Survey (BASS), which is the first all-sky, systematic survey for $\geqslant$M5 LMSs and BDs in YMGs. The whole 2MASS and AllWISE (Kirkpatrick et al. 2014) catalogs outside of the galactic plane ($|b| > 15^\circ$) were cross-matched, yielding proper motions with typical precisions of a few mas yr^{-1}. Color-quality cuts as well as the BANYAN II tool were used to select 153 high- and 21 modest-probability candidate members of YMGs, for which near-infrared (NIR) colors are consistent with $\geqslant$M5 spectral types. The BASS survey has already generated a wealth of new discoveries, including a triple M5 + M5 + planetary-mass companion in THA (Delorme et al. 2013; J. Gagné et al., in preparation), an M5+L4 host–planet system candidate member of THA (É. Artigau et al., in preparation), a new L-type candidate member of TWA (Gagné et al. 2014a) and a new low-gravity L4 β BD candidate member of ARG (Gagné et al. 2014c). A NIR and optical spectroscopic follow-up of all candidates that will be presented here is undergoing; first results were presented in Gagné et al. (2013) and more will be presented in a subsequent paper (J. Gagné et al., in preparation).

In Section 2, we detail our method for cross-matching the 2MASS and AllWISE catalogs, which we follow by a description of the various color-quality cuts applied, and how we use the BANYAN II tool to select candidates members of YMGs (Section 3). In Section 4, we present all information available in the literature for the BASS catalog, which we used to update the membership probability when relevant. In Section 5, we evaluate the recovery rate of the BASS sample for known $\geqslant$M5 candidate members and bona fide members of YMGs. We then present various characteristics of the updated BASS catalog in Section 6. In Section 7, we search for new common proper motion pairs among our sample, and we tentatively investigate mass segregation in Section 8. Conclusions are presented in Section 9. The full input sample of 98,970 potential close-by $\geqslant$M5 dwarfs is presented in Appendix A, and the low-priority BASS (LP-BASS) sample, which consists of objects only marginally redder than field dwarfs, is presented in Appendix B.

2. CROSS-MATCHING THE 2MASS AND AllWISE CATALOGS

Cross-matching the 2MASS and AllWISE catalogs (∼470 million and ∼750 million entries respectively) without the use of significant computational resources is a challenge that must be tackled in a strategic way. Fortunately, the NASA Infrared Science Archive (IRSA[5]; Groom et al. 2010) provides useful tools to achieve this. In a first step, we have built two distinct queries for the 2MASS and AllWISE catalogs to target only potential nearby $\geqslant$M5 dwarfs. We start from spectral type-color relations described in Pecaut & Mamajek (2013), Kirkpatrick et al. (2011), and Dupuy & Liu (2012) to select only targets that have NIR colors consistent with $\geqslant$M5 spectral types, which we subsequently relax to include all currently known young dwarfs in the same range of spectral types (see Gagné et al. 2014b for an extensive list of known young LMSs and BDs in the field). We target only regions of the sky located more than 15 degrees away from the galactic plane, require that measurements of J, H, K_S, $W1$, and $W2$ photometry have a reasonable quality, and that no contamination or saturation flags are problematic. We also reject sources spatially resolved in 2MASS but not in AllWISE. In Appendix A, we list the requirements in the form of two Structured Query Language (SQL) statements that were used to perform all-sky IRSA queries, which correspond to the following criteria[6].

1. The absolute galactic latitude $|b|$ of both the 2MASS and AllWISE counterparts respect $|b| > 15^\circ$.
2. $J > 2$, $H > 2$, $K_S > 2$, $W1 > 2$ and $W2 > 2$.
3. $0.506 < J - H < 2$, $0.269 < H - K_S < 1.6$ and $0.168 < W1 - W2 < 2.5$.
4. $W1 - W2 < (0.96 \times (W2 - W3) - 0.96)$ if $W3$ is detected with S/N > 5 and not saturated (Kirkpatrick et al. 2011).
5. If a 2MASS counterpart is identified in the AllWISE catalog, it must be at least at an angular distance 0.″3 from the AllWISE coordinates (i.e., to reject low proper motion objects) and respect $0.153 < K_S - W1 < 2$ in addition to the 2MASS color cuts described above.
6. The blue magnitude B, which is either the Johnson B_J magnitude of a *Tycho 2* (Høg et al. 2000) counterpart, or the photographic blue magnitude of a *USNO–A2.0* (Monet 1998) counterpart of the 2MASS object (*B_M_OPT* keyword) is either undetected or has $B - J \geqslant 4.048$.

[3] Publicly available at http://www.astro.umontreal.ca/∼malo/banyan.php.
[4] Publicly available at http://www.astro.umontreal.ca/∼gagne/banyanII.php.
[5] Available at http://irsa.ipac.caltech.edu/
[6] See the column descriptions of the 2MASS User's Guide http://www.ipac.caltech.edu/2mass/releases/allsky/doc/sec2_2a.html and the AllWISE User's Guide. See http://wise2.ipac.caltech.edu/docs/release/allwise/expsup/sec2_1a.html for additional information on the keywords.

7. The red or visible VR magnitude, which is either the Johnson V_J magnitude of a *Tycho 2* counterpart, or the photographic red magnitude of a *USNO–A2.0* counterpart of the 2MASS object (*VR_M_OPT* keyword) is either undetected or has $VR - J \geqslant 2.63$ and $B - VR \geqslant 1.3$.
8. At least two 2MASS bands have excellent (A) or good (B) photometric quality flags.
9. No 2MASS band has a poor (D, E, or F) or undetected (X or U) quality flags.
10. The AllWISE photometric quality flags of the $W1$ and $W2$ bands are either excellent (A) or good (B).
11. The angular distance between the object and its closest neighbor is at least 6.″4 in 2MASS, to ensure that they are resolved in AllWISE.
12. There are less than 0.2% of saturated pixels in the profile fitting regions of both the $W1$ and $W2$ bands in AllWISE.
13. The source is detected in the $W1$ and $W2$ AllWISE bands with a statistical significance larger than 5σ.
14. The reduced χ^2 of the profile fits for the $W1$ and $W2$ AllWISE bands both respect $\chi^2 < 5$.
15. The 2MASS read flags do not contain 0 (no detection in any band), 6 (not detected in one band) or 9 (nominally detected in one band because of confused regions) for any band.
16. The 2MASS blend flag is 1 (only one component was fit simultaneously for photometry) for all bands.
17. The 2MASS contamination flag is 0 (not contaminated) for all bands.
18. The 2MASS extragalactic contamination flag is 0 (resolved and not extended).
19. The 2MASS minor planet flag is 0 (not associated with a known solar system object).
20. The AllWISE contamination flags of the $W1$ and $W2$ bands do not correspond to potentially spurious detections (D, due to a diffraction spike; P, due to detector persistence; H, due to the scattered light of a bright nearby source; or O, due to an optical ghost caused by a nearby bright source).
21. The AllWISE extended flag is either 0 (consistent with a point source) or 1 (goodness-of-fit of the profile fitting is larger than 3 in at least one band).

These queries generated two lists: 2,762,191 objects from 2MASS and 76,883,849 objects from AllWISE. To avoid obtaining very large output file sizes, we downloaded only designations, right ascension (R.A.), and declination (decl.) positions, as well as 2MASS unique identifiers at this stage (keyword *CNTR* in the 2MASS catalog, and *2MASS_KEY* in the AllWISE catalog; the IRSA team already identified 2MASS–AllWISE cross-matches within 3″). We then locally rejected all objects located in the following star-forming regions to avoid heavily reddened contaminants: Orion ($5^h29^m <$ R.A. $< 5^h41^m$ and $-06°37' <$ decl. $< -02°25'$; Béjar et al. 1999), Taurus ($3^h50^m <$ R.A. $< 5^h15^m$ and $15° <$ decl. $< 32°$; Luhman 2004), Chamaeleon ($10^h45^m <$ R.A. $< 11^h30^m$ and $-78°30' <$ decl. $< -76°$; Luhman 2007; Alves de Oliveira et al. 2012), and Upper Scorpius ($15^h35^m <$ R.A. $< 16^h45^m$ and $-30° <$ decl. $< -21°$; Dawson et al. 2011). We subsequently counted the number of 2MASS neighbors in a 3′ radius around each target in the 2MASS subset, and rejected all those with more than 71 neighbors to avoid densely populated regions. This number was chosen so that none of the known young BDs in the field and outside of the galactic plane were rejected. This cut down the number of 2MASS targets to 2,178,389. We then locally cross-matched the unique 2MASS identifiers of both catalogs to construct list A, consisting of 169,934 2MASS sources that already had an AllWISE counterpart identified in the latter catalog. The remaining unmatched 2,008,455 2MASS sources, as well as the 75,478,161 AllWISE sources with null 2MASS keys, were saved as lists B and C, respectively. AllWISE sources with non-null 2MASS entries that were not cross-matched this way were rejected, since they must have failed at least one of the 2MASS constraints described above.

We created preliminary cross-matches by identifying the closest AllWISE entry in List C to each 2MASS entry in list B. A total of 2,001,246 of those preliminary matches were separated by distances larger than 25″ (equivalent to a proper motion $>2.''2\ \mathrm{yr}^{-1}$) or had $K_S - W1 < 0.153$ or $K_S - W1 > 2$, and were rejected. For each 2MASS component of the remaining 7209 pairs (separated by angular distances of δ), we subsequently downloaded all AllWISE entries within δ, and verified that the closest entry with a null *2MASS_KEY* corresponded to our preliminary match. We also verified that the *2MASS_KEY* was not assigned to any other nearby AllWISE source. This step has rejected 767 objects. In a final step, we downloaded all 2MASS and AllWISE entries in a radius δ+3″ around every AllWISE component of the 5876 remaining pairs, and removed all IRSA-identified cross-matches. We use a search radius of δ+3″ in this step to ensure that we retrieve all 2MASS–AllWISE matches in the AllWISE catalog in a radius δ, since those matches can be separated by up to 3″. We then verified that the closest 2MASS entry among those objects not already cross-matched by IRSA corresponded to the 2MASS component of the preliminary pairs: this filter rejected 2367 objects. The 3509 pairs that survived all these selection criteria were added to List A. We then used 2MASS and AllWISE astrometry to determine proper motions for all 173,443 objects in this supplemented List A, and rejected the 74,473 sources with a total proper motion lower than 30 mas yr^{-1}, or with a total proper motion measurement at $<5\sigma$, to reject extragalactic contaminants and red giants.

Proper motions were calculated directly from entries in both the 2MASS and AllWISE catalogs. The R.A. and decl. entries were used for the astrometric position of both catalogs; the *SIGRA* and *SIGDEC* entries of AllWISE were used as a measurement error, and the *ERR_MAJ* (σ_{MAJ}), *ERR_MIN* (σ_{MIN}) and *ERR_ANG* (σ_θ) entries of the 2MASS catalog were projected back to errors on R.A. (σ_α) and decl. (σ_δ) with:

$$\sigma_\alpha = \sqrt{(\sigma_{\mathrm{MAJ}} \sin\sigma_\theta)^2 + (\sigma_{\mathrm{MIN}} \cos\sigma_\theta)^2} \cdot \cos\delta \quad (1)$$

$$\sigma_\delta = \sqrt{(\sigma_{\mathrm{MAJ}} \cos\sigma_\theta)^2 + (\sigma_{\mathrm{MIN}} \sin\sigma_\theta)^2}, \quad (2)$$

where δ is the 2MASS decl. The epochs corresponding to these astrometric measurements were taken from the *JDATE* and *W1MJDMEAN* entries in the respective catalogs. *W1MJDMEAN* corresponds to the mean epoch of all AllWISE exposures taken in the $W1$ band. The uncertainty on the 2MASS epoch is taken to be 30 s, as described in the 2MASS User's Guide, and the uncertainty on the AllWISE epoch is taken in a conservative way as half of the maximal distance between all exposures (from the *W1MJDMAX* and *W1MJDMIN* entries). We analytically propagated all measurement errors (astrometric and temporal) of both catalogs, assuming they were all independent, to obtain the measurement errors on our 2MASS–AllWISE proper motions. The positional accuracy of the 2MASS and AllWISE catalogs vary from ∼0.″05 for bright

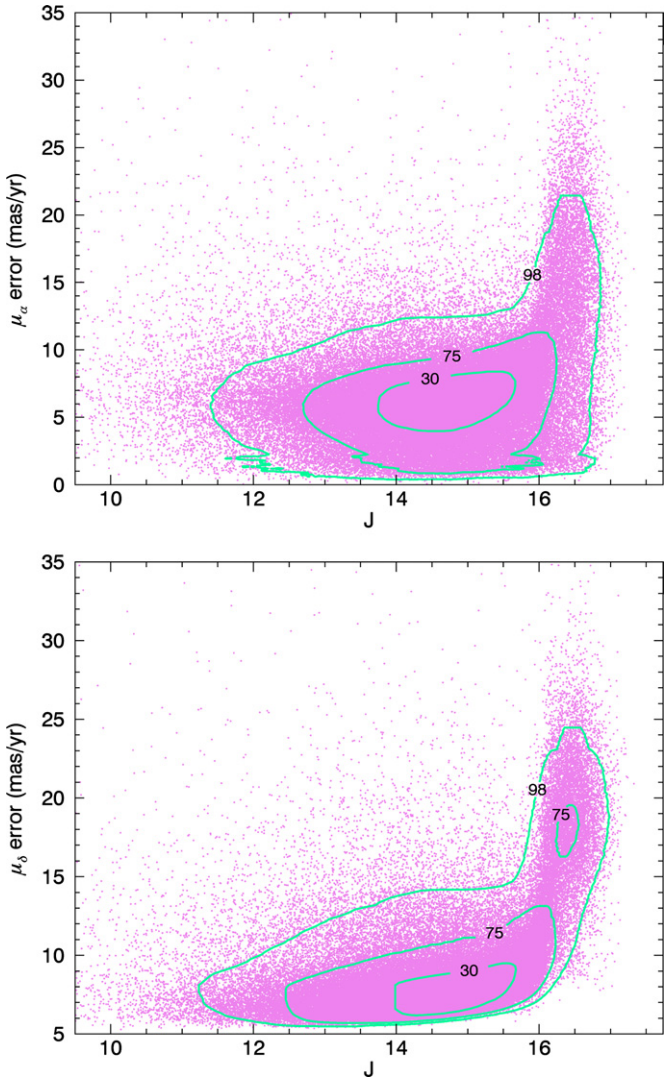

Figure 1. Proper motion precision as a function of 2MASS J magnitude in List A (pink points; see Section 2). Green contour lines include 30%, 75%, and 98% of all data points respectively. In the case of bright objects ($J < 16$), typical precisions are 3–10 mas yr^{-1} ($\mu_\alpha \cos\delta$) and 5–10 mas yr^{-1} (μ_δ), whereas they can go down to ∼25 mas yr^{-1} for fainter objects.

sources ($J \lesssim 14$), to 0.″1–0.″4 (2MASS) and 0.″06–0.″15 (AllWISE) for fainter sources. The final set of 98 970 objects contains probable nearby >M5 dwarfs with measurements of proper motion above 30 mas yr^{-1}. We list this sample in Appendix A, since it provides a great opportunity to study the kinematics of LMSs and BDs in the solar neighborhood. In Figure 1, we show that typical measurement errors on proper motions are 5–10 mas yr^{-1} for bright objects ($J < 16$), or 5–25 mas yr^{-1} for fainter objects.

We cross-matched our input sample with the Initial Gaia Source List (VizieR catalog *I/324/igsl3*) to obtain proper motions from the *UCAC3* (Zacharias et al. 2009) and the Guide Star Catalog (Lasker et al. 2008), and present in Figure 2 a comparison to the proper motions we derived from 2MASS–AllWISE. We find reduced χ^2 values of 1.27 and 1.03 for $\mu_\alpha \cos\delta$ and μ_δ, respectively, which indicates that our measurement errors are representative of the differences between our proper motions and those in the catalogs mentioned above. However, there are a few cases where the literature proper motions are significantly discrepant from the 2MASS–AllWISE measurements. We investigated the 25/3873 worst cases in *UCAC3* where either $\mu_\alpha \cos\delta$ or μ_δ were discrepant by more than 300 mas yr^{-1}. In 24/25 cases, we found other measurements in the literature that matched the 2MASS–AllWISE measurement within a few σ (typically less than 1σ), indicating that the *UCAC3* measurement might be at fault. The other case (2MASS J17274680+5200079) corresponds to a 6.″5 binary that is barely above the angular resolution of AllWISE (6.″1 in the $W1$ band and 6.″4 in the $W2$ band). Rodriguez et al. (2013) indicate that they observe a small systematic distortion (<15 mas yr^{-1}) for their $\mu_\alpha \cos\delta$ measurements from 2MASS–*WISE* as a function of galactic latitude. They propose a correction factor, which would increase our reduced χ^2 value to 1.27–1.82. This indicates that such a distortion is not clearly seen in our sample, and we thus choose not to include it in the present work. We conclude that the proper motions derived from 2MASS–AllWISE are reliable and will use only those measurements of proper motion for the remainder of this work. This will ensure that our selection criteria are more homogeneous, which will be helpful in an eventual characterization of the young population in the BASS survey.

3. IDENTIFICATION OF CANDIDATE YOUNG MOVING GROUP MEMBERS

We used BANYAN II (Gagné et al. 2014b) to compute the membership probability of all 98,970 potential close-by ⩾M5 dwarfs identified in the previous section (List A). The BANYAN II tool takes sky position, proper motion and 2MASS and AllWISE photometry as inputs and determines, using a naive Bayesian classifier, the membership probability that an object belongs to seven YMGs (TWA, βPMG, THA, COL, CAR, ARG, ABDMG) and the field population, which constitutes our eight hypotheses. Probability density functions (PDFs) are computed for every hypothesis and on each point of a regular 500 × 500 grid of distances and RVs spanning 0.1 to 200 pc and −35 to 35 km s^{-1}, respectively, by comparing galactic positions (*XYZ*) and space velocities (*UVW*) to the spatial and kinematic model (SKM) of the respective hypotheses, as well as comparing 2MASS and AllWISE magnitudes to a photometric model. All measurement errors are propagated and considered in this comparison. SKMs of YMGs were built by fitting three-dimensional ellipsoids, with unconstrained axes orientations, over the population of bona fide members with signs of youth as well as parallax and RV measurements (see Malo et al. 2013 and Gagné et al. 2014b for a complete list). For the field hypothesis, similar ellipsoids were fitted to synthetic objects drawn from the Besançon galactic model (A. C. Robin et al. in preparation; Robin et al. 2012) at distances of <200 pc. The photometric model consists of an old and a young field sequence in two CMD diagrams: absolute $W1$ as a function of $H - W2$ and absolute $W1$ as a function of $J - K_S$. The positions of maxima and characteristic widths of the resulting posterior PDFs yield a statistical distance and RV prediction, assuming the object fulfills the respective hypothesis. The same PDFs are marginalized to a final probability by numerically integrating them along the whole grid. Optionally, parallax and RV measurements can be included to derive a more robust probability. In these cases, the corresponding dimension of the marginalization grid is eliminated. The prior probabilities in the Bayesian classifier are set to the respective population estimates of each hypotheses, considering the magnitude of proper motion and galactic latitude of the object. Additionally, equal-luminosity binary hypotheses for the field and all YMGs are supplemented to

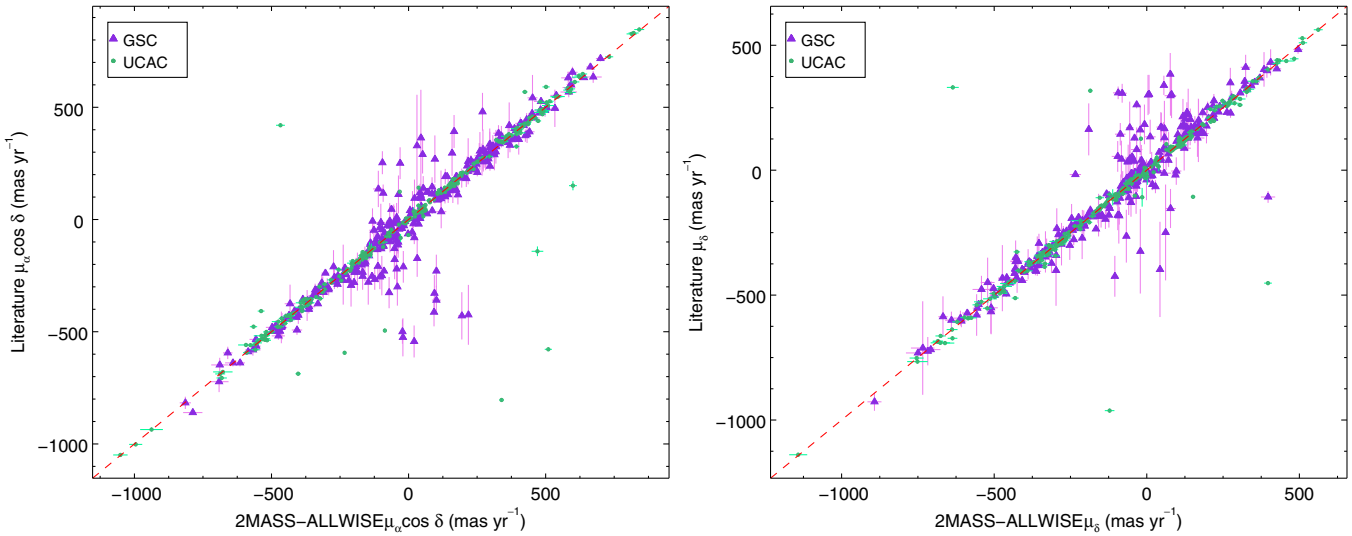

Figure 2. Comparison between proper motions determined from the 2MASS and AllWISE data sets and measurements in the literature, for a random subset of the input sample of 98,970 objects. We only display 500 random objects per bin of ∼200 mas yr^{-1}, to improve visibility. Measurements from the literature were obtained from the Initial Gaia Source List (VizieR catalog *I/324/igsl3*), which cross-matches UCAC3 (Zacharias et al. 2009; green circles) and the Guide Star Catalog (Lasker et al. 2008; purple triangles). The reduced chi-square values for $\mu_\alpha \cos\delta$ and μ_δ are 1.27 and 1.03, respectively.

our set of hypotheses, where the CMDs are shifted up by 0.75 mag. Objects for which the binary hypothesis has a higher probability will be flagged as potential binaries, and only the binary hypotheses will be used when we analyze known binary systems. A naive Bayesian classifier implicitly considers that all input parameters are independent, which is generally not the case here. Using such an analysis with dependent input parameters will generally provide a good classification; however, the Bayesian probability will be biased and thus not interpretable in an absolute way (e.g., a set of candidates with a Bayesian probabilities of 90% will not necessarily include a fraction of contaminants equal to 10%; Hand & Yu 2001; Russek et al. 1983). To address this, Gagné et al. (2014b) performed a Monte Carlo analysis using all SKM and photometric models described above to estimate the field contamination probability as a function of Bayesian probability for different hypotheses. They find that Bayesian probabilities are generally pessimistic, except for YMGs that are most subject to contamination (ARG, ABDMG, βPMG, and COL) when no parallax measurement is included. When a parallax measurement is included, the contamination probability becomes significantly lower than could be expected from the Bayesian probability alone ($\lesssim$20% when the Bayesian probability is larger than ∼10–40% depending on the YMG). These results provide a translation for the Bayesian probability output by BANYAN II to an expected contamination rate. Gagné et al. (2014b) showed that bona fide members within $<1\sigma$ of their YMG's SKM all have a Bayesian probability >95% associated with a membership to their respective YMG, whereas peripheral (1–2.5σ) ambiguous members have a Bayesian probability between 10–95%. For more details about the BANYAN II tool, the reader is referred to Gagné et al. (2014b).

After applying BANYAN II to our input sample (list A), we rejected all objects with a Bayesian probability <10% of being a member to a YMG, or with an estimated contamination rate >50%. At this point we are left with 983 candidates. We used statistical distances of the most probable hypotheses to place all candidates in the two CMDs described above, and rejected all candidates that did not have NIR colors at least 1σ redder than the field sequence. These filters cut down the candidate list to 273 objects. Another set of 275 candidates, located to the right of the field sequence by an amount less than 1σ, were used to build the low-priority BASS catalog (LP-BASS) that is discussed in Appendix B of this paper. The AllWISE catalog includes *WISE* observations that were performed in its warm phase, hence in some cases, the measurement of *W1* or *W2* can be saturated. To avoid overlooking such saturated targets, we repeated all steps described above using the *WISE* catalog instead of AllWISE, and supplemented our sample with the additional 26 objects uncovered this way (96 in the case of LP-BASS). We subsequently used the IRSA dust extinction tool[7] to remove nine objects that display a stronger extinction than 0.4 mag, potentially corresponding to distant contaminants reddened by interstellar matter in our line of sight. Another three objects listed in the 2MASS extended sources catalog (VizieR catalog *VII/233/xsc*) were rejected. In a final step, we visually inspected all Sloan Digital Sky Survey (DSS), 2MASS and AllWISE acquisition images to flag any object with a suspicious shape or evidence of interstellar absorption in the surrounding 5′. No such occurrence was found, which indicates the filters described above were efficient in preventing such contaminating objects. The resulting BASS catalog is presented in Table 2. We divide the sample in two sections: those with a contamination probability lower than 15% are grouped in a High Probability section, whereas those with a contamination probability between 15–50% are grouped in the Modest Probability section.

In Table 1, we present the fraction of members in each moving group that would fail our galactic plane and proper motion filters, assuming that our SKM models are accurate. We obtained these quantities by drawing a million synthetic objects from a Gaussian random distribution represented by each SKM and assessing what fraction fails each filter. We used the estimated recovery rate of the BANYAN II tool for each YMG (see Gagné et al. 2014b) corresponding to our tolerated field contamination of <50% and combined all these sources of incompleteness to estimate that the BASS sample is complete at the 6–90% level in the range of spectral types considered here, depending on

[7] Available at http://irsa.ipac.caltech.edu/applications/DUST/

Table 1
Expected Completeness of the BASS Survey

YMG Name	$\|b\| \leqslant 15^\circ$	$\mu \leqslant 30$ mas yr^{-1}	SFRs[a]	SFRs or $\|b\| \leqslant 15^\circ$ or $\mu \leqslant 30$ mas yr^{-1}[b]	Contamination $\geqslant$50%	Expected Completeness
ARG	42.1%	0.5%	0.6%	42.6%	89.6%	6.0%
COL	15.7%	23.4%	1.8%	36.4%	59.7%	25.6%
βPMG	25.2%	0.8%	3.4%	28.3%	60.0%	28.7%
ABDMG	20.7%	1.1%	1.6%	22.8%	59.6%	31.2%
CAR	41.2%	2.7%	0.1%	42.9%	9.9%	51.4%
TWA	19.7%	0.4%	0%	20.0%	10.3%	71.8%
THA	<0.1%	<0.1%	0%	<0.1%	10.0%	90.0%

Notes.
[a] Expected fraction of members aligned with Orion, Taurus, Chamaeleon, and Upper Scorpius (see Section 2).
[b] Filters on position and proper motion are not independent.

the YMG in question. The YMGs that would benefit the most from a search within the galactic plane are ARG and CAR, and to a lesser extent βPMG, ABDMG, and TWA. However, such a survey would present a significant challenge for two reasons; (1) a cross-match between the 2MASS and AllWISE catalogs would require the use of powerful algorithms because of crowded regions; and (2) a new free parameter would have to be added to the analysis, describing the effect of reddening by interstellar medium on the CMD sequence of field stars (e.g., this effect could be represented by a reddening vector of unknown amplitude in both CMDs that are used in the BANYAN II tool). We note that even if those two hurdles would be overcome, we expect the field contamination to remain very high within the galactic plane unless the survey benefits from RV and parallax measurements for a large number of objects. The only YMG that is significantly affected by our low proper motion cut is COL. Since this filter serves the main purpose of rejecting distant extragalactic and red giant contaminants, starting from a sample of targets with distance measurements would allow relaxing this filter and accessing to a larger number of COL candidates. The final major obstacle to efficiently identify a large number of candidate members of ARG, COL, βPMG, and ABDMG is the low recovery rate intrinsic to a naive Bayesian classifier in the situation where no information is known on the RV and distance of the input sample. It could be expected that adopting a more complex method, which could for example take account of the dependency of input parameters, would help to draw the most information possible from a sample without RV and distance measurements. However, Hand & Yu (2001) suggest otherwise by demonstrating that a naive Bayesian classifier performs much better than could be expected in these conditions. This would leave only three foreseeable options to address this aspect of our survey completeness; (1) allow for significantly more contaminants in our sample and perform an extensive spectroscopic follow-up; (2) start from a sample that includes RV and parallax measurements; or (3) identify new readily accessible observables, such as new filters in color–color diagrams, that could distinguish YMG members from field interlopers.

4. A LITERATURE SEARCH FOR ADDITIONAL INFORMATION

We searched for any additional information in the literature for all candidates in Table 2 using the SIMBAD and VizieR web tools. We found 122 objects for which at least one of RV, parallax, spectral type, signs of youth, or any other relevant information was available, including 60 known candidates or bona fide members of the YMGs considered here. There are only four known bona fide members included in those: 2MASS J00452143+1634446 (ARG; Zapatero Osorio et al. 2014 and Section 4.2), 2MASS J01231125–6921379 (THA; Gagné et al. 2014b), GJ 2022 (ABDMG; Riedel 2012; Shkolnik et al. 2012 and Riedel et al. 2014), and 2MASS J03552337+1133437 (ABDMG; Faherty et al. 2013; Liu et al. 2013a). We list these 59 objects in Table 3, with an updated Bayesian probability in light of these additional measurements. In Figure 3, we compare the BANYAN II statistical predictions for the RV and distance to measurements found in the literature, and show that the reduced χ^2 values are 1.32 and 0.84, respectively. This indicates that errors on statistical predictions are representative of the scatter observed here.

4.1. Estimates of Spectral Types

We used the 2MASS and AllWISE J, H, K_S, $W1$ and $W2$ magnitudes with the statistical distance associated to the most probable hypothesis from BANYAN II to assign a tentative spectral type to all candidates identified here. We used the Database of Ultracool Parallaxes[8] (Dupuy & Liu 2012) to compare the position of each candidate with the corresponding spectral type—magnitude sequence (spanning the M5–T9 range) and derived a PDF in each case as a function of spectral type. We then combined these PDFs in a likelihood analysis, and used the maximal position of the final PDF to assign a most probable spectral type to each object. In Figure 4, we compare our spectral type estimates to measurements available in the literature and show that these estimates are reliable to within ~2.5 subtypes.

We note a clear trend where we tend to underestimate spectral types for < M5 objects and overestimate those of >L5 objects. We used a linear fit to characterize this systematic trend and obtain a correction for our estimated spectral types :

$$\mathrm{SpT}_{\mathrm{corr}} = 1.64 + 0.81 \cdot \mathrm{SpT}_{\mathrm{estim}}, \quad (3)$$

where 0 corresponds to the M0 spectral type. We used this equation to correct all estimated spectral types listed in Tables 2 and 5. Before this correction, the reduced χ^2 value for our estimated spectral types is 2.51, and the estimated measured spectral type differences display a standard deviation of 1.1 subtypes. After the correction, the reduced χ^2 and standard deviation become 1.0 and 0.8 subtypes, respectively.

In Figure 5, we use spectral type measurements when available or estimates of spectral types otherwise to compare the BASS sample with current bona fide members in YMGs. This

[8] Available at http://www.cfa.harvard.edu/~tdupuy/plx/Database_of_Ultracool_Parallaxes.html

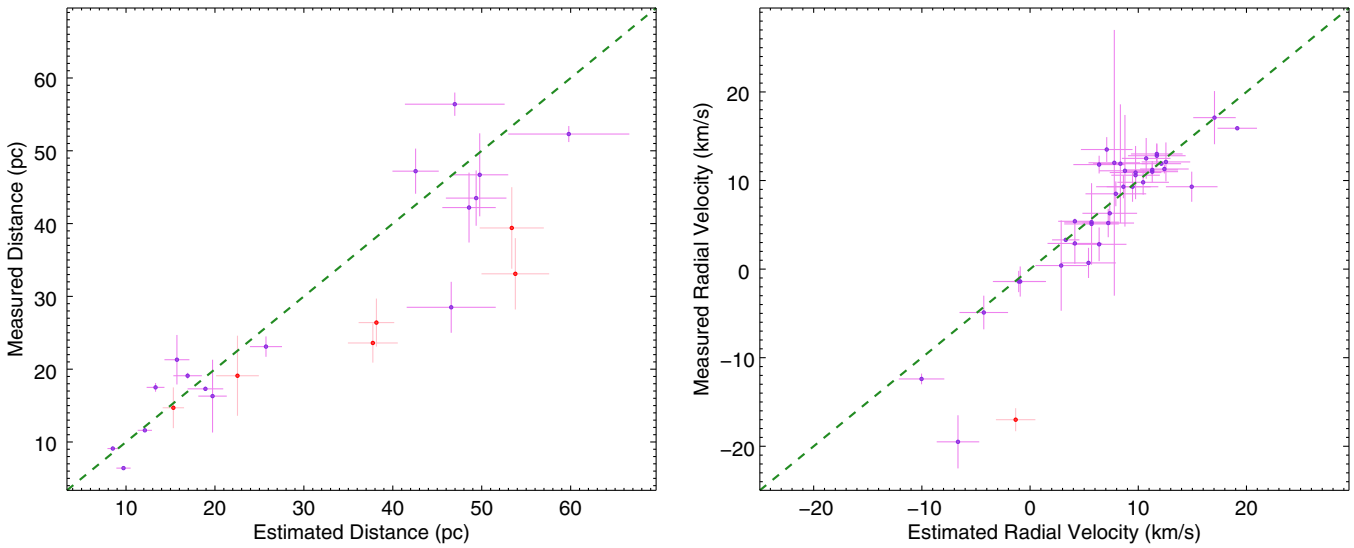

Figure 3. Comparison of statistical RV and distance predictions from BANYAN II with measurements found in the literature. The dashed green line has a unit slope and intersects with the origin. Measurements that corroborated the most probable hypothesis are displayed in purple, whereas those favoring a different YMG are displayed in red. Measurements that are significantly discrepant and thus rejecting possible YMG memberships are not displayed here.

Table 2
All-sky Search for >M5 Candidates in Young Moving Groups

2MASS	Estim.	2MASS			AllWISE		$\mu_\alpha \cos\delta$	μ_δ	Member-	Bayesian	Contamination
Designation	SpT	J	H	K_S	$W1$	$W2$	(mas yr^{-1})	(mas yr^{-1})	ship	Prob. (%)	Prob. (%)
Candidates with a High Probability											
00011217+1535355	L3.2	15.52	14.51	13.71	12.97	12.54	139.6 ± 7.8	-183.5 ± 11.8	ABDMG	79.1	1.6
00040288−6410358	L2.5	15.79	14.83	14.01	13.41	12.96	77.7 ± 3.0	-56.1 ± 8.4	THA[a]	99.9	<0.1
00041589−8747254	M5.7	12.90	12.20	11.86	11.65	11.41	77.3 ± 2.0	-29.9 ± 9.2	THA	55.4	<0.1
00065794−6436542	M6.9	13.39	12.66	12.17	11.74	11.42	92.7 ± 3.1	-71.0 ± 7.3	THA[a]	99.9	<0.1
00111532−3756553	M5.7	12.15	11.60	11.22	11.02	10.79	105.7 ± 5.0	-77.4 ± 7.4	THA	80.2	<0.1
00182834−6703130	M9.6	15.46	14.48	13.71	13.19	12.80	83.6 ± 2.9	-65.0 ± 9.3	THA[a]	99.8	<0.1
00191296−6226005	M9.7	15.64	14.62	13.96	13.38	12.96	66.1 ± 2.9	-50.6 ± 8.4	THA	99.5	<0.1
00212774−6351081	M4.0	11.02	10.48	10.11	9.91	9.66	83.0 ± 2.9	-57.6 ± 7.2	THA	99.8	<0.1
00235732−5531435	M4.5	11.11	10.55	10.24	10.07	9.87	92.3 ± 3.4	-67.7 ± 7.4	THA[a]	99.5	<0.1
00305785−6550058[b]	M2.1	9.82	9.24	8.95	8.79	8.61	70.3 ± 2.9	-51.9 ± 8.7	THA	99.1	<0.1
Candidates with a Modest Probability											
00160844−0043021	L4.0	16.33	15.23	14.54	13.84	13.39	138.3 ± 9.9	-33.7 ± 14.2	BPMG	18.8	36.4
00192626+4614078	M5.9	12.60	11.94	11.50	11.28	11.02	119.6 ± 6.1	-82.5 ± 6.9	ABDMG	53.3	17.5
00274534−0806046	M5.3	11.57	10.97	10.61	10.41	10.18	111.5 ± 7.0	-59.9 ± 6.7	BPMG	45.6	35.1
00390342+1330170	M5.1	10.94	10.37	10.06	9.84	9.65	109.8 ± 6.8	-96.5 ± 7.0	BPMG	57.9	15.3
00464841+0715177	M8.2	13.89	13.18	12.55	12.09	11.64	97.0 ± 9.2	-60.3 ± 7.3	BPMG[a]	78.5	28.4
00581143−5653326	L6.1	16.78	15.55	14.55	13.76	13.24	197.4 ± 6.2	46.0 ± 12.2	ARG	80.4	32.9
01033203+1935361	L6.2	16.29	14.90	14.15	13.18	12.70	303.0 ± 13.4	16.6 ± 7.2	ARG	31.7	16.9
01525534−6329301	M4.7	10.17	9.60	9.26	9.06	8.84	130.0 ± 3.5	7.0 ± 6.4	BPMG	71.4	22.1
02534448−7959133	M5.4	11.34	10.74	10.38	10.18	9.97	81.7 ± 2.2	90.3 ± 9.3	BPMG	71.8	24.9
03390160−2434059	M3.7	10.90	10.34	9.97	9.72	9.52	56.3 ± 5.7	-12.7 ± 6.0	COL	60.5	32.9

Notes.
[a] The binary hypothesis is more probable than the single hypothesis (see Section 3).
[b] Object from the *WISE* catalog rather than AllWISE.

figure clearly demonstrates that a significant fraction of the BASS candidates have a later spectral type than most known members of YMGs, which outlines that we are entering a yet poorly explored mass regime of the YMG population.

4.2. Comments on Individual Objects

In this section, we present comments on individual objects that deserve further discussion. All those already discussed in Gagné et al. (2014b; see the Reference column in Table 3) will not be discussed here, unless new information is available.

2MASS J00390342+1330170 has been identified by Schlieder et al. (2012a) as a candidate member of ABDMG with X-ray and near-UV emission indicative of a young, early-M dwarf; however, they do not estimate a spectral type. We find that this object has a Bayesian probability of 84.3% and 7.5% for βPMG and ABDMG, respectively. We thus assign it as a candidate member of βPMG, but we note that there is an

Table 3
Candidates with Additional Information in the Literature

2MASS Name	Measured SpT[a]	Signs of Youth[b]	RV (km s^{-1})	Trig. Dist. (pc)	Multiplicity[c]	Known Membership	Updated Membership	Updated Prob. (%)
00011217+1535355	L4:[51]	...	...	...	...	...	ABDMG	77.8
00040288−6410358	L1 γ[49]	OR[49]	...	...	...	THA[49,31]	THA	>99.9
00065794−6436542	M9:[82]	OH[72]	...	...	...	THA[31]	THA	>99.9
00160844−0043021	L5.5 [51]	...	...	...	...	...	BPMG	19.1
00192626+4614078	M8[94]	LH[83,94]	-19.5 ± 3.0[83]	...	...	ABDMG[92,31]	ABDMG	92.1
00212774−6351081	M5.5[50]	...	...	...	...	...	THA	99.8
00235732−5531435	M4.1[53]	...	5.3 ± 0.7[53]	...	...	THA[53]	THA	99.8
00325584−4405058	L0 γ[16,71]	OITRH[16,71]	...	26.4 ± 3.3[28]	...	BPMG[31]	BPMG	97.7
00354313+0233137	M5+M6[55]	...	...	...	AB[55]	...	ABDMG	88.4
00374306−5846229	L0 γ[82,16]	OR[16]	...	...	...	THA[31]	THA	99.9
00390342+1330170	...	XN[92]	...	...	...	ABDMG[92]	BPMG	91.9
00413538−5621127	M6.5+M9[94]	VHLA[90]	2.8 ± 1.9[83,34,31]	...	AB[94]	THA[31]	THA	>99.9
00452143+1634446	L2 β[82,16]	OITRH[16]	3.3 ± 0.2[4]	17.5 ± 0.6[114]	...	ARG[31]	ARG	98.0
00464841+0715177	M9[82,118]	...	...	...	...	...	BPMG	77.0
00514081−5913320	M4.4[53]	...	6.3 ± 1.3[53]	...	...	THA[53]	THA	99.9
01033203+1935361	L6 β[28,119]	OITR[27,28]	...	21.3 ± 3.4[28]	...	ARG[31]	ARG	78.2
01033563−5515561	M5.5[19,53]	OHU[19,89]	5.2 ± 1.6[68,53]	47.2 ± 3.1[89]	AB[19]	THA;CAR[19,89]	THA	99.9
01134031−5939346	M5.0[53]	...	11.9 ± 6.7[53]	...	...	THA[53]	THA	99.7
01174748−3403258	L1 β[14,2]	TRM[7,112,2]	...	...	...	THA[31]	THA	99.6
01180670−6258591	M5.1[53]	L[53]	9.3 ± 1.3[53]	...	...	THA[53]	THA	>99.9
01231125−6921379	M8[94]	UL[83]	10.9 ± 3.0[83]	42.2 ± 4.8[87]	...	THA[31 d]	THA	>99.9
01243060−3355014	M4.5[89]	OU[89]	18.3 ± 0.5[100]	25.3 ± 0.8[100,89]	C[106]	ABDMG[88,100 d]	ABDMG	>99.9
01294256−0823580	M5[81]	...	...	...	...	...	BPMG	66.2
01344601−5707564	M4.9[53]	L[53]	11.1 ± 6.3[53]	...	...	THA[53]	THA	99.8
01372781−4558261	M5.0[53]	L[53]	13.5 ± 1.4[53]	...	...	THA[53]	THA	97.8
01415823−4633574	L0 γ[120,16]	OITRHM[120,16]	12.0 ± 15.0[53]	...	...	THA[31]	THA	99.5
01443191−4604318	M5.5[76]	...	...	...	...	...	THA	99.1
01504543−5716488	M5.5[53]	L[53]	9.3 ± 1.7[53]	...	...	THA[53]	THA	>99.9
01531463−6744181	L2:[82]	...	...	...	...	...	THA	99.9
01532494−6833226	M5.1[90,53]	N[90]	9.8 ± 1.4[53]	...	...	THA[90,53]	THA	>99.9
02153328−5627175	M5.4[90,53]	LN[53]	11.3 ± 5.7[53]	...	...	THA[90,53]	THA	99.8
02180960−6657524	M4.5[53]	L[53]	11.0 ± 1.2[53]	...	...	THA[53]	THA	>99.9
02192210−3925225	M4.9[53]	L[53]	10.6 ± 0.7[53]	...	...	THA[53]	THA	>99.9
02212859−6831400	M8:[82]	OR[27]	...	39.4 ± 5.6[28]	...	...	ABDMG	40.8
02215494−5412054	M8 β[82,27]	OR[16]	...	...	...	THA[31]	THA	99.8
02235464−5815067	L0 γ[82,27]	OR[82]	...	...	...	THA[31]	THA	>99.9
02251947−5837295	M9[82,27]	O[82]	...	...	...	THA[31]	THA	99.9
02294869−6906044	M4.6[53]	L[53]	13.0 ± 1.2[53]	...	...	THA[53]	THA	>99.9
02321934−5746117	M4.4[90,53]	...	11.2 ± 0.7[53]	...	...	THA[53]	THA	>99.9
02340093−6442068	L0 γ[29]	OR[29]	...	...	...	THA[49,31]	THA	99.8
02401209−5305527	M9.5[72]	...	...	...	...	...	THA	99.9
02411151−0326587	L0 γ[64,15,16,48]	OTR[15,16,2]	...	46.7 ± 5.7[114]	...	THA[31]	THA	98.3
02435103−5432194	M9[82]	...	...	...	...	...	THA	99.9
02501167−0151295	...	...	...	33.1 ± 4.9[107]	...	...	BPMG	88.3
02523550−7831183	M4.4[53]	...	12.8 ± 1.3[53]	...	...	THA[53]	THA	98.6
02534448−7959133	M5.5[76]	H[56]	...	...	...	...	BPMG	50.1
03014892−5903021	M9[82,72]	...	...	...	...	...	THA	99.9
03032042−7312300	L2 γ[49]	OR[49]	...	...	...	THA[49,31]	THA	78.2
03050556−5317182	M5.4[90,53]	N[90]	12.1 ± 2.2[53]	...	...	THA[90,53]	THA	99.9
03093877−3014352	M4.7[53]	L[53]	12.5 ± 2.3[53]	...	...	THA[53]	THA	99.9
03114544−4719501	M4.3[90,53]	N[90]	11.3 ± 0.5[53]	...	...	THA[90,53]	THA	>99.9
03152363−5342539	M5.2[90]	N[90]	...	...	...	THA[90]	THA	99.9
03164512−2848521	L0: [14]	...	...	...	...	...	ABDMG	77.2
03231002−4631237	L0 γ[82,27]	ORL[16]	...	...	...	THA[31]	THA	99.7
03252938−4312299	M9[82,72]	...	...	...	...	...	THA	78.9
03264225−2102057	L4 [15]	ORL[15]	...	...	...	ABDMG[31]	ABDMG	98.9
03363144−2619578	M5.7[90]	N[90]	...	43.5 ± 3.8[89]	...	THA[90]	THA	99.9
03390160−2434059	M5.9[90]	N	...	...	...	COL[90]	COL	77.8
03393521−3525440	L0 β[2,44,27]	TLM[27,112,2]	9.3 ± 1.7[83,77]	6.41 ± 0.04[22]	...	CAS[86,31]	ARG	87.6
03421621−6817321	L2:[15]	R[27]	...	...	...	THA[31]	THA	99.7
03550477−1032415	M8.5[14,27]	...	...	...	...	...	BPMG	39.5
03552337+1133437	L5 γ[82,27]	OITRL[16]	11.9 ± 0.2[4]	9.1 ± 0.1[61,28]	AB[3]	ABDMG[61,31] d	ABDMG	99.7
03572695−4417305	M9 β+L1.5 β[60]	OR[16]	...	...	AB[60]	THA[31]	THA	99.9
03582255−4116060	L5[82,27]	...	...	...	...	...	BPMG	36.8
04174743−2129191	M8[15,27]	...	...	...	...	...	THA	57.7
04210718−6306022	L5 γ[82,27]	OIRL[15]	...	...	...	ARG;BPMG[31]	ARG	97.7
04362788−4114465	M8 γ[15,2]	OITR[15.2]	...	...	...	COL[31]	COL	97.6
04433761+0002051	M9 γ[15,2]	OITVRHL[27,72,31,2]	17.1 ± 3.0[83]	...	...	BPMG[31,92]	BPMG	99.8
04532647−1751543	L3:[14]	...	...	...	...	...	COL	95.8
04533604−2835349	...	...	22.5 ± 6.7[52]	...	...	...	COL	87.6
05002100+0330501	L3 γ[82,27]	...	15.9 ± 0.2[4]	...	...	...	ABDMG	62.8
05012406−0010452	L3 γ[82,16,2]	OTRL[27]	...	14.7 ± 2.8[28,114]	...	FIELD[31]	CAR	97.7
05120636−2949540	L4:[14]	R[48]	...	...	...	BPMG[31]	BPMG	33.8
05181131−3101529	M6.5[12]	...	...	...	...	...	COL	93.7

Table 3
(Continued)

2MASS Name	Measured SpT[a]	Signs of Youth[b]	RV (km s^{-1})	Trig. Dist. (pc)	Multiplicity[c]	Known Membership	Updated Membership	Updated Prob. (%)
05361998−1920396	L2 γ[29]	OITR[29,2]	...	39.0 ± 14.0[28]	...	COL[31]	COL	96.6
06022216+6336391	L1:[82]	...	...	...	...	...	ABDMG	26.1
06420559+4101599	L/Tp[65]	R[65]	...	...	...	ABDMG[31]	ABDMG	38.4
06524851−5741376	M8β[82,27]	OR[82,27]	...	32.0 ± 3.3[28]	AB[10]	ABDMG[31]	CAR	87.9
08095903+4434216	L6[51,116]	...	...	...	...	...	ARG	30.7
09455843−3253299	M4.5[85]	X[85]	...	...	...	...	ARG	89.2
09532126−1014205	L0[15]	...	...	...	...	...	CAR	63.7
10284580−2830374	M5[96]	...	...	...	...	TWA[96]	TWA	96.3
10582800−1046304	M4[91]	...	...	...	...	...	TWA	4.3
10584787−1548172	L3[36]	...	...	17.3 ± 0.3[18]	...	...	ARG	93.1
11020983−3430355	M8.5γ[28,116]	...	...	56.4 ± 1.6[104]	...	TWA[116]	TWA	99.8
11393382−3040002	M4.7[96]	...	...	...	...	TWA[96]	TWA	99.0
11395113−3159214	M8γ[38,82,2]	OITRM[38,112]	11.2 ± 2.0[69]	28.5 ± 3.5[28]	...	TWA[38,69d]	TWA	99.8
12073346−3932539	M8[48]	ORL[48,17,2]	...	52.3 ± 1.1[24]	Ab[10]	TWA[38,69d]	TWA	99.6
12074836−3900043	L1 γ[32]	OITR[32]	...	...	...	TWA[32]	TWA	99.7
12474428−3816464	M9γ[32]	ITR[32]	...	...	...	TWA[32]	TWA	47.1
13262009−2729370	L5[38,82]	...	...	...	...	...	ARG	23.3
14252798−3650229	L5[51,82]	...	5.4 ± 0.3[4]	11.6 ± 0.1[22]	...	...	ABDMG	99.6
17571539+7042011	M7.5[37]	U[57]	−12.4 ± 0.6[103,20]	19.1 ± 0.4[57]	...	...	ARG	91.0
19564700−7542270	L0 γ[15]	OR[90]	...	...	...	THA[31]	THA	85.2
20004841−7523070	M9[94]	OR[90]	11.8 ± 1.0[34]	...	...	CAS;BPMG[34,31]	BPMG	98.2
20111744−2917584	M5.5[81]	...	...	...	...	...	ARG	49.3
20224803−5645567	M5.5[12]	...	...	...	...	...	THA	59.2
20291446−5456116	M4.3[53]	...	−1.4 ± 1.2[53]	...	...	THA[53]	THA	71.4
20330186−4903105	...	...	...	16.3 ± 5.0[89]	...	...	BPMG	99.1
20334670−3733443	M5[81]	...	...	...	...	...	BPMG	80.0
20414283−3506442	L2:[15]	...	...	...	...	...	ABDMG	14.4
20423672−5425263	M4.0[53]	...	−1.4 ± 1.7[53]	...	...	THA[53]	THA	94.8
21083826−4244540	M4.4[53]	...	−4.9 ± 1.9[53]	...	...	THA[53]	THA	84.4
21265040−8140293	L3 γ[82]	OR[90]	...	...	...	THA[31]	THA	85.1
21420580−3101162	L2[58,27,8]	...	...	...	...	...	ABDMG	12.6
21490499−6413039	M4.5[85,53]	X[85]	0.4 ± 5.1[53]	...	...	THA[53]	THA	99.7
21543454−1055308	L4 β[33]	ITR[33]	...	...	...	ARG[33]	ARG	58.6
22060961−0723353	M5.5[78]	...	...	...	...	...	ABDMG	82.1
22064498−4217208	L2[14]	R[14]	...	...	...	ABDMG[31]	ABDMG	95.2
22244102−7724036	M4.2[53]	...	8.5 ± 1.4[53]	...	...	THA[53]	THA	99.2
22400144+0532162	...	...	...	23.6 ± 2.7[23]	...	...	BPMG	79.0
22443167+2043433	L6 γ[82,2]	ITRLM[90]	...	...	...	ABDMG[31]	ABDMG	99.8
22444835−6650032	M4.8[53]	L[53]	0.7 ± 1.7[53]	...	...	THA[53]	THA	99.7
22583200+1014589	...	...	...	23.1 ± 1.4[23]	...	...	ABDMG	98.3
23130558−6127077	M4.5[53]	L[53]	2.9 ± 2.3[53]	...	...	THA[53]	THA	99.8
23225240−6151114	M5[31]	...	...	...	A[31]	THA[31]	THA	98.7
23225299−6151275	L2 γ[82]	OR[16]	...	...	B[31]	THA[31]	THA	>99.9
23225384+7847386	M5[66]	UC[66]	−17.0 ± 1.3[46]	19.1 ± 5.5[66,23]	B[66]	Pleiades[74]	CAR	29.7
23255604−0259508	L3[8]	...	...	...	...	...	ABDMG	29.8
23392527+3507165	L3.5[82,8]	...	...	...	...	...	BPMG	10.6
23424333−6224564	M4.3[53]	...	5.1 ± 4.6[53]	...	...	THA[53]	THA	99.6
23520507−1100435	M7[14,58,15]	...	...	...	...	...	ABDMG	42.0

Notes.

[a] The β and γ symbols stand for low gravity and very low gravity, *p* stands for peculiar, and a semi-colon indicates an uncertain spectral type.

[b] A capital letter means the object displays the associated sign of youth. O: lower-than-normal equivalent width of atomic species in the optical spectrum, I: same but in the NIR spectrum, T: a triangular-shaped *H*-band continuum, V: high rotational velocity, X: X-ray emission, R: redder-than-normal colors for given spectral type, U: over luminous, H: Hα emission, L: Li absorption, A: signs of accretion, M: signs of low gravity from atmospheric models fitting, N: bright NUV emission, and C: companion to a young star. A question mark following a flag indicates that the result is uncertain.

[c] AB: unresolved binary, B or C: resolved companion.

[d] Bona fide member.

References. References to the table : (1) Allen et al. 2007; (2) Allers & Liu 2013; (3) Bernat et al. 2010; (4) Blake et al. 2010; (5) Bochanski et al. 2005; (6) Boyer et al. 2011; (7) Burgasser et al. 2008; (8) Burgasser et al. 2010; (9) Caballero 2007; (10) Chauvin et al. 2012; (11) Costa et al. 2005; (12) Crifo et al. 2005; (13) Cruz & Reid 2002; (14) Cruz et al. 2003; (15) Cruz et al. 2007; (16) Cruz et al. 2009; (17) da Silva et al. 2009; (18) Dahn et al. 2002; (19) Delorme et al. 2013; (20) Terrien et al. 2012; (21) Dhital et al. 2011; (22) Dieterich et al. 2014; (23) Dittmann et al. 2014; (24) Ducourant et al. 2008; (25) Dupuy & Liu 2012; (26) Finder Charts; (27) Faherty et al. 2009; (28) Faherty et al. 2012; (29) Faherty et al. 2013; (30) Forveille et al. 2005; (31) Gagné et al. 2014b; (32) Gagné et al. 2014a; (33) Gagné et al. 2014c; (34) Gálvez-Ortiz et al. 2010; (35) Gatewood & Coban 2009; (36) Geballe et al. 2002; (37) Gizis et al. 2000; (38) Gizis 2002; (39) Gould & Chanamé 2004; (40) Guenther & Wuchterl 2003; (41) Gizis et al. 1997; (42) Hearty et al. 1999; (43) Janson et al. 2012; (44) Jenkins et al. 2009; (45) Kendall et al. 2007; (46) Kharchenko et al. 2007; (47) Khovritchev et al. 2013; (48) Kirkpatrick et al. 2008; (49) Kirkpatrick et al. 2010; (50) Kirkpatrick et al. 2011; (51) Knapp et al. 2004; (52) Kordopatis et al. 2013; (53) Kraus et al. 2014; (54) Lane et al. 2011; (55) Law et al. 2008; (56) Lee et al. 2010; (57) Lépine & Simon 2009; (58) Liebert & Gizis 2006; (59) Liu et al. 2008; (60) Liu et al. 2010; (61) Liu et al. 2013a; (62) Liu et al. 2013b; (63) Looper et al. 2007; (64) Luhman et al. 2009; (65) Mace et al. 2013; (66) Makarov 2007; (67) Malo et al. 2013; (68) Malo et al. 2014a; (69) Mamajek 2005; (70) Mann et al. 2013; (71) Marocco et al. 2013; (72) Martín et al. 2010; (73) Mason et al. 2001; (74) Montes et al. 2001; (75) Newton et al. 2014; (76) Phan-Bao & Bessell 2006; (77) Reid et al. 2002; (78) Reid et al. 2003; (79) Reid et al. 2004; (80) Reid et al. 2006; (81) Reid et al. 2007; (82) Reid et al. 2008a; (83) Reiners & Basri 2009; (84) Reylé et al. 2006; (85) Riaz et al. 2006; (86) Ribas 2003; (87) A. Riedel et al., in preparation; (88) Riedel 2012; (89) Riedel et al. 2014; (90) Rodriguez et al. 2013; (91) Rojas-Ayala et al. 2012; (92) Schlieder et al. 2012a; (93) Schlieder et al. 2012b; (94) Schmidt et al. 2007; (95) Schmidt et al. 2010; (96) Schneider et al. 2012b; (97) Schneider et al. 2014; (98) Seifahrt et al. 2010; (99) Shkolnik et al. 2009; (100) Shkolnik et al. 2012; (101) Zwitter et al. 2008; (102) Subasavage et al. 2005; (103) Tanner et al. 2010; (104) Teixeira et al. 2008; (105) Bonnefoy et al. 2009; (106) Thé & Staller 1974; (107) Tinney 1996; (108) Tinney 1996; (109) van Leeuwen 2007; (110) Vrba et al. 2004; (111) West et al. 2008; (112) Witte et al. 2011; (113) Zacharias et al. 2012; (114) Zapatero Osorio et al. 2014; (115) Nidever et al. 2002; (116) Scholz et al. 2005; (117) Chiu et al. 2006; (118) Wilson et al. 2003; (119) Kirkpatrick et al. 2000; (120) Kirkpatrick et al. 2006.

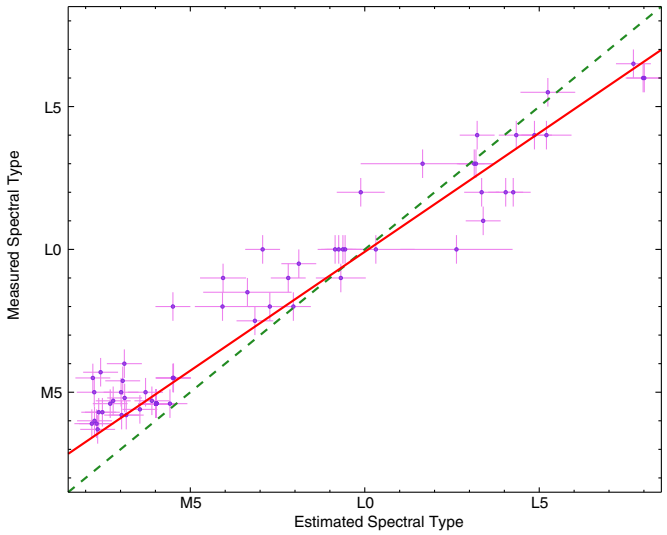

(a) Before Correction

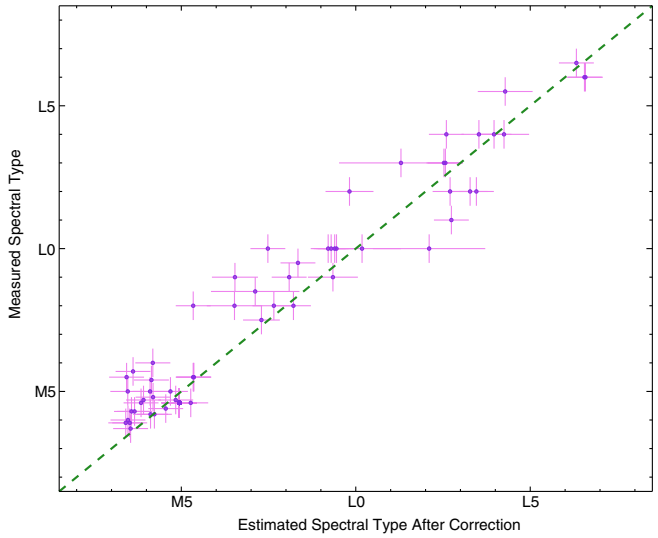

(b) After Correction

Figure 4. Estimated spectral types obtained from 2MASS and AllWISE photometry as well as statistical distances from BANYAN II compared with measurements available in the literature from optical or NIR spectroscopy. The dashed green line has a unit slope and intersects with the origin. Our estimates are reliable within ∼1.5 subtype in the M5–L6 range, but tend to overestimate (underestimate) later (earlier) spectral types. To account for this effect, we adjusted a linear correction to the estimated spectral types (red dashed line; top panel). Corrected estimations of spectral types are displayed in the bottom panel.

expected ∼10% contamination rate from ABDMG to βPMG for such a result (see Gagné et al. 2014b).

2MASS J00452143+1634446 was reported by Gagné et al. (2014b) as a candidate member of ARG with unusually red NIR colors for its L2 spectral type. Blake et al. (2010) measured an RV of 3.4 ± 0.2 km s^{-1}, and Zapatero Osorio et al. (2014) measured a trigonometric distance of 17.5 ± 0.6, pc, which brings the Bayesian probability of the ARG membership hypothesis to 98.0%. Zapatero Osorio et al. (2014) also derived an isochronal age of 10–100 Myr and detected lithium in its atmosphere. As noted by Zapatero Osorio et al. (2014), all evidence points toward a membership to ARG, hence we propose that this ∼15 $M_{\rm Jup}$ object is a bona fide member of this association.

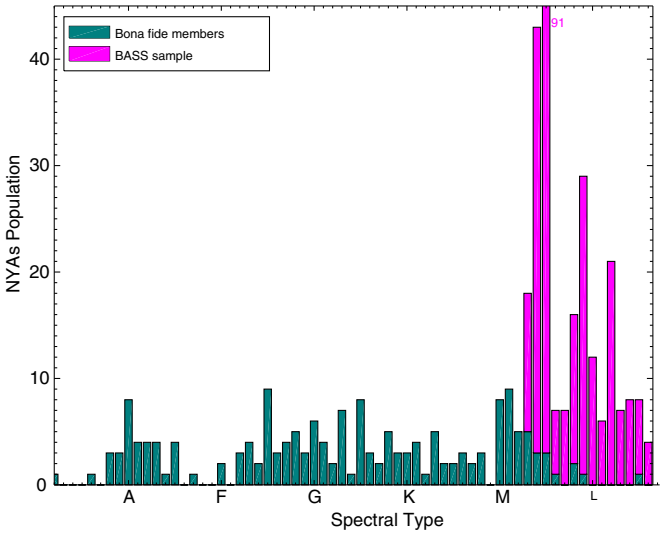

Figure 5. Estimated spectral types (violet bars) for the BASS sample, compared with the current bona fide population of all YMGs considered here (green bars). The M5 spectral bin has a value of 91: the vertical range has been shortened for clarity. The BASS sample targets YMG candidates in a range of spectral types that is yet largely unexplored.

2MASS J01033563–5515561 was first identified as a highly probable candidate to THA in early versions of the BASS sample. Delorme et al. (2013) used high contrast imaging to search for low-mass companions around BASS candidates and demonstrated that this object is in fact an M5+M5, 0.″26 tight binary harboring a 12–14 $M_{\rm Jup}$ substellar companion at a separation of 1.″78. They note that the NIR colors of the companion are indicative of a young L-type object, which is consistent with the THA membership. Subsequently, Kraus et al. (2014) and Malo et al. (2014a) independently measured RVs of 4.0 ± 2.0 km s^{-1} and 7.3 ± 2.6 km s^{-1} respectively, whereas the latter independently identifies it as a candidate member of THA. We combined both RV measurements to obtain RV = 5.2 ± 1.6 km s^{-1}. Riedel et al. (2014) measured a trigonometric distance of 47.2 ± 3.1 pc, in good agreement with our statistical distance of 42.3 ± 3 pc (which is at 1.1σ from the measurement). Without using any RV measurement, they argue that its kinematics are more consistent with CAR rather than THA. They also use empirical isochrones for YMGs to show that the system is overluminous for THA or CAR even when binarity is taken into account, which could mean that it is possibly younger, or an even higher-order multiple system. When not using the RV measurement in BANYAN II, we obtain a Bayesian probability of 98.9%, 0.7%, and 2 × 10^{-7} for THA, ABDMG, and CAR, respectively. The statistical RVs associated to these hypotheses are, respectively, 7.2±2.5 km s^{-1}, 10.8±1.8 km s^{-1}, and 14.0 ± 2.0 km s^{-1}. Both measured RVs are consistent with the THA hypothesis (at 0.7σ) and not consistent with CAR (at 3.0σ), which strengthens the THA hypothesis even more. Once we include the RV measurement, the THA hypothesis clearly dominates with a Bayesian probability of 99.9% for THA and 2 × 10^{-10} for CAR. We thus suggest that this system is a bona fide member of THA, since it has all measurements needed to be considered as such (i.e., complete $XYZUVW$ kinematics and signs of youth). This system will be discussed in more detail in a subsequent paper (J. Gagné et al., in preparation).

2MASS J01243060–3355014 (GJ 2022 B) was identified by Jao et al. (2003) as a co-moving companion to the 1.″8 M4.5 + M4.5 binary GJ 2202 AC. Shkolnik et al. (2009) used

the X-ray emission and low K I equivalent width (EW) of the latter to constrain its age between 40–300 Myr, and Shkolnik et al. (2012) measured a trigonometric distance of 25.1 ± 1.0 pc and an RV of 18.3 ± 1.5 km s^{-1} for GJ 2022 B. They used this information to identify this object as a new bona fide member of ABDMG. Riedel et al. (2014) subsequently measured a trigonometric distance of 25.8 ± 1.4 pc; we combined both distance measurements in an error-weighted average to obtain 25.3 ± 0.8 pc. We find that the ABDMG membership, distance and RV measurements are all consistent with our results from BANYAN II; the predicted RV of 18.3 ± 2.0 km s^{-1} is consistent with the measurement, and the statistical distance of 26.1 ± 1.6 pc is at $<1\sigma$ of the combined distance measurements. Including youth, RV, distance, and spectral types in our analysis yields a membership probability of 99.98% for the ABDMG hypothesis, associated with a field contamination probability of <0.1%. This is consistent with the conclusions of Shkolnik et al. (2012) and Riedel et al. (2014) that this system is a bona fide member of ABDMG. We note that Shkolnik et al. (2012) refer to the wide companion as GJ 2022 C, whereas Jao et al. (2003) and Riedel et al. (2014) refer to it as GJ 2022 B. We adopt the latter to preserve historical nomenclature, as proposed by Riedel et al. (2014).

2MASS J01303563–4445411 was identified as an M9 dwarf by Reid et al. (2008b) and Faherty et al. (2009). Subsequently, Dhital et al. (2011) resolved this system as an M9+L6 pair with a 3.″2 separation. They noted that the companion displays red colors for its spectral type, at 1.7σ of the field L6 BDs, but the primary has normal NIR colors for its spectral type, which could be an indication that the companion has an unusually dusty atmosphere. They showed that the optical spectrum of the primary does not display Hα or Li, which indicates a minimal age of 250 Myr. Furthermore, a resolved NIR spectrum of the L6 companion does not display typical signs of youth such as a triangular *H*-band continuum. We thus conclude that this system must be a false positive in our analysis, despite its 90.6% Bayesian probability of being a member of THA, since its age is not consistent with any YMG in the solar neighborhood.

2MASS J02212859–6831400 has been identified as an M8 dwarf by Reid et al. (2008b), and Faherty et al. (2009) indicate that it is unusually red and for its spectral type and displays signs of low gravity. Faherty et al. (2012) measured a trigonometric distance of 39.4 ± 5.6 pc. This object was not considered as a strong candidate member of any YMG in Gagné et al. (2014b), but here we find it as a candidate member of ABDMG with a Bayesian probability of 40.8% and a contamination probability of <0.1%. This discrepancy is due to the 2MASS–AllWISE proper motion, which is at 2.2σ or 5.0 mas yr^{-1} ($\mu_\alpha \cos\delta$) and 1.7σ or 9.1 mas yr^{-1} (μ_δ) of the proper motion used in the analysis of Gagné et al. (2014b, which was measured by Faherty et al. (2012). We visually inspected the 2MASS and AllWISE Atlas images and found that our cross-match between both catalogs is unambiguous; however, it is possible that this candidate is a false positive in our analysis. A measurement of RV will be necessary to better constrain the membership of this object.

2MASS J02401209–5305527 was reported as an M9.5 BD by Martín et al. (2010). They measured the EW of the Na I doublet at 8170–8200 Å to be EW $= 5.5 \pm 0.8$ Å. It is well known that low-gravity objects have a lower-than-normal Na I EW; however, no classification scheme using this measurement in the optical extends to such a late spectral type. We note that this EW is low compared with other M9.5 BDs in their sample, for which Na I EWs range from 5.9 to 9.7 Å with an average and standard deviation of 7.3 and 1.3 Å, respectively. However, it is higher than the Na I EW of low-gravity field BDs in their sample (2MASS J04433761+0002051 with 3.6 ± 0.8 Å and 2MASS J06085283–2753583 with 5.0 ± 0.7 Å). NIR spectroscopy would be useful to clarify the age of 2MASS J02401209–5305527.

2MASS J03014892–5903021 and 2MASS J03252938–4312299 have both been identified as M9 dwarfs by Reid et al. (2008b). Martín et al. (2010) measured the EW of their 8170–8200 Å Na I doublets and find 4.5 ± 0.8 Å and 5.1 ± 0.8 Å, respectively. They revised the spectral type of 2MASS J03252938–4312299 to M8.5. In a similar way to 2MASS J02401209–5305527, they have not flagged either objects as low-gravity, but both display the lowest Na I EW of all dwarfs in their sample with similar spectral types, except for Upper Scorpius candidates. NIR spectroscopy would be useful in clearly identifying potential signs of low-gravity in these objects.

2MASS J03393521–3525440 (LP 944–20) was identified as an M9 dwarf by Leggett et al. (2001). They used their lithium detection to constrain its age below 1 Gyr. Allers & Liu (2013) updated its spectral classification to an intermediate gravity L0 β; Reid et al. (2002) and Reiners & Basri (2009) measured an RV which Gagné et al. (2014b) combined to obtain 9.3 ± 1.7 km s^{-1}; Dieterich et al. (2014) measured a trigonometric distance of 6.41 ± 0.04 pc. Gagné et al. (2014b) used a previous parallax measurement from Tinney (1996); 5.0 ± 0.1 pc) with the BANYAN II tool to derive a Bayesian probability of 17.5% that this is a member of ARG. However, Ribas (2003) indicated that it is a candidate member to the purported ~200 Myr old Castor moving group (CAS; Barrado y Navascués 1998). They thus use an alternate Bayesian analysis similar to BANYAN I (Malo et al. 2013) but including a SKM of CAS built from members reported by Barrado y Navascués (1998) and find a significantly larger Bayesian probability for CAS (99.7%). More recently, Mamajek et al. (2013) used updated distance and RV measurements of the original CAS members to demonstrate that they are too far apart in velocity space to be a part of a moving group of common origin. They thus argue that CAS is likely a dynamical stream rather than a moving group, which is in line with the results of Mamajek (2012), Monnier et al. (2012), and Zuckerman et al. (2013). The difference in UVW space between LP 944–20 and ARG is considerable (9.7 km s^{-1}) and comparable to its distance to Fomalhaut (13.5 km s^{-1}). We conclude that LP 944–20 is likely a contaminant in our analysis, which could possibly be explained by the fact that our SKM model of field stars, derived from the Besançon galactic model (Robin et al. 2014, 2012), does not explicitly include such dynamical streams that could act as an additional source of contamination.

2MASS J05002100+0330501 was identified as an L4 dwarf by Reid et al. (2008b) and Blake et al. (2010) measured an RV of 15.9 ± 0.2 km s^{-1}, from which we obtain a 62.8% membership probability associated with ABDMG. However, Reid et al. (2008b) specified that this object displays no notable peculiarities and would be a good spectral standard. While NIR spectroscopy could unambiguously rule out low gravity, it is likely that this object is a field contaminant in our analysis.

2MASS J05012406–0010452 has been identified by Reid et al. (2008b) as an L4 BD with signs of low gravity in its optical spectrum. Cruz et al. (2009) updated its classification to L4 γ using its optical spectrum, and Allers & Liu (2013) classified it as L3 γ using NIR spectroscopy. Faherty et al. (2012) measured

a trigonometric distance of 13.1 ± 0.8 pc. Gagné et al. (2014b) considered this object and found no obvious candidacy to any YMG considered here. However, we find that it has a 64.7% Bayesian probability of being a member of COL, associated with a 2.3% contamination probability. The discrepancy between this result and that of Gagné et al. (2014b) is due to the μ_δ proper motion measurement from 2MASS–AllWISE, which is at 2.8σ of the value they used, which was measured by Faherty et al. (2012). We visually inspected the 2MASS and AllWISE Atlas images and found that our cross-match between both catalogs is unambiguous. Much like the case of 2MASS J02212859–6831400, an RV measurement will be needed to better constrain the membership of this object, but it is plausible that this object is a false positive in our analysis.

2MASS J10584787–1548172 (DENIS–P J1058.7–1548) has been identified as an L3 dwarf by Geballe et al. (2002) and Dahn et al. (2002) measured a trigonometric distance of 17.3 ± 0.3 pc, from which we obtain a 93.1% membership probability to ARG. Reid et al. (2008b) measured Hα emission in its optical spectrum, but reported no further peculiarities. Schneider et al. (2014) subsequently measured the gravity-sensitive $H_2(K)$ in its NIR spectrum and obtain a value of 1.021, which is consistent with a field L3 dwarf. It is thus likely that this object is a field contaminant in our analysis.

2MASS J12474428–3816464 has been identified by Gagné et al. (2014a) as a low-gravity M9 γ candidate member of TWA, as part of the initial follow-up of the BASS survey. They note that its kinematics are discrepant with TWA albeit its low probability of being a field contaminant: its kinematics would match with TWA if it was placed further away; however, this would make it over-luminous compared to young BDs of the same spectral type and age. It could be expected that this is a contaminant from the Lower Centaurus Crux region (LCC; ~10–20 Myr; de Zeeuw et al. 1999) of the Scorpius–Centaurus complex, but its distance (~120 pc) would also make it overluminous. It is possible that this object could be an unresolved binary and located further away, between TWA and LCC: this is reminiscent of TWA 29 and TWA 31, and might strengthen the proposition of Song et al. (2003; see also Schneider et al. 2012a) that TWA could actually be part of the LCC.

2MASS J14252798–3650229 has been identified as an L5 BD by Faherty et al. (2009). Including RV and trigonometric distance measurements from Blake et al. (2010) and Riedel et al. (2014), respectively, we find a 99.6% probability that this object is a member of ABDMG, with 0.1% contamination probability. Only signs of youth need to be confirmed before we can consider this object as a new bona fide member of ABDMG; however, we note that its has NIR colors $J - K_S = 1.94$, hence 1σ redder than field L5 dwarfs, which could be an indication of youth.

2MASS J17571539+7042011 (LP 44–162) has been identified as an M7.5 dwarf by Gizis et al. (2000). Tanner et al. (2010) and Terrien et al. (2012) measured its RV, which we combine in an error-weighted mean to obtain -12.4 ± 0.6 km s^{-1}. Lépine et al. (2009) measured a trigonometric distance of 19.1 ± 0.4 pc and reported that it is significantly overluminous compared to dwarfs of the same colors, and proposed that it might be an unresolved multiple. We find a Bayesian probability of 91.0% that this is a member of ARG. However, Deshpande et al. (2012) obtained high-resolution NIR spectroscopy and reported pseudo-EWs of K I lines in the J band that are consistent with M7.5 field dwarfs (e.g., see Allers & Liu 2013). It is thus plausible that this object is a false positive in our analysis, despite its high probability.

SIMP J21543454–1055308 has been independently discovered in the *SIMP* survey for field BDs (Artigau et al. 2009; J. Robert et al., in preparation). A NIR spectroscopic follow-up revealed that this object is a low-gravity L4 β BD with an estimated mass of $10 \pm 0.5\ M_{\rm Jup}$, well into the planetary regime, if it is a member of ARG as suspected (Gagné et al. 2014c).

2MASS J23225384+7847386 has been identified as an M5 proper motion companion to V 368 Cep and LSPM J2322+7847 by Makarov et al. (2007). Using the X-ray luminosity of V 368 Cep as well as an isochrone analysis on all three components, they estimated an age of ~50 Myr for the system. Using the RV measurement from Kharchenko et al. (2007), and combined trigonometric distance measurements from Kharchenko et al. (2007) and Dittmann et al. (2014), we find that this object has a 29.7% probability of being a member of CAR, with a contamination probability of 1.0%. The estimated age of this system is consistent with that of CAR, which makes it a compelling candidate member, even if its Bayesian probability is somewhat low. This low probability is a consequence of its galactic position $XYZ = (-8.7 \pm 2.5, 16.1 \pm 4.6, 5.5 \pm 1.6)$ pc, at 2.5σ of our spatial model for CAR. We note however that its kinematics are a very good match to CAR with $UVW = (-10.1 \pm 5.2, -23.5 \pm 2.9, -6.3 \pm 1.0)$, at only 0.5σ of our kinematic model. This could be an indication that CAR is in fact spatially larger than our present model, which would not be surprising since it was built from the only seven currently known bona fide members. We thus suggest that 2MASS J23225384+7847386 is probably a member in CAR, and that we might be currently missing more objects like this one as a result of our SKM for this association being too narrowly confined. Finding additional objects like this one will be needed to better constrain the SKM of CAR. Montes et al. (2001) suggested that V 368 Cep is a member of the Pleiades moving group (PMG; also called the Local Association); however, we find that its kinematics are much more consistent with those of CAR, at only 1.5 km s^{-1} of our dynamical model, compared to a difference of 5.5 km s^{-1} with the kinematics of the PMG (Montes et al. 2001). Famaey et al. (2005) demonstrated that the PMG is likely a dynamical stream with a large spread in age rather than a coeval moving group, hence the age constraint acts as a further indication that a membership to CAR is more likely.

5. RECOVERY OF KNOWN CANDIDATES AND MEMBERS OF YOUNG MOVING GROUPS

In this section, we assess the fraction of known $\geqslant$M5 candidate members of YMGs that are recovered in the BASS and LP-BASS catalogs. We identified a total of 98 candidate members of the YMGs considered here in the literature (Schlieder et al. 2012b; Shkolnik et al. 2012; Malo et al. 2013; Rodriguez et al. 2013; Gagné et al. 2014b; Kraus et al. 2014 and references therein). We do not include low-probability candidates from Gagné et al. (2014b) here, since they have a contamination probability of >50% by definition, which ensures that they are not listed in the BASS catalog. We find that a total of 55/98 of all these candidates are recovered in BASS (see Table 3), whereas 8 others are recovered in LP-BASS (see Appendix B), hence making up for 64% of currently known candidate members. All 35 candidates not recovered here are listed in Table 4, along with a list of the filters that caused them to be rejected. We note that 17 of those 36 candidates were missed only because they were cut from our input sample because of quality filters (i.e., low galactic latitude, low proper motion, large number of 2MASS neighbors, poor 2MASS or AllWISE photometric quality, or

Table 4
Known YMG Candidate Members not Recovered in BASS

2MASS Designation	Measured SpT[a]	Known Candidacy	Reason for Rejection[b]
00332386−1521309	L4 β	ARG[31]	$HW2_{CMD}$
00470038+6803543	L7 p	ABDMG[31]	b, $2M_{\#}$
01112542+1526214	M5+M6	βPMG[67]	$W1_{SAT}$
01291221+3517580	L4	ARG[31]	$HW2_{CMD}$
01424687−5126469	M6.5	COL[90]	$J-H$, $2M_{PH}$, $\sigma\mu$, μ, P, C
02535980+3206373	M7p	βPMG[31]	$HW2_{CMD}$, P
03214475−3309494	M5.8	COL[90]	$V-J$, $2M_{PH}$, P, C
03244305−2733230	M5.5	COL[90]	K_S-W1, μ, P, C
03350208+2342356	M8.5	βPMG[100]	$W1_{SAT}$, $W2_{SAT}$, C
04062677−3812102	L0 γ	COL[31]	P, C
05184616−2756457	L1 γ	COL[31]	μ
06195260−2903592	M6	COL[31]	μ
06322402−5010349	L3	ABDMG[31]	$HW2_{CMD}$, $\sigma\mu$, C
07285117−3015527	M5	ABDMG[100]	b, $W1_{SAT}$, $2M_{\#}$
09445422−1220544	M5	ARG[67]	$W1-W2$, $W1_{SAT}$
10042066+5022596	L3 β	ABDMG[31]	$W1_{SAT}$, P, C
10172689−5354265	M5	βPMG[105]	b, $J-H$, $W1_{SAT}$, $2M_{\#}$
11321831−3019518	M5	TWA[67]	$H-K_S$, K_S-W1
11324116−2652090	M5	TWA[69]	$H-K_S$, K_S-W1, $2M_{CC}$, $W1_{SAT}$, W_{CC}
12242443−5339088	M5	βPMG[67]	b, K_S-W1, $HW2_{CMD}$, $2M_{\#}$
12451416−4429077	M9.5 p	TWA[31]	$2M_{\#}$
13142039+1320011	M7	ABDMG[93]	P
16002647−2456424	M7.5 p	ABDMG[31]	JK_{CMD}, $HW2_{CMD}$, USco, $2M_{\#}$, P, C
16471580+5632057	L9 p	ARG[31]	P, C
17410280−4642218	L7 p	βPMG;ABDMG[97]	b, $2M_{CC}$, $2M_{\#}$
18450097−1409053	M5	ARG[67]	b, $W1-W2$, $2M_{CC}$, $2M_{PROX}$, $W1_{SAT}$, $W2_{SAT}$, $2M_{\#}$, P
21011544+1756586	L7.5	ABDMG[31]	$2M_{PH}$, $2M_{CC}$, $2M_{\#}$
21103096−2710513	M5	βPMG[67]	$WISE$
21140802−2251358	L7	βPMG[62]	$2M_{PH}$
21354554−4218343	M5.2	THA[53]	$B-V$, P, C
21374019+0137137	M5	βPMG[93]	$H-K_S$, $W1_{SAT}$
21481633+4003594	L6	ARG[31]	b, $2M_{\#}$
22081363+2921215	L3 γ	βPMG[31]	P, C
23204705−6723209	M5	THA[67]	$V-J$, $2M_{PH}$, $2M_{CC}$, $\sigma\mu$
23512200+3010540	L5.5	ARG[31]	$B-J$, χ^2_{W1}, $2M_{BL}$, $HW2_{CMD}$

Notes.
[a] Measured in the NIR unless symbol otherwise specified.
[b] This column contains codes corresponding to the filters that rejected an object from the BASS catalog; (1) *WISE*: no entry in the *WISE* and AllWISE catalogs, (2) b: absolute galactic latitude is too low, (3) $B-V$ color is too blue, (4) $B-J$ color is too blue, (5) $V-J$ color is too blue, (6) $J-H$ color is too blue, (7) $H-K_S$ color is too blue, (8) K_S-W1 color is too blue, (9) $W1-W2$ color is too blue, (10) χ^2_{W1}: the reduced χ^2 from the adjusted profile in the $W1$ band is too large, (11) $2M_{PH}$: 2MASS photometric quality is too low, (12) $2M_{BL}$: a blend flag is suspicious in 2MASS, (13) $2M_{CC}$: a contamination flag is suspicious in 2MASS, (14) $2M_{PROX}$: a close-by 2MASS source is unresolved in AllWISE, (15) $W1_{SAT}$: $W1$ magnitude is saturated, (16) $W2_{SAT}$: $W2$ magnitude is saturated, W_{CC}: a contamination flag is suspicious in AllWISE, (17) JK_{CMD}: the object falls to the left of the M_{W1} versus $J-K_S$ field sequence using its statistical distance, (18) $HW2_{CMD}$: the object falls to the left of the M_{W1} versus $H-W2$ field sequence using its statistical distance, (19) Usco: the object is too close to Upper Scorpius, (20) $2M_{\#}$: the object has too many immediate neighbors in 2MASS, (21) $\sigma\mu$: the 2MASS–AllWISE proper motion is not precise enough, (22) μ: the proper motion is too low, (23) P: the Bayesian probability is too low, (24) C: the contamination probability is too high. See Sections 2–3 for detailed descriptions of these respective filters.
References to this table are identical to those of Table 3.

NIR colors too blue), whereas 18 were missed at least because of a low Bayesian probability, high contamination probability, or position in a CMD diagram derived from its statistical distance. Considering only the known candidate members that were part of our input search sample, the BASS and LP-BASS catalogs thus recover 68% of them.

6. THE UPDATED BASS SAMPLE

We present in Table 5 a complete list of the BASS sample, which contains only objects respecting all criteria mentioned in Sections 2–3 after taking account of all information available in the literature. We list in this table the contamination probability of all objects, obtained from the Monte Carlo analysis described in Section 3, as well as statistical estimates for their distance and RV. We refer to this list as the BASS sample for the remainder of this work. We used the individual contamination probability of all candidate members to estimate an average contamination fraction from field stars of 2.4% and 29.5% for the high probability and modest probability samples, respectively. These estimates of contamination do not take account of possible cross-contamination between the YMGs considered here or other,

Table 5
The Complete BASS Catalog

2MASS Designation	Spectral Type[a]	Probable Membership	Bayesian Prob. (%)	Contamination Prob. (%)	Estimated Mass Range ($M_{\rm Jup}$)	Statistical Distance (pc)	Statistical RV (km s^{-1})
Candidates with a High Probability							
00011217+1535355	L4:	ABDMG	77.8	1.8	$17.5^{+0.8}_{-1.1}$	27.3 ± 1.6	-6.5 ± 2.0
00040288−6410358	L1 γ	THA	>99.9	<0.1	12.8 ± 0.3	45.0 ± 2.4	6.5 ± 2.5
00041589−8747254	(M5.7)	THA	55.4	<0.1	$60.9^{+8.8}_{-7.1}$	51.8 ± 3.6	11.3 ± 2.2
00065794−6436542	M9:	THA	>99.9	<0.1	$20.5^{+1.1}_{-13.9}$	41.4 ± 2.4	6.2 ± 2.4
00111532−3756553	(M5.7)	THA	80.2	<0.1	$60.6^{+8.6}_{-6.7}$	$38.2^{+2.0}_{-2.4}$	1.5 ± 2.2
00182834−6703130	(M9.6)	THA	99.8	<0.1	13.3 ± 0.3	$43.8^{+2.8}_{-2.4}$	6.9 ± 2.5
00191296−6226005	(M9.7)	THA	99.5	<0.1	$13.3^{+0.3}_{-0.4}$	$46.6^{+2.4}_{-2.8}$	6.7 ± 2.5
00192626+4614078	M8	ABDMG	92.1	4.1	$87.1^{+8.5}_{-8.6}$	37.8 ± 3.2	-19.5 ± 3.0
00212774−6351081	M5.5	THA	99.8	<0.1	$158.3^{+19.9}_{-18.5}$	$44.2^{+2.8}_{-2.4}$	6.8 ± 2.4
00235732−5531435	M4.1	THA	99.8	<0.1	$133.1^{+17.4}_{-14.6}$	41.4 ± 2.4	5.3 ± 0.7
Candidates with a Modest Probability							
00160844−0043021	L5.5	BPMG	19.1	36.1	9.6 ± 0.3	$30.9^{+2.8}_{-3.2}$	3.3 ± 1.8
00274534−0806046	(M5.3)	BPMG	45.6	35.1	66.9 ± 4.2	32.1 ± 2.8	4.4 ± 1.5
00464841+0715177	M9	BPMG	77.0	26.9	$15.0^{+0.1}_{-0.3}$	$33.8^{+2.8}_{-3.2}$	3.2 ± 1.7
00581143−5653326	(L6.1)	ARG	80.4	32.9	$10.3^{+0.7}_{-0.3}$	$25.3^{+2.8}_{-2.4}$	2.6 ± 2.0
01525534−6329301	(M4.7)	BPMG	71.4	22.1	$107.6^{+6.8}_{-7.8}$	23.7 ± 2.4	14.7 ± 1.7
02534448−7959133	M5.5	BPMG	50.1	30.9	66.9 ± 4.9	$28.9^{+2.8}_{-3.2}$	12.0 ± 2.1
03390160−2434059	M5.9	COL	77.8	31.9	$204.7^{+6.6}_{-3.5}$	$59.4^{+5.6}_{-6.0}$	18.6 ± 1.8
03473987−4114014	(M5.3)	COL	38.0	45.4	$77.2^{+11.0}_{-10.5}$	$71.0^{+8.8}_{-8.0}$	19.7 ± 1.7
03510460−5701469	(M5.1)	COL	17.6	47.4	$88.3^{+12.0}_{-11.7}$	$68.6^{+8.8}_{-8.0}$	19.1 ± 1.7
03550477−1032415	M8.5	BPMG	39.5	38.5	$26.4^{+3.5}_{-4.2}$	$35.0^{+4.4}_{-4.8}$	17.7 ± 1.8

Notes.
[a] Spectral types in parentheses were estimated from 2MASS–AllWISE colors (see Section 4.1).
[b] The binary hypothesis is more probable than the single hypothesis (see Section 3).

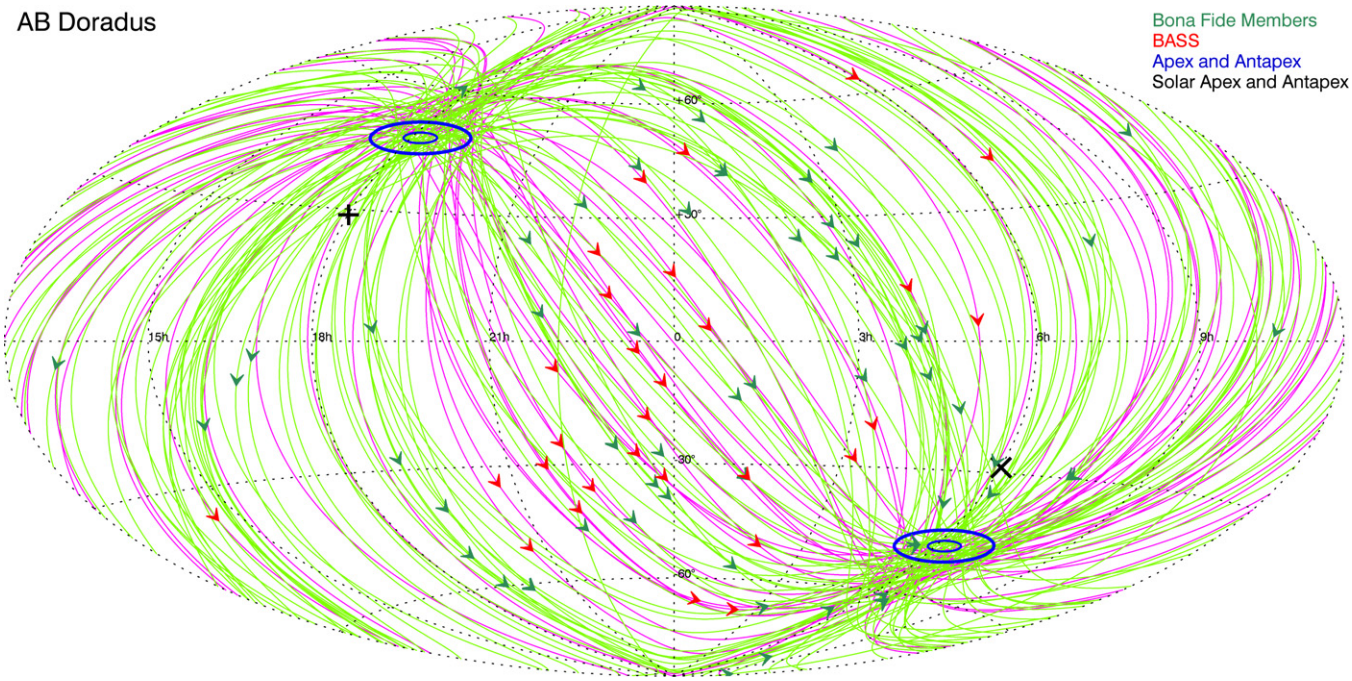

Figure 6. Proper motion as a function of sky position for candidate members of AB Doradus in the BASS Catalog (red arrows and lines) compared with currently known bona fide members (light green; see Gagné et al. 2014b). The proper motions of candidate members and bona fide members all converge to the apex and antapex of ABDMG (blue circles), which is a well-known property of YMGs.

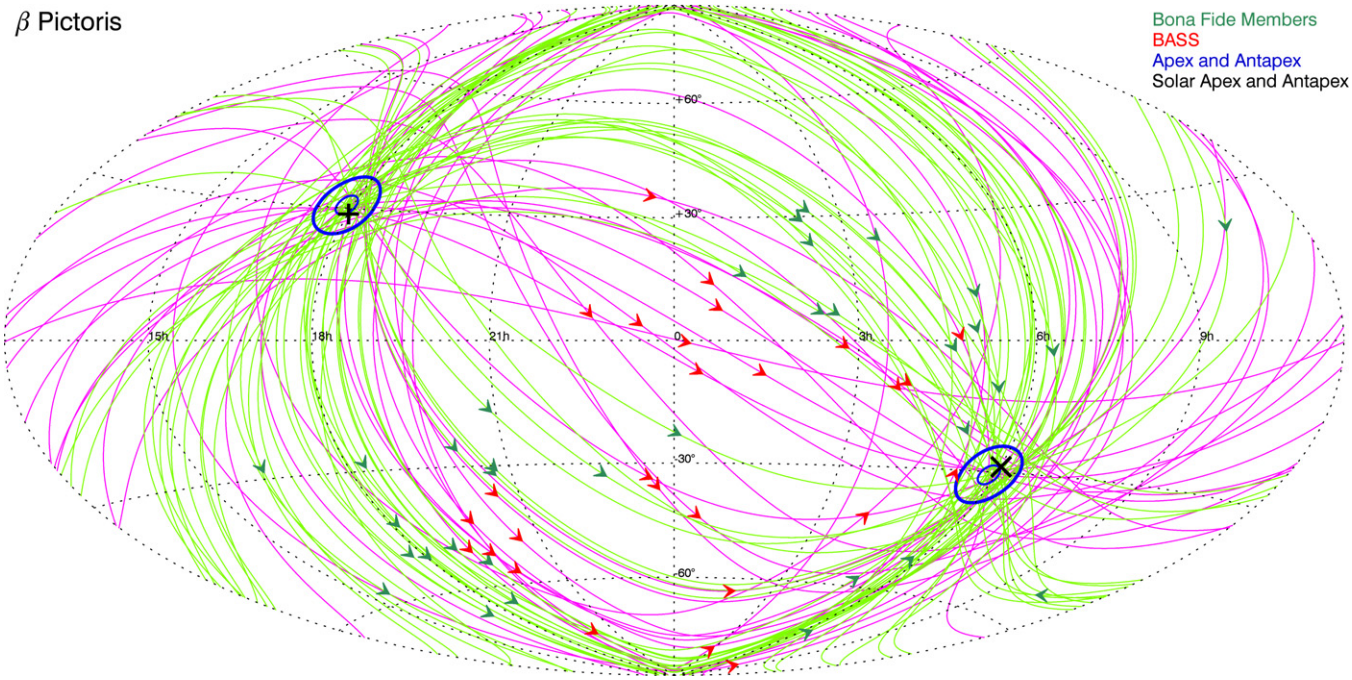

Figure 7. Proper motion as a function of sky position for BASS candidate members and bona fide members of βPMG. Colors and symbols are defined in the same way as in Figure 6.

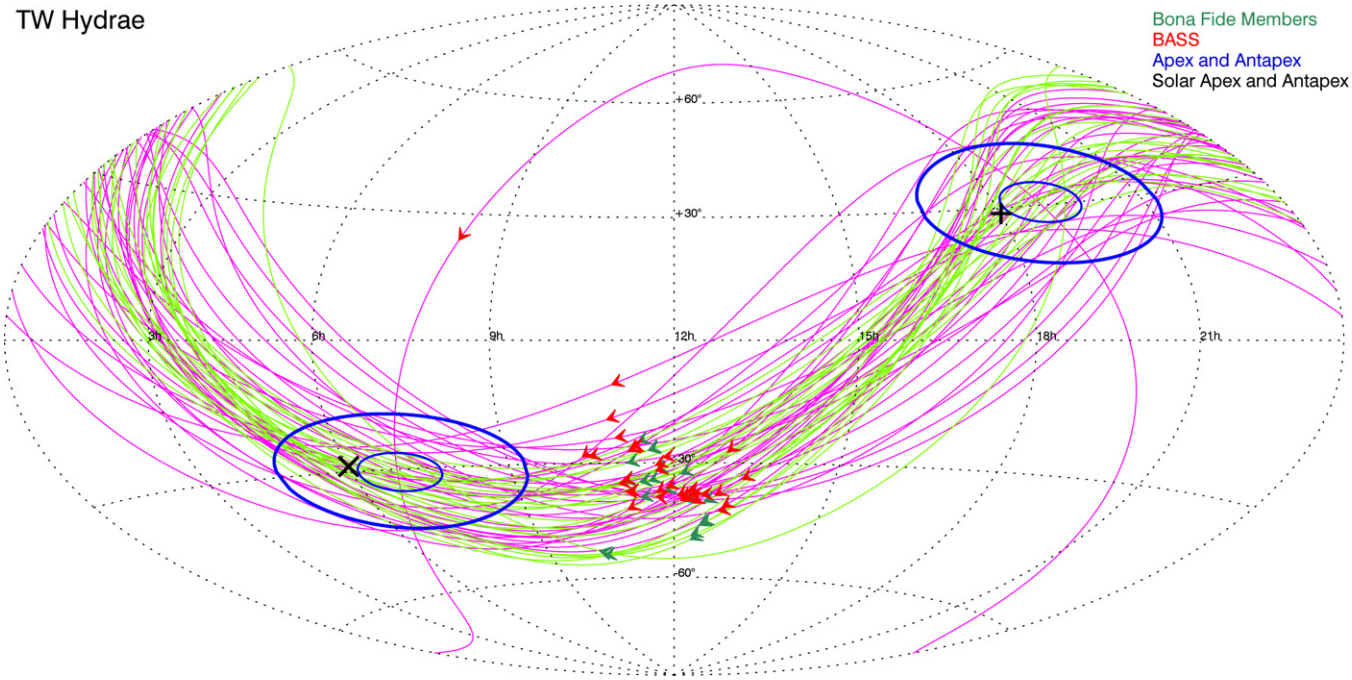

Figure 8. Proper motion as a function of sky position for BASS candidate members and bona fide members of TWA. Colors and symbols are defined in the same way as in Figure 6.

older nearby associations not considered, e.g., Carina-Near (∼200 Myr; Zuckerman et al. 2006), the Ursa Major moving group (∼500 Myr; King et al. 2003), and the Hercules–Lyra association (∼250 Myr; Eisenbeiss et al. 2013). Another way to assess a minimal contamination rate is to count the fraction of candidates with RV, distance, or spectra in the literature that were rejected from these measurements. This estimate yields a larger contamination rate of 12.6% (11/87) for the high probability candidates. Small number statistics prevent an accurate estimation for the low-probability candidates: only 37 had such measurements in the literature, from which 4 were rejected. We rather choose to scale the observed 12.6% contamination fraction of the high-probability sample with the ratio of predicted contamination fractions of both samples to estimate a more reliable expected contamination fraction of ∼71% for the modest probability BASS sample.

In Figures 6–12, we compare proper motions and sky positions of the BASS sample with currently known bona fide members of YMGs; it can be seen that, as expected, trajectories of candidates in the BASS sample projected on the

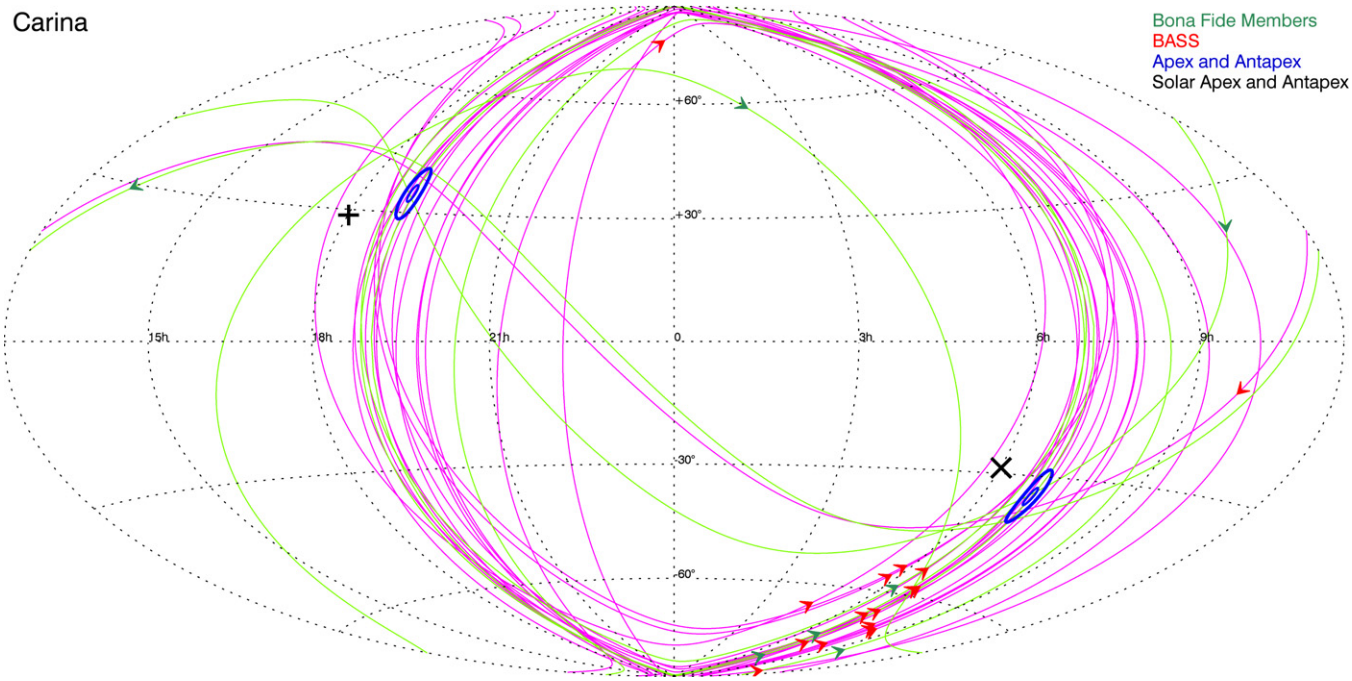

Figure 9. Proper motion as a function of sky position for BASS candidate members and bona fide members of CAR. Colors and symbols are defined in the same way as in Figure 6.

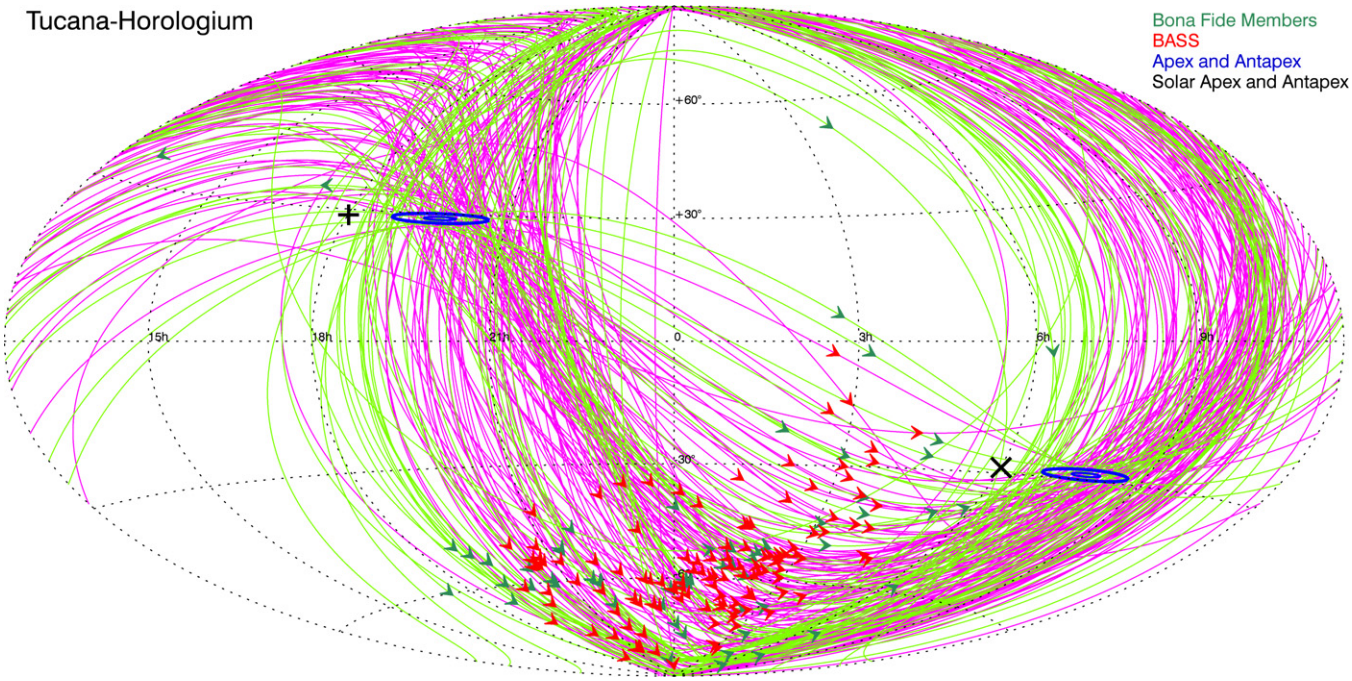

Figure 10. Proper motion as a function of sky position for BASS candidate members and bona fide members of THA. Colors and symbols are defined in the same way as in Figure 6.

celestial sphere are consistent with known bona fide members. In Figure 13, we use the statistical distances from BANYAN II to display the position of candidates of the BASS sample in two CMDs: absolute $W1$ as a function of $H-W2$, and absolute $W1$ as a function of $J-K_S$. These two CMDs are used as observable in the BANYAN II tool as they are useful to distinguish young >M5 dwarfs from their field counterparts. In Figures 14–20, we compare the statistical predictions for galactic positions (XYZ) and space velocity (UVW) of all BASS candidates with those of currently known bona fide members of YMGs, as well as the 1.557σ contours of the SKM ellipsoids used in BANYAN II. We use 1.557σ as the three-dimensional analog to 1σ in one dimension in the sense that it encompasses 68% of objects drawn from a Gaussian random PDF. In Figure 21, we show the sky position of all BASS candidate members as well as known bona fide members of the YMGs considered here. We display the galactic plane ($b>15^\circ$) as well as star-forming regions that were avoided in our search (see Section 2).

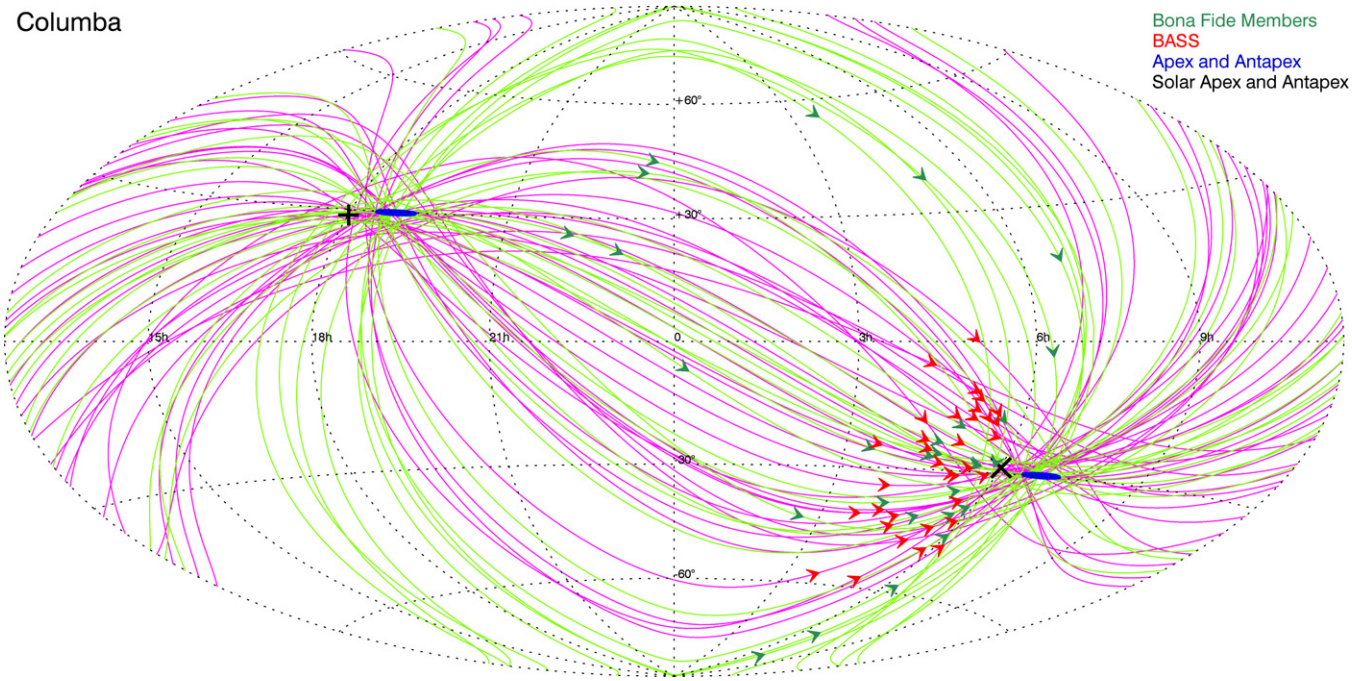

Figure 11. Proper motion as a function of sky position for BASS candidate members and bona fide members of COL. Colors and symbols are defined in the same way as in Figure 6.

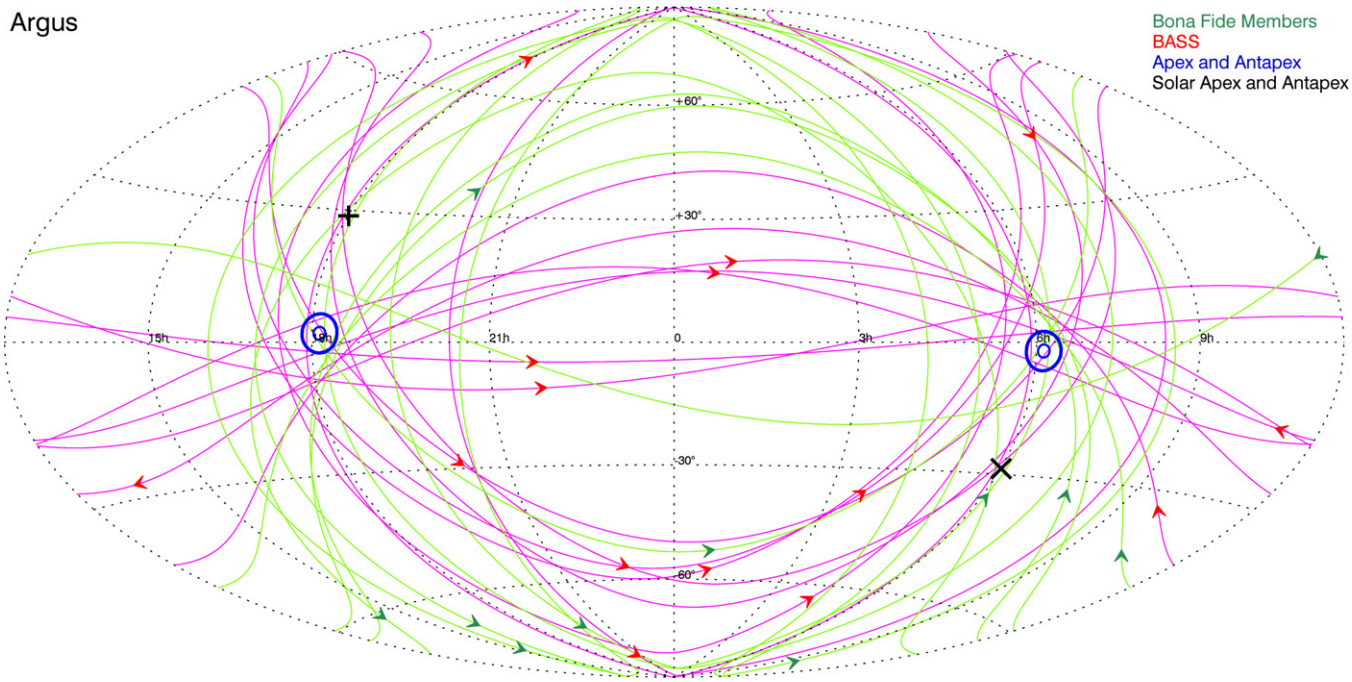

Figure 12. Proper motion as a function of sky position for BASS candidate members and bona fide members of ARG. Colors and symbols are defined in the same way as in Figure 6.

6.1. Mass Estimates

We used the YMG age and statistical distance associated to the most probable hypothesis from BANYAN II and the AMES-Cond isochrones (Baraffe et al. 2003) in combination with the CIFIST2011 BT-Settl atmosphere models (Allard et al. 2013; Rajpurohit et al. 2013) to estimate the mass of all candidates presented here. A uniform distribution spanning the age range of each YMG was used to compare their absolute J, H, K_S, $W1$, and $W2$ magnitudes with model isochrones in a maximum likelihood analysis. Mass estimates are listed in Table 5. The BASS sample comprises 79 new candidate young BDs and 22 candidate planetary-mass objects.

7. A SEARCH FOR NEW COMMON PROPER MOTION PAIRS

Since the 2MASS and AllWISE catalogs provide a fast way to determine proper motions for a large number of targets, we performed a search for common proper motion objects around all candidates in the BASS sample. We used the BANYAN II statistical distance of each candidate to define a projected

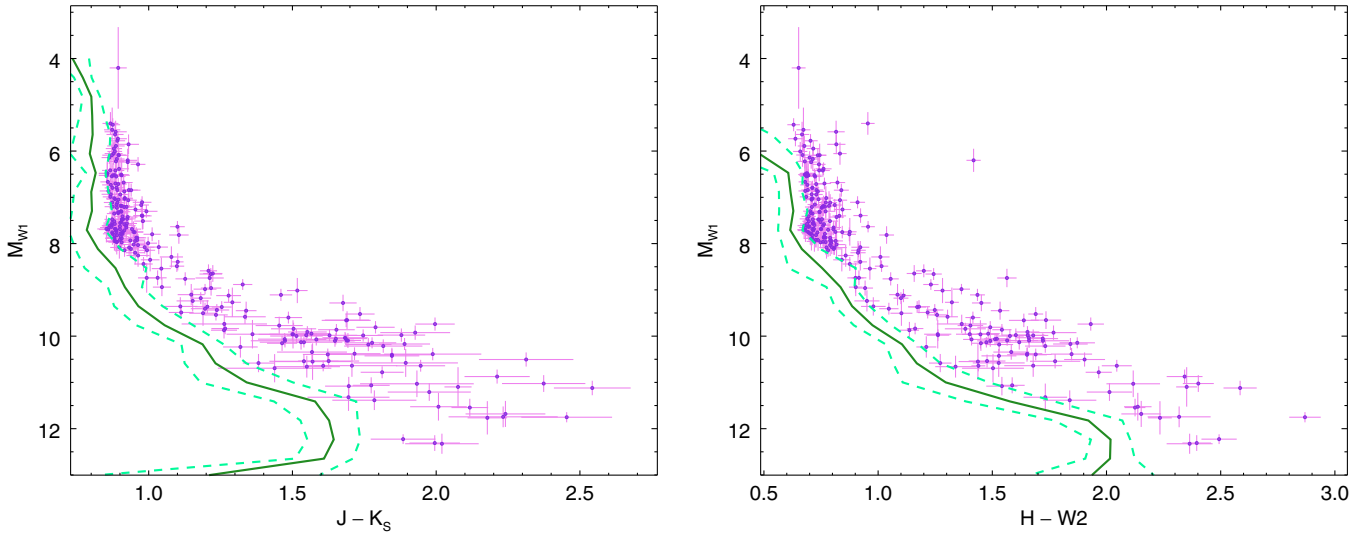

Figure 13. Positions of all objects in the BASS sample in two different CMDs (purple points), compared with the field sequence (thick green line) and its scatter (dashed green lines). We used the statistical distances of the most probable hypothesis from the BANYAN II tool to compute absolute magnitudes. The positions of all BASS candidates are consistent with them being young objects brighter and/or redder than the field sequence.

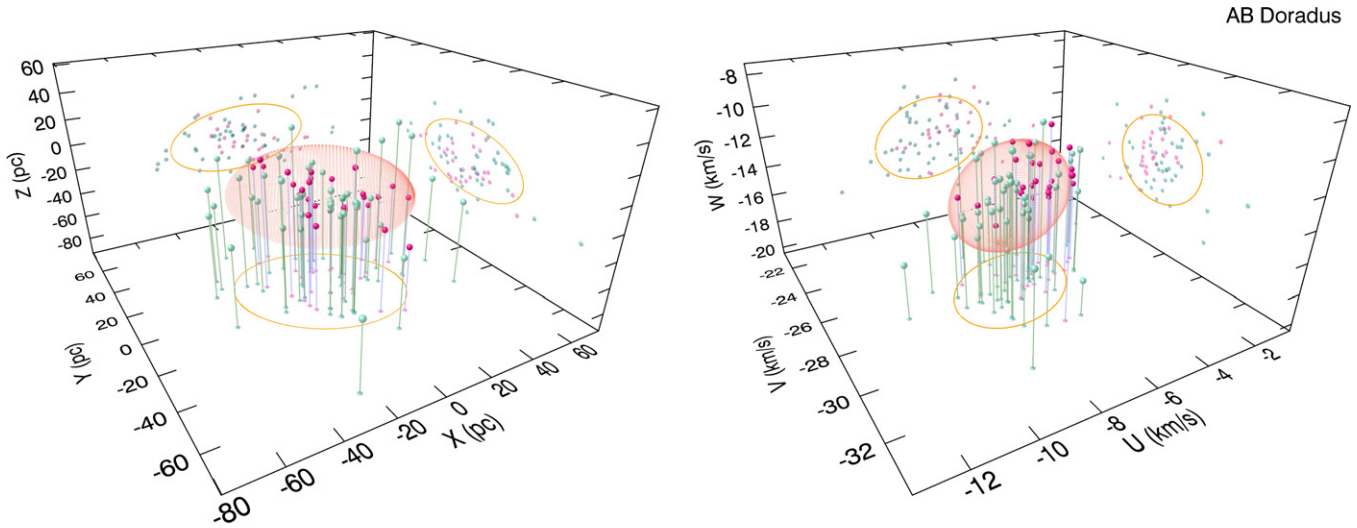

(a) *XYZ* (b) *UVW*

Figure 14. Most probable galactic positions *XYZ* and space velocities *UVW* based on BANYAN II statistical distances and RVs for all BASS candidate members in ABDMG (red points) compared with bona fide members (green points), as well as the spatial and kinematic ellipsoid models used in BANYAN II (orange ellipsoids; see Gagné et al. 2014b for more details). All points and models are projected on the three normal planes for a better clarity.

separation radius of 10,000 AU, within which we have searched for any other object with a proper motion respecting the criteria of Lépine & Bongiorno (2007), albeit with a more conservative filter on the allowed proper motion difference. This requires that the separation $\Delta\theta$ (measured in arcseconds) and the proper motion difference $\Delta\mu$ (measured in mas yr^{-1}) obey the following equations:

$$\Delta\theta\ \Delta\mu < 1,000 \cdot (\mu/150)^{3.8},$$
$$\Delta\mu < 50.$$

These criteria should ensure that the majority of genuine proper motion pairs are recovered, with a minimal amount of contamination from chance alignments. This search allowed us to find 5 new common proper motion pairs and recover 10 that were already known in the literature. Those already known are:

1. 2MASS J00451358+0015509* (M3.8) and 2MASS J00451098+0015117 (HD 4271; F8; Newton et al. 2014)
2. 2MASS J01243060–3355014* (GJ 2022 B; M4.5) and 2MASS J01242767–3355086 (GJ 2022 AC; M4.5+M4.5; Thé & Staller 1974)
3. 2MASS J02033222+0648588* (estimated M4.5) and 2MASS J02032589+0648008 (estimated early M; Zacharias et al. 2012)
4. 2MASS J02420204–5359147* (M4.6) and 2MASS J02420404–5359000 (estimated early M; Zacharias et al. 2012)
5. 2MASS J03114240–1537183* (LP 722–14; estimated M5.0) and 2MASS J03114269–1537327 (LP 722–15; estimated M2.2; Luyten 1980)
6. 2MASS J03283911–1537333* (GJ 3229 B; M3.5) and 2MASS J03283893–1537171 (GJ 3228 A; M3.5; Gliese & Jahreiß 1991)
7. 2MASS J03505949+1414017* (M5) and 2MASS J03510078+1413398 (M4; Mason et al. 2001)

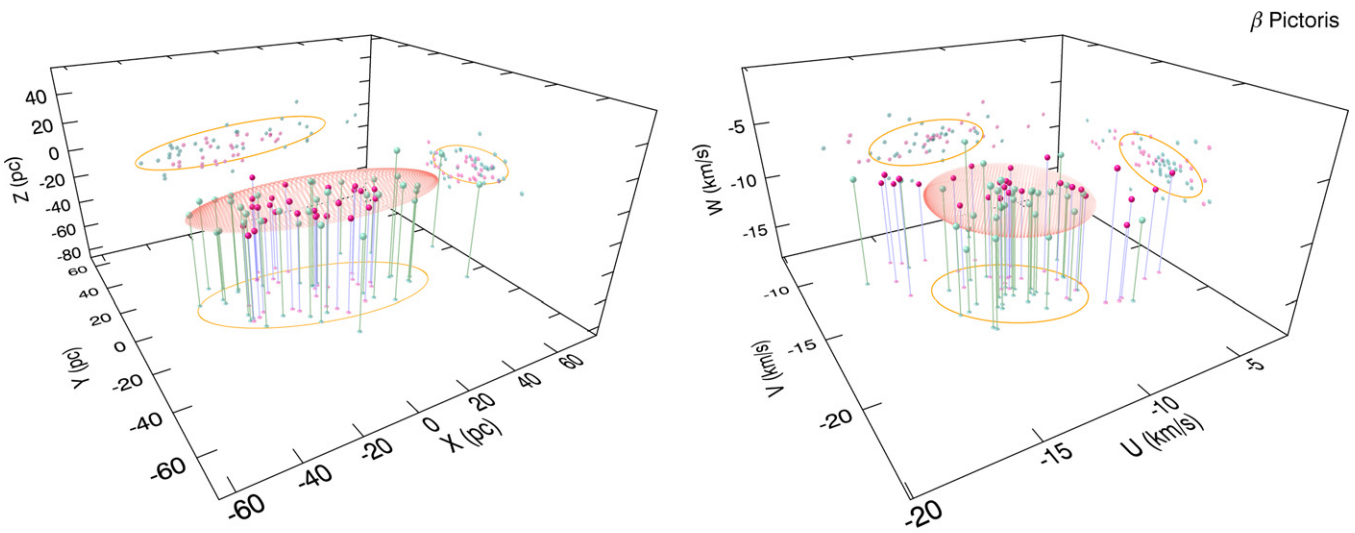

(a) *XYZ* (b) *UVW*

Figure 15. Most probable galactic positions *XYZ* and space velocities *UVW* based on BANYAN II statistical distances and RVs for all BASS candidate members in βPMG compared with bona fide members. Colors and symbols are defined in the same way as in Figure 14.

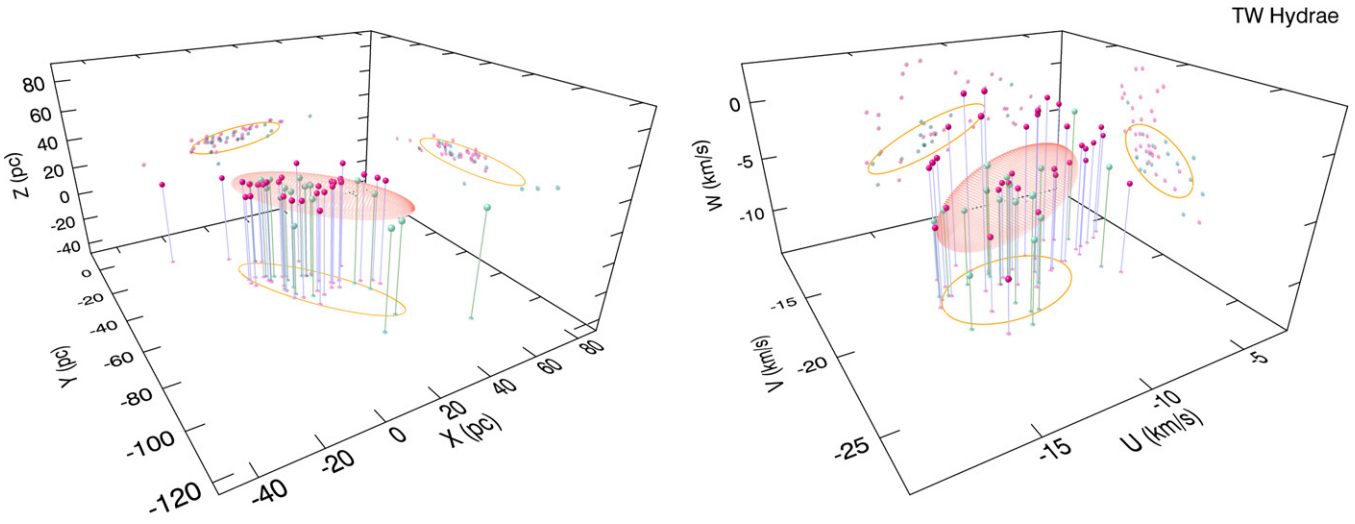

(a) *XYZ* (b) *UVW*

Figure 16. Most probable galactic positions *XYZ* and space velocities *UVW* based on BANYAN II statistical distances and RVs for all BASS candidate members in TWA compared with bona fide members. Colors and symbols are defined in the same way as in Figure 14. We note that a fraction of BASS candidates have kinematics slightly discrepant with those of TWA. It is possible that contamination from the Lower Centaurus Crux causes this (i.e., Schneider et al. 2012a), however a follow-up of these candidates will be needed to confirm this.

8. 2MASS J21440795+1704372* (GJ 126–30; M4.5) and 2MASS J21440900+1703348 (GJ 126–31; M4; Mason et al. 2001)
9. 2MASS J23225240–6151114* (M5) and 2MASS J23225299–6151275* (L2 γ; Gagné et al. 2014b)
10. 2MASS J23102196–0748531* (M5) and 2MASS J23102196–0748531 (HIP 114424; K0; Mann et al. 2014).

We identified components present in the BASS or LP-BASS catalogs with an asterisk. Any potentially useful information from these matches were already taken into account in Section 4. We discuss the new potential common proper motion pairs below:

2MASS J04353042–6449570 from BASS (estimated M8.4 with $J = 15.27$) seems to be co-moving with 2MASS J04352709–6450042 ($J = 15.16$) at an angular separation of 22.″4 and a proper motion difference of 0.4 mas yr^{-1} (0.05σ) with respect to a total proper motion of 53.2 mas yr^{-1}. However, we note that 2MASS J04352709–6450042 is only 0.11 mag brighter in the J band, and yet its NIR colors are significantly bluer: it has $J - K_S = 0.42$ and $H - W2 = 0.02$, versus $J - K_S = 1.34$ and $H - W2 = 1.30$ for the BASS candidate. These very blue colors would be indicative of a spectral type earlier than M, which is not consistent with it being at the same distance than the primary, even if the latter was a multiple system. For this reason, BANYAN II rejects it as a probable candidate member of CAR, but if we do not include photometry, then its Bayesian probability for CAR is 31.4%, with a contamination probability of 21.9%. We conclude nonetheless that the secondary is most probably not a member of CAR and

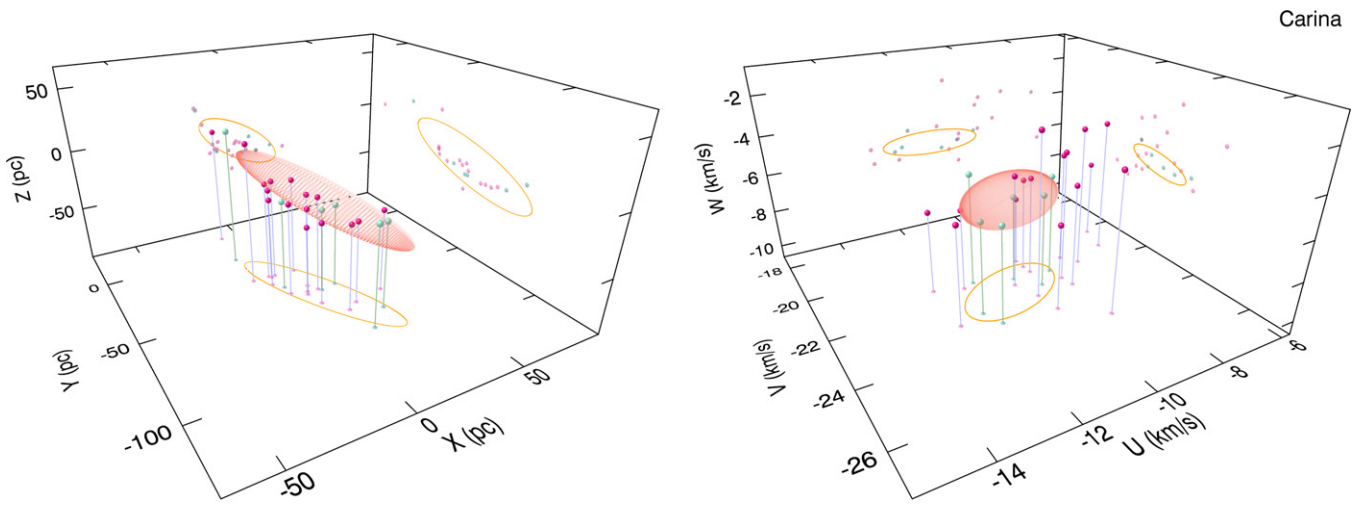

(a) *XYZ* (b) *UVW*

Figure 17. Most probable galactic positions *XYZ* and space velocities *UVW* based on BANYAN II statistical distances and RVs for all BASS candidate members in CAR compared with bona fide members. Colors and symbols are defined in the same way as in Figure 14. We note that the SKMs presented here (orange ellipsoids) are based on only seven bona fide members, and they are thus most probably incomplete (see Gagné et al. 2014b for a discussion). It can be seen that BASS candidates preferentially fall in a region slightly outside of the kinematic model, which potentially points out to an overlooked region of CAR members in the kinematic space.

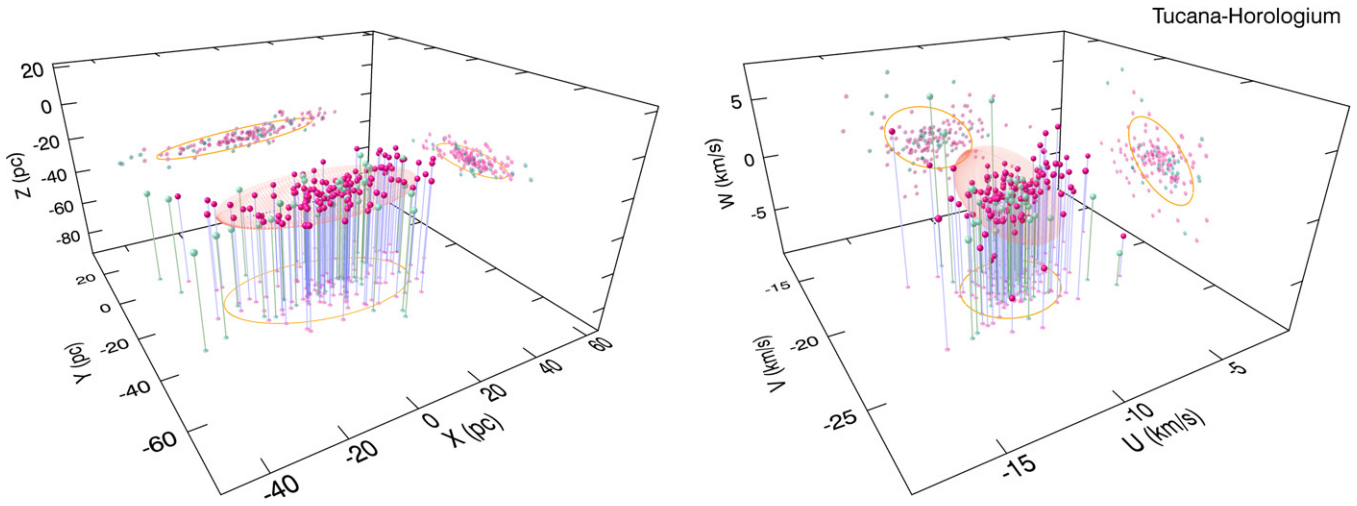

(a) *XYZ* (b) *UVW*

Figure 18. Most probable galactic positions *XYZ* and space velocities *UVW* based on BANYAN II statistical distances and RVs for all BASS candidate members in THA compared with bona fide members. Colors and symbols are defined in the same way as in Figure 14. As noted by Kraus et al. (2014), the spatial distribution of THA is significantly thinner in the *Z* direction and thus forms a plane in the *XYZ* space.

that this system is possibly a chance alignment, since otherwise it would be hard to reconcile the very different colors and the similar apparent *J* magnitudes of its components. We note that Lépine & Bongiorno (2007) used their common proper motion criteria only on stars with $\mu > 150$ mas yr^{-1}, hence it is possible that it does not perform as well on this system, which has only $\mu = 53.2$ mas yr^{-1}.

2MASS J05121347+0131539 (NLTT 14667) from LP-BASS (estimated M4.9 with $J = 10.36$) seems to be co-moving with 2MASS J05121170+0131154 ($J = 16.39$) at an angular separation of 46.″8 and a proper motion difference of 28.6 mas yr^{-1} (0.9σ) with respect to a total proper motion of 212.4 mas yr^{-1}. The contrast is significant with $\Delta J = 6.03$, which would point to a late-T spectral type for the secondary if it is at the same distance than the primary. However, we note that the secondary is most probably a contaminating object, since an extended PSF is visible within 10″ of its 2MASS position in the red DSS filter.

2MASS J14415883–1649008 (WT 2090) from LP-BASS (M4.5 with $J = 10.23$) is co-moving with 2MASS J14415908–1653133 (Wolf 1501; M3 with $J = 9.35$) at an angular separation of 252.″5 and a proper motion difference of 3.8 mas yr^{-1} (0.3σ) with respect to a total proper motion of 290.3 mas yr^{-1}. Kirkpatrick et al. (2010) obtained a NIR spectral type of M3 for Wolf 1501. We note that the contrast ratio $\Delta J = 0.88$ is large for their respective spectral types of M3 and M4.5. Both objects are weak candidate members of ABDMG, with respective Bayesian probabilities of 5.4% and 3.8% and contamination probabilities of 23.4% and 26.9%.

2MASS J21500933+0558102 from LP-BASS (estimated M4.9 with $J = 10.66$) is co-moving with 2MASS

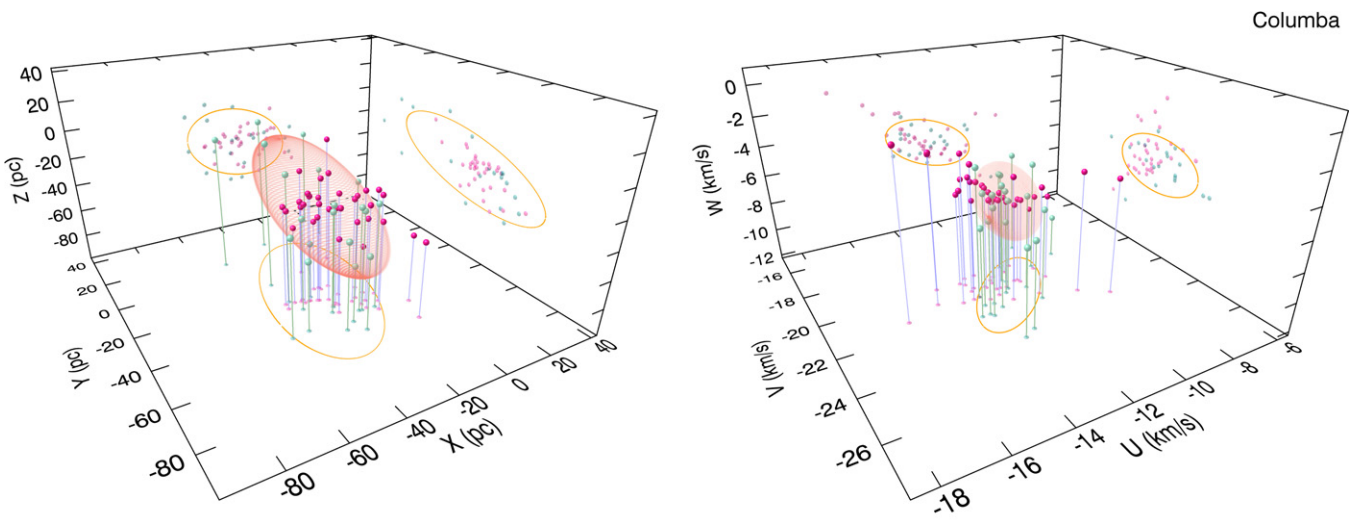

(a) *XYZ* (b) *UVW*

Figure 19. Most probable galactic positions *XYZ* and space velocities *UVW* based on BANYAN II statistical distances and RVs for all BASS candidate members in COL compared with bona fide members. Colors and symbols are defined in the same way as in Figure 14.

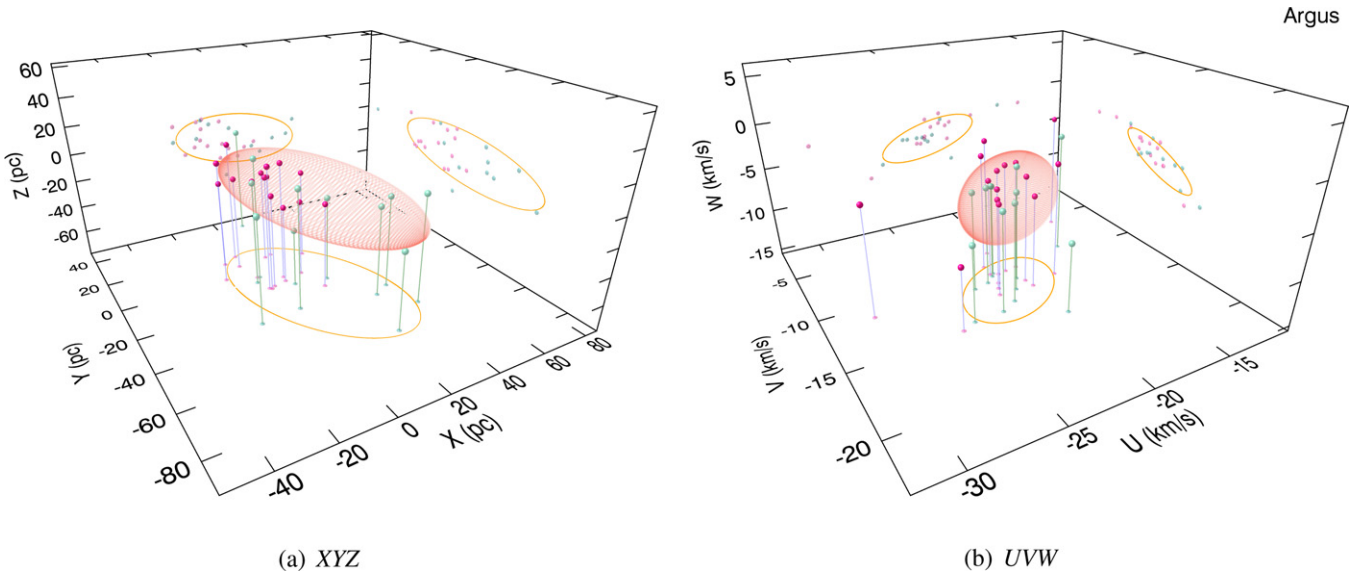

(a) *XYZ* (b) *UVW*

Figure 20. Most probable galactic positions *XYZ* and space velocities *UVW* based on BANYAN II statistical distances and RVs for all BASS candidate members in ARG compared with bona fide members. Colors and symbols are defined in the same way as in Figure 20.

J21501011+0558137 from LP-BASS (estimated M4.9 with $J = 10.74$) at an angular separation of $12''$ and a proper motion difference of 21.9 mas yr^{-1} (0.8σ) with respect to a total proper motion of 146.9 mas yr^{-1}. Their contrast ratio is relatively small with $\Delta J = 0.08$, which is consistent with their similar estimated spectral types. The direction of their 2MASS–AllWISE proper motions is slightly different, which favors ARG for the primary and βPMG for the secondary. However, both have a somewhat ambiguous membership between ARG and βPMG; the primary has respective Bayesian probabilities of 8.0% and 15.6%, whereas the secondary has 16.6% and 3.0%. We thus regard this system as an ambiguous, low-probability candidate member of βPMG and ARG.

2MASS J23133055–5352079 from LP-BASS (estimated M5.7 with $J = 12.08$) is co-moving with 2MASS J23133024–5351389 (HD 219046; $J = 8.59$) at an angular separation of $29\farcs1$ and a proper motion difference of 17.0 mas yr^{-1} (1.5σ). The contrast ratio is consistent with the latter component being a K-type star. We find no additional information in the literature for this system.

8. A PRELIMINARY INVESTIGATION ON MASS SEGREGATION

According to the virial theorem, it is expected that all components of a gravitationally bound astrophysical system will end up with the same average kinetic energy after relaxing to the equilibrium state. Hence, the lower-mass members of stellar associations are expected to have a larger velocity than their higher-mass siblings; this effect referred to as mass segregation. It has already been demonstrated for globular clusters (Hasan & Hasan 2011; Olczak et al. 2011; Pang et al. 2013); however, no signs of mass segregation have yet been identified for YMGs. The BASS catalog provides a unique sample on which to test for this effect, since it potentially contains the latest-type, lowest-mass members known to all YMGs.

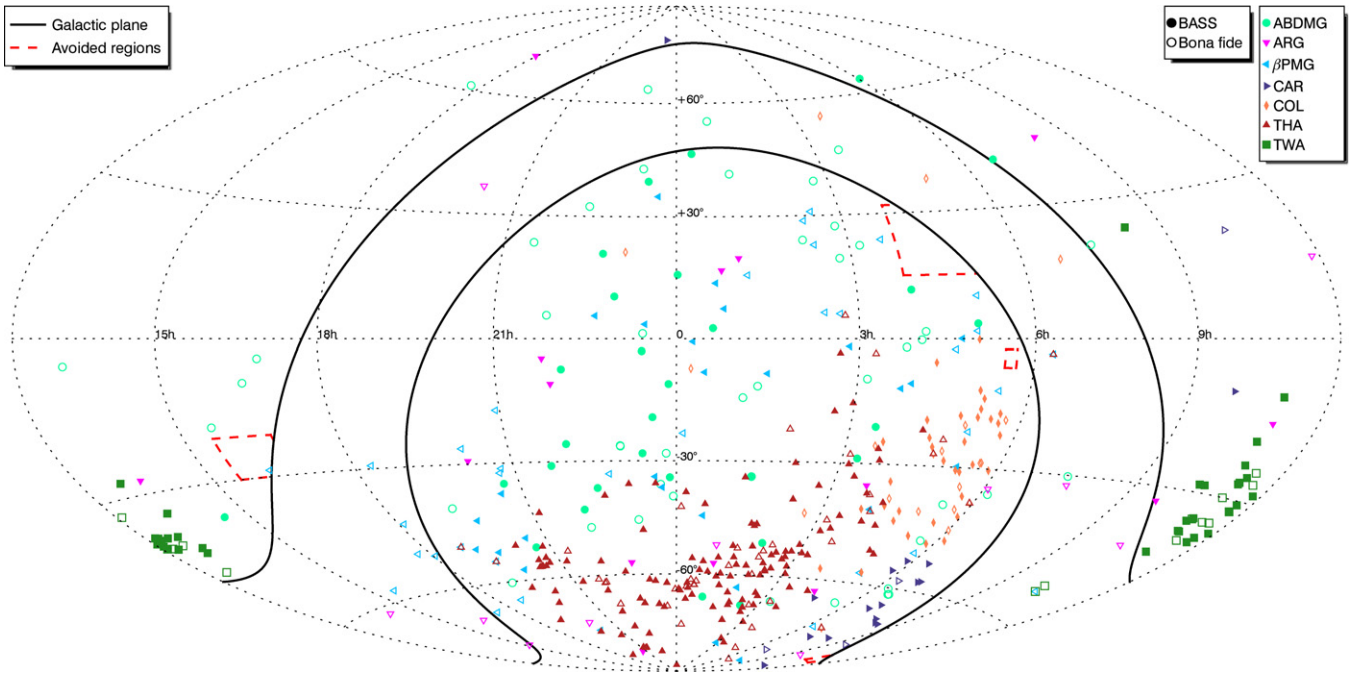

Figure 21. Sky position of all BASS candidates (filled symbols), compared with currently known bona fide members (open symbols) of each YMG considered here. Thick black lines delimit the galactic plane within ±15° of galactic latitude, and the dashed red lines delimit regions that were avoided in our search for YMG candidates (see Section 2).

Instead of relying on mass estimates that are dependent on physical hypotheses inherent to evolutionary models, we use statistical distance predictions from BANYAN II to obtain absolute $W1$ magnitudes for all high probability candidates in the BASS sample. Since members of YMGs are expected to be coeval, their absolute $W1$ magnitude should depend on their mass in a monotonic way, thus providing a more direct way to bring out mass segregation. The AllWISE $W1$ band is preferred to 2MASS bands since it is less affected by clouds in the atmospheres of BDs, which could introduce errors in the absolute magnitude–mass relation. Since the UVW separation to the center of mass of a given YMG is directly related to the kinetic energy of a member with respect to the YMG, it is expected that mass segregation would cause fainter (less massive) objects to be more scattered in the UVW space (i.e., dynamical mass segregation). As a consequence of this, one would also expect that they be more scattered spatially at a given moment in the XYZ space (i.e., spatial mass segregation).

Allison et al. (2009) devised a quantitative way to assess mass segregation in associations of stars that is more sensitive than a simple visual characterization, and more importantly, that is not dependent on the geometry of the members' distribution. They base this characterization on the principle of minimum spanning trees (MSTs). For a given distribution of coordinates (e.g., R.A. and decl. in a bi-dimensional space that is most often used in the case of open clusters), a MST is the shortest network of straight lines that connects all individual points without creating any loop. A mass segregation ratio (MSR) is then defined as

$$\Lambda_{\rm MSR} = \frac{\langle l_{\rm norm} \rangle}{l_{\rm massive}} \pm \frac{\sigma_{\rm norm}}{l_{\rm massive}},$$

where $l_{\rm massive}$ is the total length of the MST of the N most massive stars in an association, and $\langle l_{\rm norm} \rangle$ and $\sigma_{\rm norm}$ are respectively the average and standard deviation of a set of Monte Carlo simulations in which the MST network length is determined for a set of N stars randomly selected from the sample. If mass segregation is present, it is expected that $\Lambda_{\rm MSR}$ will have a value above unity. On the other hand, a value below unity would indicate that massive stars are more scattered than other members. We performed this analysis in both the XYZ and UVW three-dimensional spaces, using the algorithm described by Cartwright & Whitworth (2004) to build the MSTs. We determined the MSR for values of N spanning 3 to the total number of stars in each YMG, using 100 random subsets in each Monte Carlo simulation. We show the resulting MSTs for the full set of N bona fide members and high probability BASS candidates of each YMG in Figures 22 and 23. We sorted stars according to their increasing absolute $W1$ magnitudes instead of decreasing mass when we determined $\Lambda_{\rm MSR}$, for the reasons mentioned above. This was done for only the bona fide members in a first step, and then for bona fide members and all high probability candidates of the BASS catalog taken together.

We show in Figures 24 and 25 the resulting MSRs as a function of N for only bona fide members of each YMG. A MSR larger than one indicates that massive stars are more concentrated toward the center of the distribution, whereas a MSR smaller than one indicates the inverse situation. In most cases with a large statistical significance, the MSR ratio is above unity, which is expected from the physical considerations mentioned above. ABDMG is the only case where both the maximal spatial and dynamical mass segregation are present at $>2\sigma$, with 2.5σ and 2.4σ, respectively. βPMG displays a spatial mass segregation at 2.4σ and COL displays a dynamical mass segregation at 2.9σ. In some cases (βPMG, TWA, and THA), an inverse spatial or dynamical mass segregation is apparent between 1σ and 2σ, but never at a larger statistical significance. The inclusion of high priority BASS candidates in this analysis (see Figures 26 and 27) generally increases the significance of the previous results, the only exception being COL. As a consequence, ABDMG, THA, and COL display both a maximal

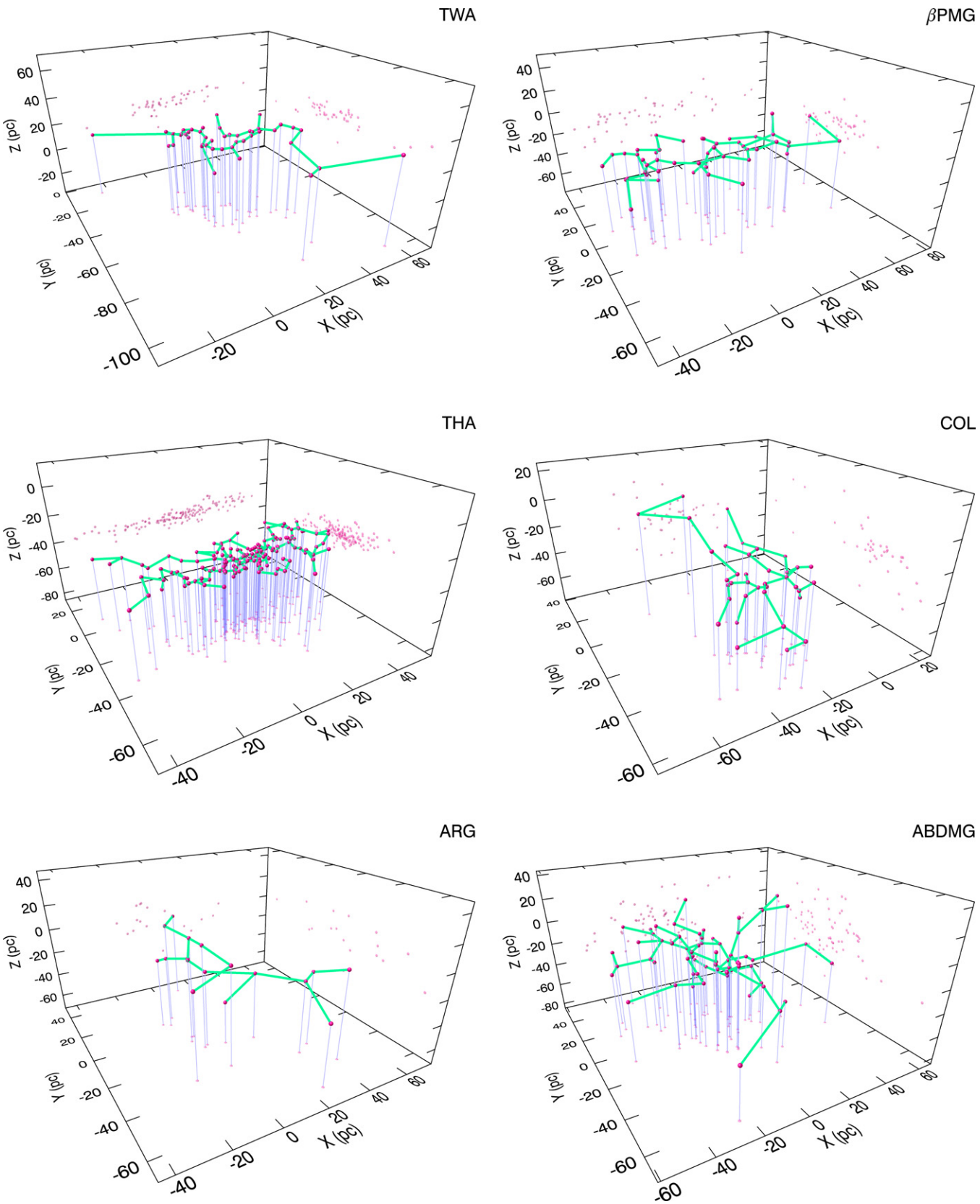

Figure 22. Minimum spanning trees (MSTs; green lines) in *XYZ* space for bona fide members and high probability BASS candidates (red points and their projections). Blue lines link each data point to its projection on the XZ plane for clarity. The total length of the MSTs for the brightest subsets of objects, compared with a random subset, is a useful diagnosis to determine the presence of mass segregation.

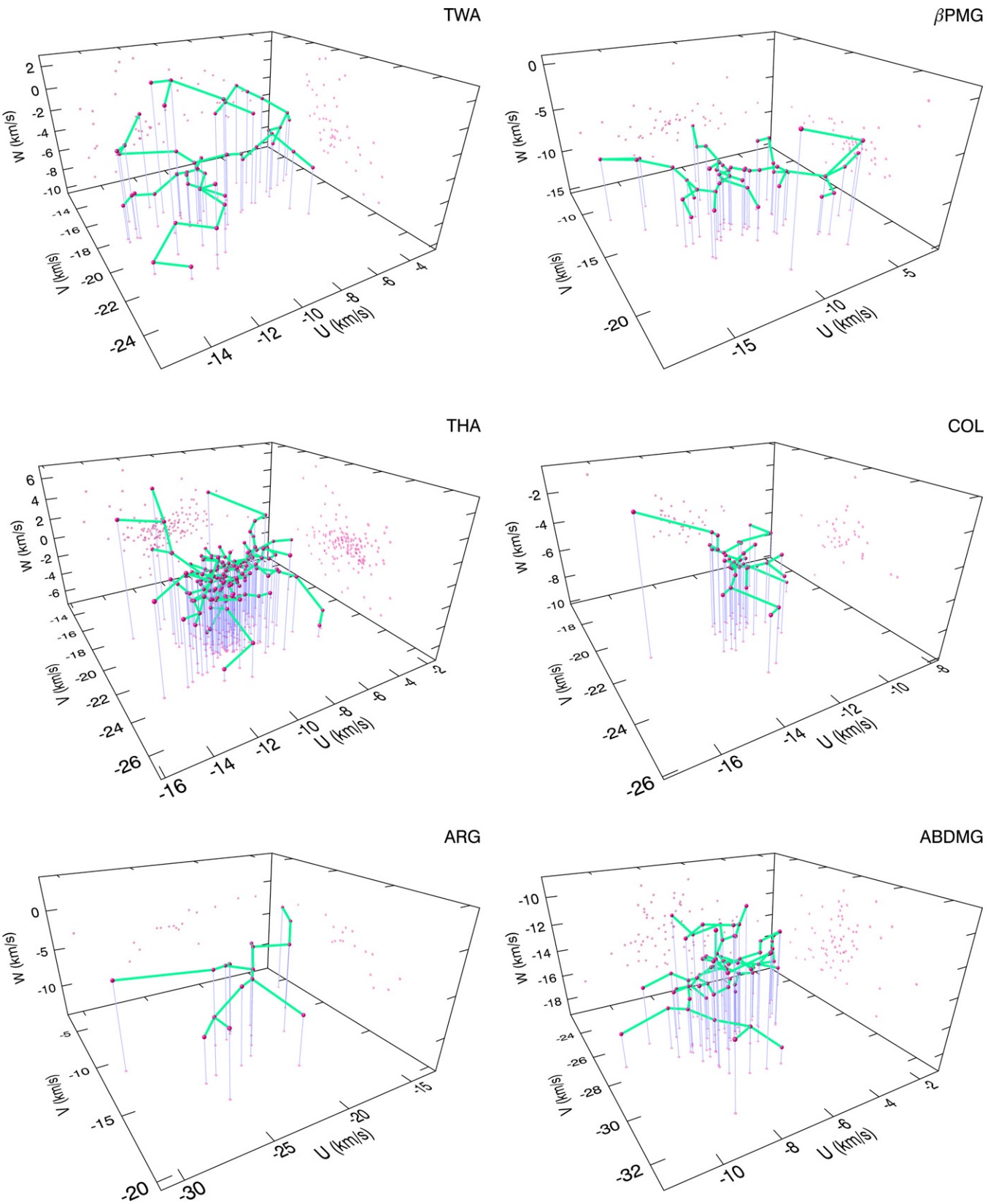

Figure 23. Minimum spanning trees (MSTs; green lines) in *UVW* space for bona fide members and high probability BASS candidates (red points and their projections). Blue lines link each data point to its projection on the *UV* plane for clarity. The total length of the MSTs for the brightest subsets of objects, compared with a random subset, is a useful diagnosis to determine the presence of mass segregation.

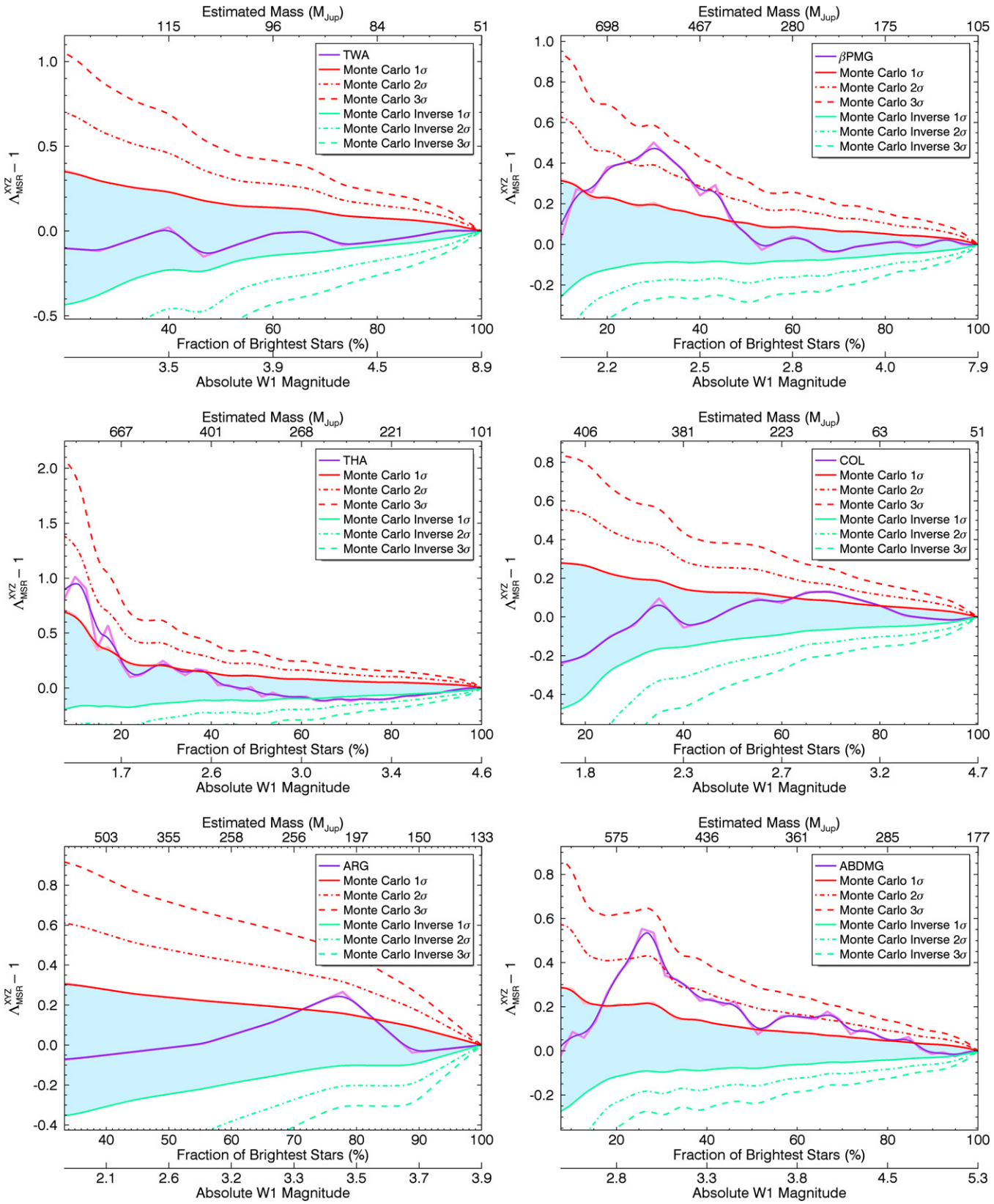

Figure 24. Spatial mass segregation ratios (MSRs) for bona fide members of YMGs considered here except CAR, as a function of the population fraction of brightest stars that were used in the calculation. Purple curves represent the departure of the MSR from unity, whereas red curves represent results of the Monte Carlo simulation where random stars were chosen instead of the brightest ones. Green curves delimit the region below which the MSR would be smaller than unity with statistical significance (i.e., least massive stars more concentrated toward the center). A MSR (purple curve) located inside the pale blue region indicates no significant difference between the scatter of the brightest or faintest objects. Darker, thick lines represent smoothed versions of the light-colored lines. The segregation mass ratio of CAR does not significantly depart from unity for any value of *N*.

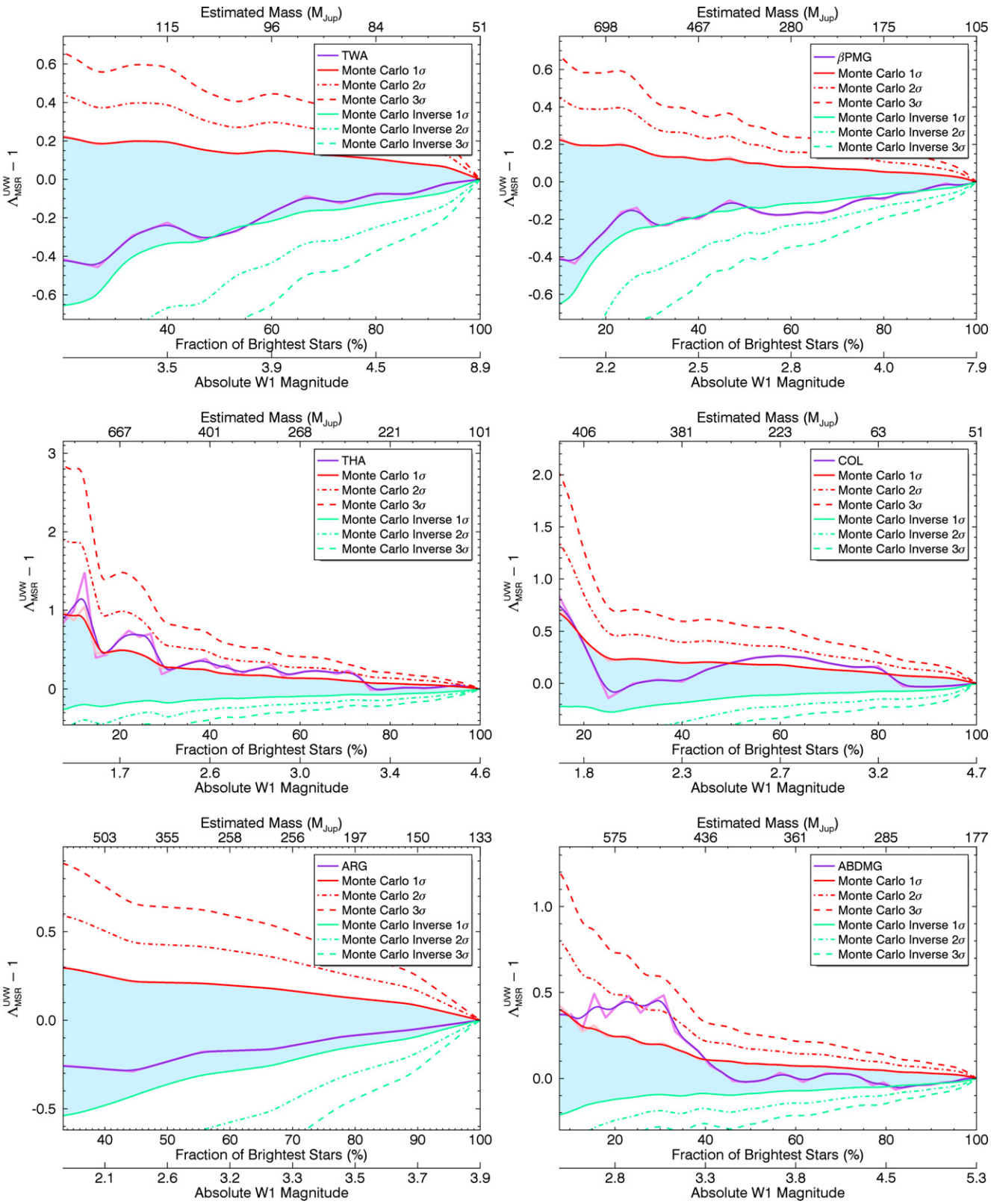

Figure 25. Same as Figure 24 for dynamical mass segregation.

dynamical and spatial mass segregation at 2–4σ in this situation. Spatial segregation is also apparent for ARG and BPMG at 3.2σ and 3.4σ, respectively. We note that in most cases that are statistically significant, mass segregation only starts appearing at masses lower than 0.3–0.5 $M_{\odot}$. However, we stress that a follow-up of the BASS sample must be completed before cases other than ABDMG can be considered as significant. We add that even in the case of ABDMG, securing more members will be necessary to increase the statistical significance of this tentative result.

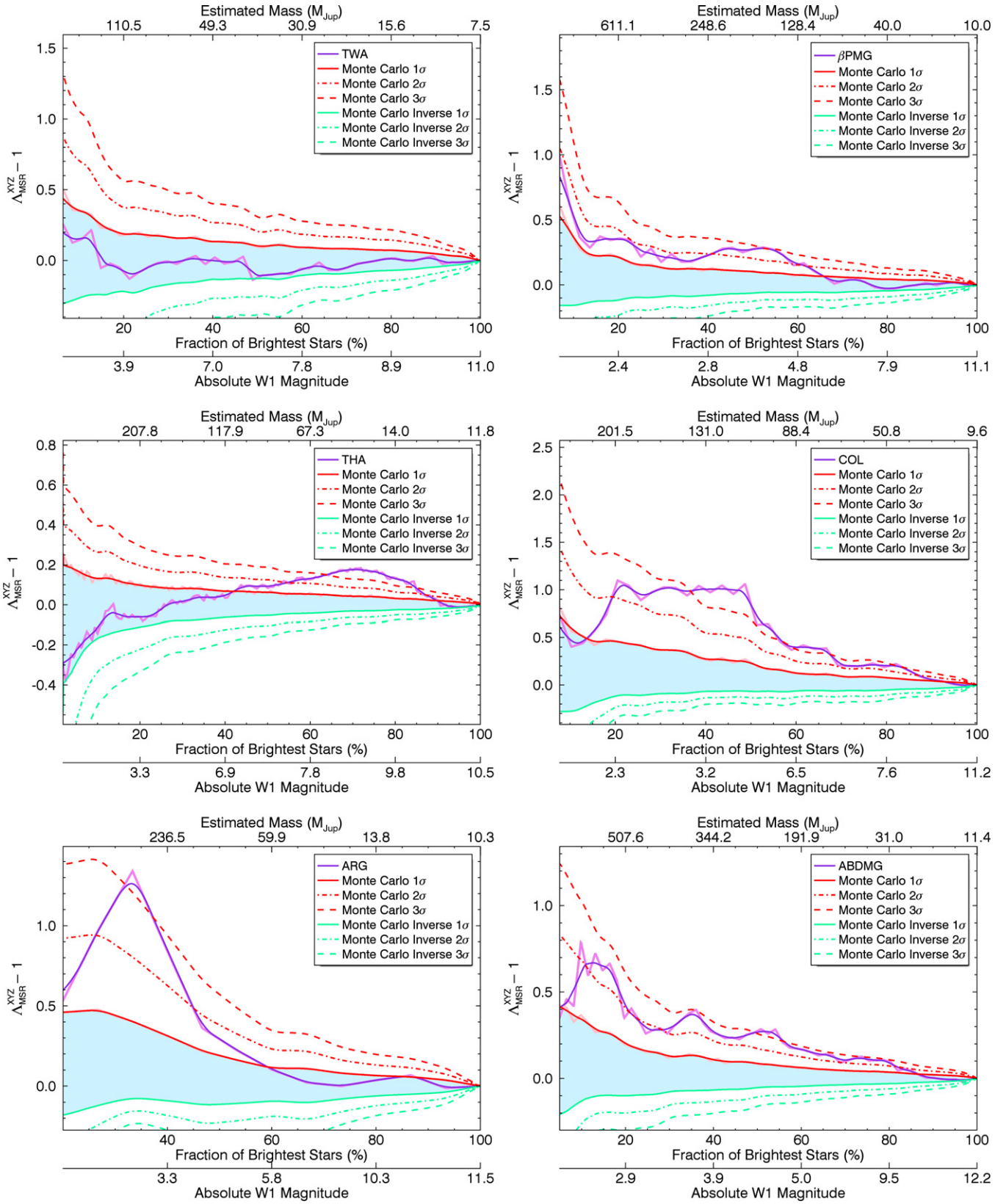

Figure 26. Same as Figure 24 with high probability BASS candidates added to the set of bona fide members.

Our analysis does not take account of two effects that could bias our results: (1) the selection criteria imposed to the BASS survey; and (2) the effect of unresolved binaries. To investigate the former effect, we performed a Monte Carlo simulation in which we have drawn a million synthetic objects from each SKM, and rebuilt 500 times the MST corresponding to a random subset of 100 synthetic objects. We repeated this with and without applying the selection filters described in Section 2

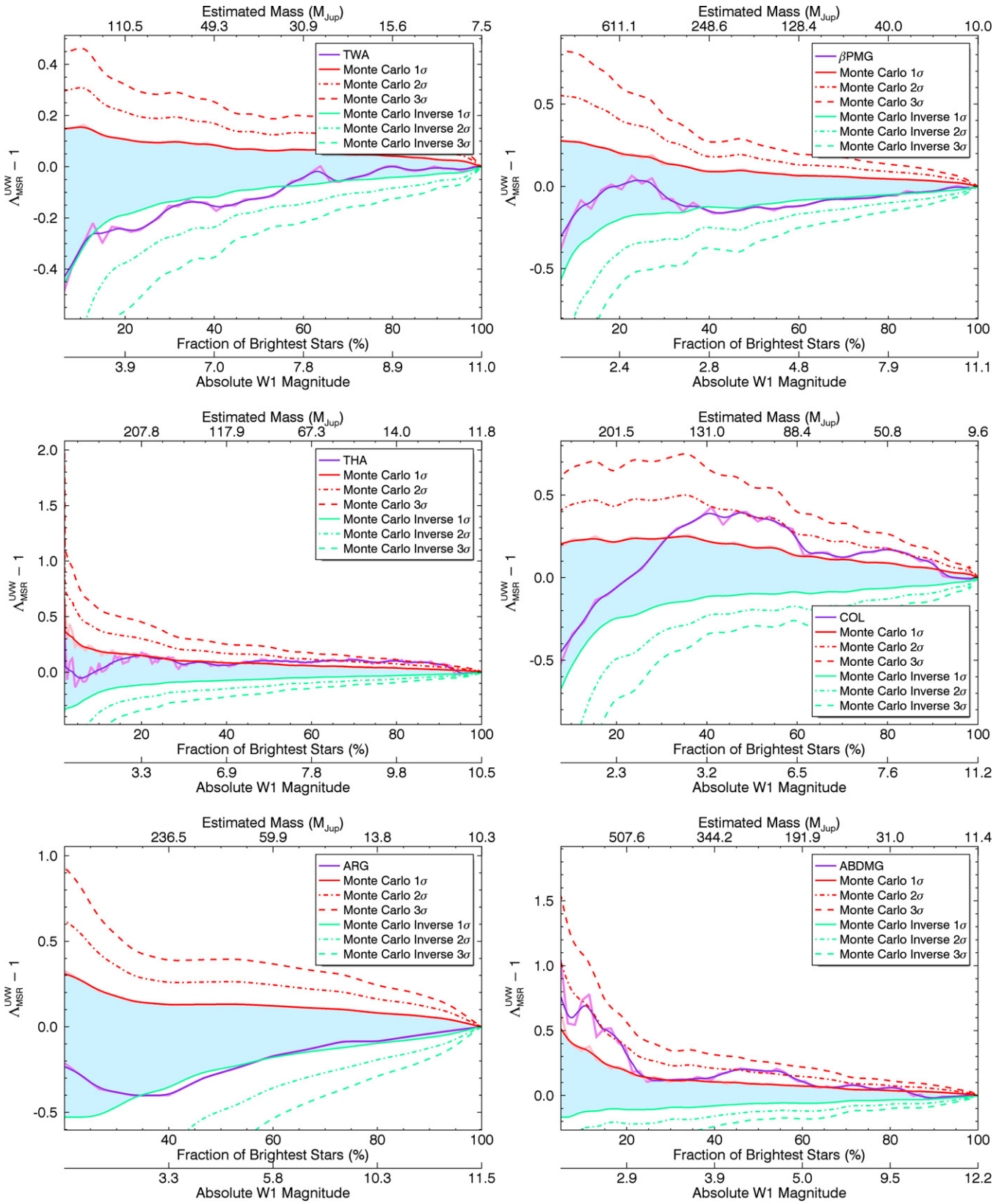

Figure 27. Same as Figure 25 with high probability BASS candidates added to the set of bona fide members.

to assess whether they have any systematic effect on the length of the MST. Any such systematic bias will only affect BASS candidates, which all have masses lower than currently known bona fide members. Hence, if this bias systematically shrinks the MST length, we will have underestimated mass segregation in the analysis described above, and vice versa. We found that our selection bias did not significantly affect the dynamical mass segregation: in all cases, they decreased the length of

Table 6
All-sky Input Sample of Nearby Potential >M5 Objects

2MASS				AllWISE			μ_α	μ_δ
Designation	J	H	K_S	Designation	$W1$	$W2$	(mas yr^{-1})	(mas yr^{-1})
00000027−1534494	10.47 ± 0.02	9.90 ± 0.02	9.63 ± 0.02	000000.46−153448.4	9.40 ± 0.02	9.22 ± 0.02	240.5 ± 9.3	87.4 ± 7.4
00000058−2621542	12.83 ± 0.02	12.27 ± 0.02	11.98 ± 0.02	000000.60−262154.9	11.78 ± 0.02	11.59 ± 0.02	27.2 ± 5.2	−63.1 ± 6.2
00000160−7721530	15.66 ± 0.08	15.09 ± 0.09	14.76 ± 0.13	000002.10−772152.6	14.33 ± 0.03	14.06 ± 0.04	151.6 ± 3.8	32.9 ± 10.0
00000296+2541349	13.34 ± 0.02	12.82 ± 0.02	12.51 ± 0.03	000002.98+254134.4	12.29 ± 0.02	12.09 ± 0.02	29.0 ± 5.2	−40.4 ± 6.1
00000497+3740328	15.66 ± 0.05	15.15 ± 0.08	14.82 ± 0.10	000004.96+374033.4	14.57 ± 0.03	14.32 ± 0.05	−16.0 ± 6.7	56.3 ± 9.6
00000540−5418547	14.23 ± 0.03	13.70 ± 0.04	13.39 ± 0.04	000005.29−541855.4	13.20 ± 0.02	13.03 ± 0.03	−85.2 ± 3.7	−64.8 ± 8.5

the dynamical MST with a statistical significance between 0 and 0.1σ. However, the spatial mass segregation was affected by our selection filters: in all cases, the average length of the MST has also decreased, with statistical significances of ∼1.5σ (ABDMG), ∼1.8σ (ARG and TWA), ∼2.2σ (CAR), ∼2.8σ (βPMG), and ∼3σ (COL; THA was unaffected). We have thus likely underestimated any positive spatial mass segregation in our analysis, as well as overestimated any negative spatial mass segregation. Since all of the statistically significant spatial mass segregation ratios obtained here are positive (less massive objects are more spread out), this does not change the conclusions of our analysis, except that we might generally underestimate the statistical significance of these conclusions.

Since we did not account of known and unknown unresolved binaries in our analysis and because the $W1$ flux of an object always falls rapidly when decreasing its mass, we will have systematically overestimated the total mass of unresolved systems. However, there is no apparent reason that would cause the fraction of multiple systems in a given YMG to correlate with *XYZUVW*. Hence, the effect of ignoring unresolved systems will be the same as overestimating the mass and luminosity of a random subset of members that we considered as single objects. This addition of noise will thus tend to draw the MSR closer to unity, as well as increase the measurement error on the MSR. As a consequence, this simplification made us less sensitive to the detection of any mass segregation, whether it be positive or negative.

9. SUMMARY AND CONCLUSIONS

We used the 2MASS and AllWISE surveys to perform the first systematic all-sky survey for ⩾M5 candidate members of YMGs. We identified a total of 275 M4–L7 candidate members, from which 153 are new strong candidates with an expected overall contamination of 13% from field stars. Seventynine of these candidates are expected to be BDs, and 22 are expected to be planetary-mass objects. We searched for all additional information available in the literature for the BASS sample to update membership probability, and show that we recover 60% of known ⩾M5 candidates to YMGs, whereas most of the remaining 40% were missed due to the quality filters used to minimize false positives. Three new common proper motion pairs were discovered among low-probability candidates. We finally used this unique sample to tentatively identify signs of mass segregation in YMGs. We find marginal evidence for mass segregation in ABDMG even when considering only bona fide members, and this result extends to THA and COL when high probability BASS candidates are taken into account. The BASS sample will open the door to the identification of BD members of YMGs, and has already proved extremely fruitful from a number of discoveries previously published. Extensive NIR and optical spectroscopic follow-ups are ongoing and have already enabled the discovery of several new young BDs that will be presented in upcoming papers. Complementary data can be found at http://www.astro.umontreal.ca/∼gagne, and the BANYAN II web tool is publicly available at http://www.astro.umontreal.ca/∼gagne/banyanII.php.

We thank the anonymous referee of this paper, who provided us with valuable comments that significantly increased the quality of this work. The authors also thank Kelle Cruz, Jacqueline K. Faherty, Philippe Delorme, Adric Riedel, Loïc Albert, Rebecca Oppenheimer, Eric Mamajek, Brendan Bowler, David Blank, and Amélie Simon for useful comments and discussions and Adric Riedel for sharing data. This work was supported in part through grants from the Fond de Recherche Québécois-Nature et Technologie and the Natural Science and Engineering Research Council of Canada. This research has benefitted from the SpeX Prism Spectral Libraries, maintained by Adam Burgasser at http://pono.ucsd.edu/∼adam/browndwarfs/spexprism, and the Database of Ultracool Parallaxes at http://www.cfa.harvard.edu/∼tdupuy/plx/Database_of_Ultracool_Parallaxes.html. This research made use of; the SIMBAD database and VizieR catalog access tools, operated at Centre de Données astronomiques de Strasbourg, France (Ochsenbein et al. 2000); data products from the Two Micron All Sky Survey, which is a joint project of the University of Massachusetts and the Infrared Processing and Analysis Center (IPAC)/California Institute of Technology (Caltech), funded by the National Aeronautics and Space Administration (NASA) and the National Science Foundation (Skrutskie et al. 2006); data products from the Wide-field Infrared Survey Explorer, which is a joint project of the University of California, Los Angeles, and the Jet Propulsion Laboratory (JPL)/Caltech, funded by NASA (Wright et al. 2010); the NASA/IPAC Infrared Science Archive, which is operated by the JPL, Caltech, under contract with NASA; the M, L, and T dwarf compendium housed at http://DwarfArchives.org and maintained by Chris Gelino, Davy Kirkpatrick, and Adam Burgasser.

APPENDIX A

THE INPUT SAMPLE OF NEARBY POTENTIAL >M5 DWARFS

We present in Table 6 the complete sample of 98,970 potential >M5 nearby objects in which we searched for candidate members of YMGs. This sample will be useful to study the kinematics of such red objects. This table includes all observables that were fed to BANYAN II to determine the Bayesian probability: 2MASS and AllWISE magnitudes, sky position and proper

Table 7
LP-BASS Candidates with Additional Information in the Literature

2MASS Designation	Measured SpT[a]	Signs of Youth[b]	RV (km s^{-1})	Trig. Dist. (pc)	Multiplicity[c]	Known Membership	Updated Membership	Updated Prob. (%)
00165057−7122387	...	...	-3.4 ± 3.0[54]	...	...	...	THA	36.6
00192753−3620153	M5.5[12]	...	...	...	...	...	THA	11.5
00281434−3227556	M5[85]	...	...	...	...	...	BPMG	30.4
00303013−1450333	L7[14,47]	...	...	26.7 ± 3.2[110]	...	...	ARG	24.1
00425349−6117384	M4.2[53]	...	6.9 ± 1.0[53]	...	...	THA[53]	THA	99.9
00455663+3347109	M4.5+M5.5[55]	...	...	18.1 ± 1.3[47,23]	AB[55]	...	ARG	89.7
00551459+4511019	...	...	...	35.8 ± 3.3[23]	...	...	ABDMG	19.3
00584253−0651239	L0[14,48,27]	...	...	29.6 ± 3.5[71]	...	...	BPMG	88.6
01000219−6156270	M6[12]	...	...	...	...	...	THA	99.1
01044008+1129485	...	N[92]	...	...	...	ABDMG[92]	BPMG	76.5
01234181−3833496	M4.5[78]	...	18.4 ± 6.3[101]	...	...	...	BPMG	0.6
01253196−6646023	M4.2[53]	...	7.1 ± 5.1[53]	...	...	THA[53]	THA	99.7
01275875−6032243	M4.2[90,53]	N	9.1 ± 2.5[53]	...	...	THA[90,53]	THA	>99.9
01283025−4921094	M4.1[53]	...	6.5 ± 5.7[53]	...	...	THA[53]	THA	99.3
01375879−5645447	M3.9[53]	...	8.5 ± 0.6[53]	...	...	THA[53]	THA	99.9
01534955+4427284	...	...	...	20.2 ± 1.2[23]	...	...	ARG	98.5
02001992−6614017	M4.3[90,53]	N	11.8 ± 1.1[53]	...	...	THA[90,53]	THA	>99.9
02025788−3136262	M4.0[90]	N	...	...	...	FIELD[90]	COL	40.7
02030658−5545420	M4.5[90]	N	...	...	...	ABDMG[90]	THA	99.9
02033222+0648588	...	...	...	...	C[113]	ABDMG[92]	BPMG	64.5
02123372−6049185	M6.5[34]	...	13.1 ± 0.2[34]	...	...	...	THA	94.8
02190228+2352550	M3.6[99]	X[99]	15.7 ± 0.7[100]	20.6 ± 0.8[23]	...	...	ARG	72.2
02294569−5541496	M4.8[53]	L[53]	11.5 ± 1.0[53]	...	...	THA[53]	THA	>99.9
02341866−5128462	M4.3[53]	...	10.9 ± 0.9[53]	...	...	THA[53]	THA	>99.9
02351494+0247534	...	...	...	17.8 ± 1.0[23]	...	...	BPMG	77.6
02383255−7528065	M4.1[53]	...	12.3 ± 0.6[53]	...	...	THA[53]	THA	98.9
02412721−3049149	M4.7[90,53]	ON[90]	18.2 ± 1.1[53]	...	...	THA[90,53]	BPMG	88.3
02420204−5359147	M4.6[90,53]	N	11.5 ± 2.3[53]	...	...	THA[90,53]	THA	>99.9
02591904−5122341	M5.4[53]	L[53]	11.0 ± 2.3[53]	...	...	THA[53]	THA	>99.9
03090022−4924513	M4.5[84]	...	...	...	...	...	ARG	18.8
03104941−3616471	M4.3[90,53]	N	13.8 ± 1.6[53]	...	...	THA[90,53]	THA	>99.9
03341065−2130343	M6[14]	...	19.0 ± 0.8[34]	...	...	IC 2391?[34]	BPMG	22.9
03370359−1758079	L4.5[1]	...	...	...	...	...	ARG	11.6
03561624−3915219	M5.0[90,53]	N	16.7 ± 0.7[53]	...	...	THA[90,53]	THA	99.9
04032484+0824508	...	X[92]	...	...	...	ABDMG[92]	BPMG	96.7
04054799−1515399	M8[45]	...	...	...	...	...	THA	70.1
04111790−0556489	M9[111]	...	20.1 ± 5.0[111]	...	...	...	COL	20.6
04133609−4413325	M3.9[90,53]	N	16.4 ± 1.4[53]	...	...	THA[90,53]	THA	99.6
04231498−1533245	...	...	...	22.4 ± 1.0[23]	AB[26]	...	BPMG	93.3
04390494−0959012	M6[13]	...	...	...	...	...	ABDMG	15.4
04475779−5035200	M4.0[53]	...	18.6 ± 0.9[53]	...	...	THA[53]	COL	72.0
05195412−0723359	M4+M4.5[85,43]	X[85]	...	...	AB[43]	...	COL	89.7
06142994−6318559	...	...	...	...	Ab[73]	...	ARG	89.0
06313103−8811365	M5[102]	...	...	...	...	...	ARG	28.1
07135309−6545115	...	...	...	...	AB[26]	...	CAR	91.5
07140394+3702459	M8[94,82,27]	...	...	12.5 ± 0.7[23]	...	...	ARG	74.9
07355465+3333459	M4.5[78]	...	...	32.4 ± 2.5[23]	...	...	ABDMG	26.2
10023100−2814280	M4+M6[80]	...	...	...	AB[43]	...	CAR	93.7
10134260−2759586	M5[38]	...	...	...	...	TWA[38]	CAR	43.5
10451718−2607249	M8[38,82,27]	...	...	...	...	...	ABDMG	18.2
15031325−2840134	M5[78]	...	...	...	...	...	ABDMG	4.3
20042845−3356105	M4.5[85]	X[85]	...	...	...	...	BPMG	93.8
21144103−4339531	...	...	2.7 ± 0.3[34]	...	...	CAS[34]	ABDMG	74.5
21272613−4215183	M8[82]	...	-7.6 ± 0.3[34]	34.6 ± 7.5[108]	...	Pleiades[34]	BPMG	82.5
21380269−5744583	M3.7[53]	...	-0.5 ± 1.3[53]	...	...	THA[53]	THA	98.7
21414678−2704542	M4.5[78]	...	...	...	...	...	ABDMG	45.7
22021125−1109461	M6.5[77]	...	-9.4 ± 1.0[40]	...	...	...	ABDMG	84.9
22043859−1832204	M4.5[5]	...	-7.2 ± 3.8[52]	...	...	...	BPMG	26.3
22294830−4858285	M4.5[80]	...	...	...	...	...	BPMG	21.1
22302626−0142063	M4[5]	...	...	...	...	...	ABDMG	14.6
22541103+1606546	M4[42]	...	...	30.2 ± 1.3[23]	...	...	ARG	68.8
23261182+1700082	M4.5+M6[43]	...	...	...	AB[43]	...	BPMG	66.8
23301129−0237227	M6[81]	...	...	...	...	...	BPMG	42.8
23310161−0406193	M8+L3[9]	...	-12.86 ± 0.09[9,115]	26.1 ± 0.4[109]	AB[9]	...	ABDMG	0.5
23524562−5229593	M4.6[53]	L[53]	3.1 ± 0.7[53]	...	...	THA[53]	THA	99.9

Notes.
[a] The β and γ symbols stand for low gravity and very low gravity, *p* stands for peculiar, and a semi-colon indicates an uncertain spectral type.
[b] A capital letter means the object displays the associated sign of youth. O: lower-than-normal equivalent width of atomic species in the optical spectrum, I: same but in the NIR spectrum, T: a triangular-shaped *H*-band continuum, V: high rotational velocity, X: X-ray emission, R: redder-than-normal colors for given spectral type, U: overluminous, H: Hα emission, L: Li absorption, A: signs of accretion, M: signs of low gravity from atmospheric models fitting, N: bright NUV emission, and C: companion to a young star. A question mark following a flag indicates that the result is uncertain.
[c] AB: unresolved binary, B or C: resolved companion.
References to this table are identical to those of Table 3.

Table 8
The Complete LP-BASS Catalog

2MASS Designation	Spectral Type[a]	Probable Membership	Bayesian Prob. (%)	Contamination Prob. (%)	Estimated Mass Range ($M_{\rm Jup}$)	Statistical Distance (pc)	Statistical RV (km s^{-1})
Candidates with a High Probability							
00081980−2559449	(M5.8)	ABDMG	60.1	5.3	$87.1^{+8.2}_{-7.8}$	$36.2^{+2.4}_{-2.0}$	10.0 ± 2.0
00091768+0603461	(M5.2)	ABDMG	36.6	2.4	$156.3^{+14.4}_{-12.8}$	25.3 ± 1.6	-2.0 ± 2.0
00165057−7122387	(M5.7)	THA	36.6	<0.1	$57.7^{+8.1}_{-6.3}$	47.4 ± 3.2	-3.4 ± 3.0
00165242−7640540	(M5.3)	THA	31.8	<0.1	$85.0^{+11.1}_{-8.9}$	$45.4^{+3.2}_{-2.8}$	6.4 ± 2.4
00200551−5359372	(M6.2)	THA	98.9	<0.1	$36.2^{+9.3}_{-6.7}$	$39.8^{+2.4}_{-2.0}$	5.3 ± 2.4
00303013−1450333	L7	ARG	24.1	2.6	$10.4^{+0.6}_{-0.4}$	26.7 ± 3.2	4.3 ± 2.0
00381489−6403529	(M8.6)	THA	99.7	<0.1	$15.3^{+0.7}_{-6.1}$	44.2 ± 2.4	7.5 ± 2.4
00425349−6117384	M4.2	THA	99.9	<0.1	$123.0^{+15.6}_{-13.1}$	42.6 ± 2.4	6.9 ± 1.0
00455663+3347109	M4.5+M5.5	ARG	89.7	0.1	$86.4^{+8.4}_{-7.7}$	18.1 ± 1.3	4.3 ± 1.4
00474453+4159428	(M3.7)	BPMG	49.0	14.4	$169.0^{+10.5}_{-11.0}$	30.5 ± 2.8	-3.2 ± 2.2
Candidates with a Modest Probability							
00085614−2813211	(L8.9)	BPMG	21.5	21.8	6.1 ± 0.1	16.1 ± 1.2	5.8 ± 1.5
00102936−0746487	(M6.2)	ABDMG	18.2	19.9	$74.3^{+7.0}_{-6.6}$	$43.8^{+3.2}_{-2.8}$	3.3 ± 2.1
00192753−3620153	M5.5	THA	11.5	43.0	$60.3^{+8.6}_{-6.8}$	$37.8^{+2.0}_{-2.4}$	0.9 ± 2.2
00193193−0554404	(M5.0)	BPMG	30.8	44.2	$89.9^{+6.4}_{-6.1}$	$33.8^{+3.6}_{-3.2}$	3.2 ± 1.7
00281434−3227556	M5	BPMG	30.4	45.7	$168.7^{+10.6}_{-11.1}$	$32.1^{+2.8}_{-3.2}$	8.1 ± 1.5
00324451+2744454	(M5.0)	BPMG	17.4	36.0	93.9 ± 5.6	35.8 ± 3.2	-3.6 ± 2.0
00465095+3822416	(M5.5)	ARG	15.8	28.2	$77.3^{+7.9}_{-8.2}$	$33.8^{+3.2}_{-3.6}$	2.3 ± 1.7
00473149−1424425	(M4.8)	BPMG	54.3	34.2	$100.0^{+5.7}_{-6.3}$	30.9 ± 2.8	6.9 ± 1.5
00584590+2430511	(M5.8)	BPMG	24.8	27.3	46.8 ± 2.6	31.3 ± 2.8	2.2 ± 2.1
01012488−2412472	(M6.0)	BPMG	12.1	30.2	$41.5^{+2.8}_{-2.5}$	23.3 ± 2.0	9.3 ± 1.5

Notes.
[a] Spectral types in parentheses were estimated from 2MASS–AllWISE colors (see Section 4.1).
[b] The binary hypothesis is more probable than the single hypothesis (see Section 3).

motion determined from the 2MASS–AllWISE cross-match. This list was built from the selection criteria described in Section 2, which produced the two following SQL statements that we used to query the 2MASS and AllWISE all-sky catalogs, respectively, using the IRSA service:

2MASS:
```
(GLAT > 15 OR GLAT < -15) AND (J_M-H_M) >= 0.506 AND (J_M-H_M) < 2 AND (H_M-K_M) >= 0.269 AND (H_M-K_M) < 1.6 AND (NOT rd_flg LIKE ' %0%') AND (NOT rd_flg LIKE '%6%') AND (NOT rd_flg LIKE '%9%') AND bl_flg = '111' AND cc_flg = '000' AND gal_contam = '0' AND J_M > 2 AND H_M > 2 AND K_M > 2 AND (NOT ph_qual LIKE '%D%') AND (NOT ph_qual LIKE '%E%') AND (NOT ph_qual LIKE '%F%') AND (NOT ph_qual LIKE '%X%') AND (NOT ph_qual LIKE '%U%') AND (NOT ph_qual LIKE '%CC%') AND (NOT ph_qual='CAC') AND (NOT ph_qual='CBC') AND PROX > 6.4 AND mp_flg = '0' AND (b_m_opt is null OR (b_m_opt - J_M) >= 4.048) AND (vr_m_opt is null OR (vr_m_opt - J_M) >= 2.63) AND (b_m_opt is null OR vr_m_opt is null OR (b_m_opt - vr_m_opt) >= 1.3)
```

AllWISE:
```
(GLAT > 15 OR GLAT < -15) AND (W1MPRO - W2MPRO) >= 0.168 AND (W1MPRO - W2MPRO) < 2.5 AND (W3SNR < 5 OR (NOT W3SAT = 0) OR((W1MPRO - W2MPRO) > (0.96*(W2MPRO - W3MPRO)-0.96))) AND (cc_flags NOT LIKE ' _D__ ' AND cc_flags NOT LIKE ' D___ ' AND cc_flags NOT LIKE ' _O__ ' AND cc_flags NOT LIKE ' O___ ' AND cc_flags NOT LIKE ' _P__ ' AND cc_flags NOT LIKE ' P___ ' AND cc_flags NOT LIKE ' _H__ ' AND cc_flags NOT LIKE ' H___ ') AND (EXT_FLG = '0' OR EXT_FLG = '1') AND W1SNR > 5 AND W2SNR > 5 AND W1RCHI2 < 5 AND W2RCHI2 < 5 AND W1MPRO > 2 AND W2MPRO > 2 AND W1SAT < 0.002 AND W2SAT < 0.002 AND (PH_QUAL LIKE ' AA%' OR PH_QUAL LIKE 'AB%' OR PH_QUAL LIKE 'BA%' OR PH_QUAL LIKE 'BB%') AND (tmass_key is null OR (R_2MASS >= 0.3 AND (j_m_2MASS - h_m_2MASS) >= 0.506 AND (j_m_2MASS - h_m_2MASS) < 2 AND (h_m_2MASS - k_m_2MASS) >= 0.269 AND (h_m_2MASS - k_m_2MASS) < 1.6 AND (k_m_2MASS - w1mpro) >= 0.153 AND (k_m_2MASS - w1mpro) < 2))
```

APPENDIX B

MARGINALLY RED CANDIDATES

We present here the low-priority BASS (LP-BASS) sample, consisting of all candidates that were rejected from the BASS sample because they were less than 1σ redder than the field sequence in the M_{W1} versus $J - K_S$ and M_{W1} versus $H - W2$ CMD diagrams, as indicated by the statistical distance of their most probable BANYAN II membership. However, we still only include candidates that are redder than the field sequence. Using the same method as described in the paper, we estimate contamination fractions of ∼26% and ∼80% in the high and modest-probability LP-BASS samples. We thus discourage the use of this sample for statistical studies or time-consuming

follow-ups. However, since the spread in the NIR colors of young objects in the two CMD mentioned above are large, we expect that a fraction of young objects will be rejected by our conservative filter, which requires candidates to be $>1\sigma$ redder than the field. It is thus likely that this sample contains a considerable fraction of true members of YMGs. Candidate members in the LP-BASS are also being following spectroscopically to identify signs of youth, albeit with a lower priority. Results will be presented in subsequent papers.

In Table 7, we show all measurements in the literature that are useful in constraining the membership of the LP-BASS candidate members. We use these measurements to refine results from BANYAN II, and report the final probability and most probable YMG for all LP-BASS objects in Table 8.

We note that 2MASS J00455663+3347109 (G 132–25) had three distinct trigonometric distance measurements in the literature, one of which is significantly discrepant. Reid & Cruz (2002) reported 68.0 ± 18.5 pc from the Yale catalog (van Altena et al. 1995), Khovritchev et al. (2013) measured 20.1 ± 2.1 pc, and Dittmann et al. (2014) measured 17.4 ± 1.3 pc. We thus consulted the Yale catalog directly to verify the measurement. Sky coordinates are reported as of 1900 in the catalog; we thus used the *precess* IDL routine from the Astronomy Users Library[9] to precess the coordinates of G 132–25 back to this epoch. We find R.A. $= 00^{h}40^{m}32\overset{s}{.}625$, decl. $= 33°14'21\overset{''}{.}78$. The closest entry in the Yale catalog is that of LP 294–2, at a distance of $4'$. Since LP 294–2 has a distinct 2MASS counterpart (2MASS J00461297+3350108), we conclude the most probable explanation is that the trigonometric distance of LP 294–2 has been misattributed to G 132–25 in Reid & Cruz (2002). We thus rejected this measurement and combined the two others to obtain 18.1 ± 1.3 pc in Table 7.

[9] Available at http://idlastro.gsfc.nasa.gov/

REFERENCES

Allard, F., Homeier, D., Freytag, B., Schaffenberger, W., & Rajpurohit, A. S. 2013, MmSAI, 24, 128
Allen, P. R., Cruz, K. K., Koerner, D. W., McElwain, M. W., & Reid, N. I. 2007, AJ, 133, 971
Allers, K. N., & Liu, M. C. 2013, ApJ, 772, 79
Allison, R. J., Goodwin, S. P., Parker, R. J., et al. 2009, MNRAS, 395, 1449
Alves de Oliveira, C., Moraux, E., Bouvier, J., & Bouy, H. 2012, A&A, 539, 151
Artigau, É., Lafrenière, D., Doyon, R., et al. 2009, in Proc. AIP Conf. Ser. 1094, Cool Stars, Stellar Systems, and the Sun, ed. E. Stempels (Melville, NY: AIP), 493
Baraffe, I., Chabrier, G., Barman, T. S., Allard, F., & Hauschildt, P. H. 2003, A&A, 402, 701
Barenfeld, S. A., Bubar, E. J., Mamajek, E. E., & Young, P. A. 2013, ApJ, 766, 6
Barrado y Navascués, D. 1998, A&A, 339, 831
Béjar, V. J. S., Zapatero Osorio, M. R., & Rebolo, R. 1999, ApJ, 521, 671
Bernat, D., Bouchez, A. H., Ireland, M., et al. 2010, ApJ, 715, 724
Binks, A. S., & Jeffries, R. D. 2014, MNRAS, 438, L11
Blake, C. H., Charbonneau, D., & White, R. J. 2010, ApJ, 723, 684
Bochanski, J. J., Gizis, J. E., Hawley, S. L., et al. 2005, AJ, 130, 1871
Bonnefoy, M., Chauvin, G., Dumas, C., et al. 2009, A&A, 506, 799
Bonnefoy, M., Chauvin, G., Lagrange, A.-M., et al. 2014, A&A, 562, 127
Bowler, B. P., Liu, M. C., Shkolnik, E. L., & Dupuy, T. J. 2013, ApJ, 774, 55
Bowler, B. P., Liu, M. C., Shkolnik, E. L., & Tamura, M. 2012a, ApJ, 756, 69
Bowler, B. P., Liu, M. C., Shkolnik, E. L., et al. 2012b, ApJ, 753, 142
Boyer, M. L., Srinivasan, S., van Loon, J. T., et al. 2011, AJ, 142, 103
Burgasser, A. J., Cruz, K. K., Cushing, M. C., et al. 2010, ApJ, 710, 1142
Burgasser, A. J., Cruz, K. K., Liu, M. C., Ireland, M. J., & Dupuy, T. J. 2008, ApJ, 681, 579
Caballero, J. A. 2007, ApJ, 667, 520
Cartwright, A., & Whitworth, A. P. 2004, MNRAS, 348, 589
Chauvin, G., Lowrance, P., Faherty, J. K., et al. 2012, A&A, 548, 33
Chiu, K., Fan, X., Leggett, S. K., et al. 2006, AJ, 131, 2722
Costa, E., Méndez, R. A., Jao, W. C., et al. 2005, AJ, 130, 337
Crifo, F., Phan-Bao, N., Delfosse, X., et al. 2005, A&A, 441, 653
Cruz, K. K., Kirkpatrick, D. J., & Burgasser, A. J. 2009, AJ, 137, 3345
Cruz, K. K., Lowrance, P., Reid, N. I., Liebert, J., & Kirkpatrick, D. J. 2003, AJ, 126, 2421
Cruz, K. K., & Reid, N. I. 2002, AJ, 123, 2828
Cruz, K. K., Reid, N. I., Kirkpatrick, D. J., et al. 2007, AJ, 133, 439
Dahn, C. C., Gizis, J. E., Harris, H. C., et al. 2002, AJ, 124, 1170
da Silva, L., Torres, C. A. O., de La Reza, R., et al. 2009, A&A, 508, 833
Dawson, P., Scholz, A., & Ray, T. P. 2011, MNRAS, 418, 1231
de La Reza, R., Torres, C. A. O., Quast, G., Castilho, B. V., & Vieira, G. L. 1989, ApJL, 343, L61
Delorme, P., Gagné, J., Girard, J. H., et al. 2013, A&A, 553, L5
Delorme, P., Gagné, J., Malo, L., et al. 2012, A&A, 548, 26
Deshpande, R., Martín, E. L., Montgomery, M. M., et al. 2012, AJ, 144, 99
de Zeeuw, P. T., Hoogerwerf, R., de Bruijne, J. H. J., Brown, A. G. A., & Blaauw, A. 1999, AJ, 117, 354
Dhital, S., Burgasser, A. J., Looper, D. L., & Stassun, K. G. 2011, AJ, 141, 7
Dieterich, S. B., Henry, T. J., Jao, W.-C., et al. 2014, AJ, 147, 94
Dittmann, J. A., Irwin, J. M., Charbonneau, D., & Berta-Thompson, Z. K. 2014, ApJ, 784, 156
Ducourant, C., Teixeira, R., Chauvin, G., et al. 2008, A&A, 477, L1
Dupuy, T. J., & Liu, M. C. 2012, ApJS, 201, 19
Eisenbeiss, T., Ammler-von Eiff, M., Roell, T., et al. 2013, A&A, 556, 53
Faherty, J. K., Burgasser, A. J., Cruz, K. K., et al. 2012, ApJ, 752, 56
Faherty, J. K., Cruz, K. K., Burgasser, A. J., et al. 2009, AJ, 137, 1
Faherty, J. K., Cruz, K. K., Rice, E. L., Mamajek, E. E., & Núñez, A. 2013, AJ, 145, 2
Famaey, B., Jorissen, A., Luri, X., et al. 2005, A&A, 430, 165
Forveille, T., Beuzit, J.-L., Delorme, P., et al. 2005, A&A, 435, L5
Gagné, J., Faherty, J. K., Cruz, K. K., et al. 2014a, ApJL, 785, L14
Gagné, J., Lafrenière, D., Doyon, R., Malo, L., & Artigau, É. 2014b, ApJ, 783, 121
Gagné, J., Lafreniere, D., Doyon, R., et al. 2013, MmSAI, 84, 916
Gagné, J., Lafrenière, D., Doyon, R., et al. 2014c, ApJL, 792, L17
Gálvez-Ortiz, M. C., Clarke, J. R. A., Pinfield, D. J., et al. 2010, MNRAS, 409, 552
Gatewood, G., & Coban, L. 2009, AJ, 137, 402
Geballe, T. R., Knapp, G. R., Leggett, S. K., et al. 2002, ApJ, 564, 466
Gizis, J. E. 2002, ApJ, 575, 484
Gizis, J. E., Hawley, S. L., & Reid, N. I. 1997, AJ, 113, 1458
Gizis, J. E., Monet, D. G., Reid, N. I., et al. 2000, AJ, 120, 1085
Gliese, W., & Jahreiß, H. 1991, NASA STI/Ricon Tech. Rep. A, 92, 33932
Gould, A., & Chanamé, J. 2004, ApJS, 150, 455
Groom, S., Howell, J. H., & Teplitz, H. I. 2010, BAAS, 215, 438.05
Guenther, E. W., & Wuchterl, G. 2003, A&A, 401, 677
Hand, D. J., & Yu, K. 2001, Int. Stat. Rev., 69, 385
Hasan, P., & Hasan, S. N. 2011, MNRAS, 413, 2345
Hearty, T., Magnani, L., Caillault, J. P., et al. 1999, A&A, 341, 163
Hinkley, S., Pueyo, L., Faherty, J. K., et al. 2013, ApJ, 779, 153
Høg, E., Fabricius, C., Makarov, V. V., et al. 2000, A&A, 355, L27
Janson, M., Hormuth, F., Bergfors, C., et al. 2012, ApJ, 754, 44
Jao, W.-C., Henry, T. J., Subasavage, J. P., et al. 2003, AJ, 125, 332
Jenkins, J. S., Ramsey, L. W., Jones, H. R. A., et al. 2009, ApJ, 704, 975
Kastner, J. H., Zuckerman, B., Weintraub, D. A., & Forveille, T. 1997, Science, 277, 67
Kendall, T. R., Jones, H. R. A., Pinfield, D. J., et al. 2007, MNRAS, 374, 445
Kharchenko, N. V., Scholz, R. D., Piskunov, A. E., Röeser, S., & Schilbach, E. 2007, AN, 328, 889
Khovritchev, M. Y., Izmailov, I. S., & Khrutskaya, E. V. 2013, MNRAS, 435, 1083
King, J. R., Villarreal, A. R., Soderblom, D. R., Gulliver, A. F., & Adelman, S. J. 2003, AJ, 125, 1980
Kirkpatrick, D. J., Barman, T. S., Burgasser, A. J., et al. 2006, ApJ, 639, 1120
Kirkpatrick, D. J., Cushing, M. C., Cruz, K. K., et al. 2011, ApJS, 197, 19
Kirkpatrick, D. J., Gizis, J. E., Reid, N. I., et al. 2000, AJ, 120, 447
Kirkpatrick, D. J., Looper, D. L., Burgasser, A. J., et al. 2010, ApJS, 190, 100
Kirkpatrick, D. J., Lowrance, P., Cruz, K. K., et al. 2008, ApJ, 689, 1295
Kirkpatrick, D. J., Schneider, A. C., Fajardo-Acosta, S., et al. 2014, ApJ, 783, 122
Kiss, L. L., Moór, A., Szalai, T., et al. 2011, MNRAS, 411, 117
Knapp, G. R., Leggett, S. K., Fan, X., et al. 2004, AJ, 127, 3553
Kordopatis, G., Gilmore, G., Steinmetz, M., et al. 2013, AJ, 146, 134
Kraus, A. L., Shkolnik, E. L., Allers, K. N., & Liu, M. C. 2014, AJ, 147, 146
Lane, R. R., Kiss, L. L., Lewis, G. F., et al. 2011, A&A, 530, 31

Lasker, B. M., Lattanzi, M. G., McLean, B. J., et al. 2008, AJ, 136, 735
Law, N. M., Hodgkin, S. T., & Mackay, C. D. 2008, MNRAS, 384, 150
Lee, K.-G., Berger, E., & Knapp, G. R. 2010, ApJ, 708, 1482
Leggett, S. K., Allard, F., Geballe, T. R., Hauschildt, P. H., & Schweitzer, A. 2001, ApJ, 548, 908
Lépine, S., & Bongiorno, B. 2007, AJ, 133, 889
Lépine, S., & Simon, M. 2009, AJ, 137, 3632
Lépine, S., Thorstensen, J. R., Shara, M. M., & Rich, R. M. 2009, AJ, 137, 4109
Liebert, J., & Gizis, J. E. 2006, PASP, 118, 659
Liu, M. C., Dupuy, T. J., & Allers, K. N. 2013a, AN, 334, 85
Liu, M. C., Dupuy, T. J., & Ireland, M. J. 2008, ApJ, 689, 436
Liu, M. C., Dupuy, T. J., & Leggett, S. K. 2010, ApJ, 722, 311
Liu, M. C., Magnier, E. A., Deacon, N. R., et al. 2013b, ApJL, 777, L20
Looper, D. L., Bochanski, J. J., Burgasser, A. J., et al. 2010a, AJ, 140, 1486
Looper, D. L., Burgasser, A. J., Kirkpatrick, D. J., & Swift, B. J. 2007, ApJL, 669, L97
Looper, D. L., Mohanty, S., Bochanski, J. J., et al. 2010b, ApJ, 714, 45
Luhman, K. L. 2004, ApJ, 617, 1216
Luhman, K. L. 2007, ApJS, 173, 104
Luhman, K. L., Cruz, K. K., Mamajek, E. E., & Allen, P. R. 2009, ApJ, 703, 399
Luhman, K. L., Stauffer, J. R., & Mamajek, E. E. 2005, ApJL, 628, L69
Luyten, W. J. 1980, Proper Motion Survey with the 48-inch Schmidt Telescope, Vol. 55 (Minneapolis, MA: Univ. Minnesota), 1
Mace, G. N., Lowrance, P., Kirkpatrick, D. J., et al. 2013, ApJS, 205, 6
Makarov, V. V. 2007, ApJ, 658, 480
Makarov, V. V., & Urban, S. 2000, MNRAS, 317, 289
Makarov, V. V., Zacharias, N., Hennessy, G. S., Harris, H. C., & Monet, A. K. B. 2007, ApJL, 668, L155
Malo, L., Artigau, É., Doyon, R., et al. 2014a, ApJ, 788, 81
Malo, L., Doyon, R., Feiden, G. A., et al. 2014b, ApJ, 792, 37
Malo, L., Doyon, R., Lafrenière, D., et al. 2013, ApJ, 762, 88
Mamajek, E. E. 2005, ApJ, 634, 1385
Mamajek, E. E. 2012, ApJL, 754, L20
Mamajek, E. E., Barlett, K. L., Scifahrt, A., et al. 2013, AJ, 146, 154
Mamajek, E. E., & Bell, C. P. M. 2014, MNRAS, 445, 2169
Manjavacas, E., Bonnefoy, M., Schlieder, J. E., et al. 2014, A&A, 564, 55
Mann, A. W., Brewer, J. M., Gaidos, E., Lépine, S., & Hilton, E. J. 2013, AJ, 145, 52
Mann, A. W., Deacon, N. R., Gaidos, E., et al. 2014, AJ, 147, 160
Marocco, F., Andrei, A. H., Smart, R. L., et al. 2013, AJ, 146, 161
Martin, D. C., Fanson, J., Schiminovich, D., et al. 2005, ApJL, 619, L1
Martín, E. L., Phan-Bao, N., Bessell, M., et al. 2010, A&A, 517, 53
Mason, B. D., Wycoff, G. L., Hartkopf, W. I., Douglass, G. G., & Worley, C. E. 2001, AJ, 122, 3466
Monet, D. 1998, USNO-A2.0 (Flagstaff, AZ: United States Naval Observatory)
Monnier, J. D., Che, X., Zhao, M., et al. 2012, ApJL, 761, L3
Montes, D., López-Santiago, J., Gálvez, M. C., et al. 2001, MNRAS, 328, 45
Moór, A., Szabó, G. M., Kiss, L. L., et al. 2013, MNRAS, 435, 1376
Naud, M.-E., Artigau, É., Malo, L., et al. 2014, ApJ, 787, 5
Newton, E. R., Charbonneau, D., Irwin, J., et al. 2014, AJ, 147, 20
Nidever, D. L., Marcy, G. W., Butler, R. P., Fischer, D. A., & Vogt, S. S. 2002, ApJS, 141, 503
Ochsenbein, F., Bauer, P., & Marcout, J. 2000, A&AS, 143, 23
Olczak, C., Spurzem, R., & Henning, T. 2011, A&A, 532, 119
Pang, X., Grebel, E. K., Allison, R. J., et al. 2013, ApJ, 764, 73
Pecaut, M. J., & Mamajek, E. E. 2013, ApJS, 208, 9
Perryman, M. A. C., Lindegren, L., Kovalevsky, J., et al. 1997, A&A, 323, L49
Phan-Bao, N., & Bessell, M. S. 2006, A&A, 446, 515
Rajpurohit, A. S., Reylé, C., Allard, F., et al. 2013, A&A, 556, 15
Reid, N. I., & Cruz, K. K. 2002, AJ, 123, 2806
Reid, N. I., Cruz, K. K., & Allen, P. R. 2007, AJ, 133, 2825
Reid, N. I., Cruz, K. K., Burgasser, A. J., & Liu, M. C. 2008a, AJ, 135, 580
Reid, N. I., Cruz, K. K., Lewitus, E., Allen, P. R., & Burgasser, A. J. 2006, AJ, 132, 891
Reid, N. I., Cruz, K. K., Lowrance, P., et al. 2003, AJ, 126, 3007
Reid, N. I., Cruz, K. K., Lowrance, P., et al. 2004, AJ, 128, 463
Reid, N. I., Gizis, J. E., Kirkpatrick, D. J., et al. 2002, AJ, 124, 519
Reid, N. I., Lowrance, P., Cruz, K. K., et al. 2008b, AJ, 136, 1290
Reiners, A., & Basri, G. 2009, ApJ, 705, 1416
Reylé, C., Scholz, R. D., Schultheis, M., Robin, A. C., & Irwin, M. 2006, MNRAS, 373, 705
Riaz, B., Gizis, J. E., & Harvin, J. 2006, AJ, 132, 866
Ribas, I. 2003, A&A, 400, 297
Rice, E. L., Faherty, J. K., & Cruz, K. K. 2010, ApJL, 715, L165
Riedel, A. R. 2012, PhD thesis, Georgia State Univ.
Riedel, A. R., Rodriguez, D., Finch, C. T., et al. 2014, AJ, 147, 85
Robin, A. C., Marshall, D. J., Schultheis, M., & Reylé, C. 2012, A&A, 538, 106
Robin, A. C., Reylé, C., Fliri, J., et al. 2014, A&A, 569, 13
Rodriguez, D., Bessell, M. S., Zuckerman, B., & Kastner, J. H. 2011, ApJ, 727, 62
Rodriguez, D., Zuckerman, B., Kastner, J. H., et al. 2013, ApJ, 774, 101
Rojas-Ayala, B., Covey, K. R., Muirhead, P. S., & Lloyd, J. P. 2012, ApJ, 748, 93
Russek, E., Kronmal, R. A., & Fisher, L. D. 1983, Comput. Biomed. Res., 16, 537
Schlieder, J. E., Lépine, S., & Simon, M. 2010, AJ, 140, 119
Schlieder, J. E., Lépine, S., & Simon, M. 2012a, AJ, 143, 80
Schlieder, J. E., Lépine, S., & Simon, M. 2012b, AJ, 144, 109
Schmidt, S. J., Cruz, K. K., Bongiorno, B. J., Liebert, J., & Reid, N. I. 2007, AJ, 133, 2258
Schmidt, S. J., West, A. A., Hawley, S. L., & Pineda, J. S. 2010, AJ, 139, 1808
Schneider, A. C., Cushing, M. C., Kirkpatrick, D. J., et al. 2014, AJ, 147, 34
Schneider, A. C., Melis, C., & Song, I. 2012a, ApJ, 754, 39
Schneider, A. C., Song, I., Melis, C., Zuckerman, B., & Bessell, M. 2012b, ApJ, 757, 163
Scholz, R. D., McCaughrean, M. J., Zinnecker, H., & Lodieu, N. 2005, A&A, 430, L49
Seifahrt, A., Reiners, A., Almaghrbi, K. A. M., & Basri, G. 2010, A&A, 512, 37
Shkolnik, E. L., Anglada-Escude, G., Liu, M. C., et al. 2012, ApJ, 758, 56
Shkolnik, E. L., Liu, M. C., & Reid, N. I. 2009, ApJ, 699, 649
Skrutskie, M. F., Gizis, J. E., Kirkpatrick, D. J., et al. 2006, AJ, 131, 1163
Song, I., Zuckerman, B., & Bessell, M. S. 2003, ApJ, 599, 342
Subasavage, J. P., Henry, T. J., Hambly, N. C., Brown, M. A., & Jao, W.-C. 2005, AJ, 129, 413
Tanner, A. M., Law, N. M., & Gelino, C. R. 2010, PASP, 122, 1195
Teixeira, R., Ducourant, C., Chauvin, G., et al. 2008, A&A, 489, 825
Terrien, R. C., Mahadevan, S., Bender, C. F., et al. 2012, ApJL, 747, L38
Thé, P. S., & Staller, R. F. A. 1974, A&A, 36, 155
Tinney, C. G. 1996, MNRAS, 281, 644
Torres, C. A. O., da Silva, L., Quast, G. R., de La Reza, R., & Jilinski, E. 2000, AJ, 120, 1410
Torres, C. A. O., Quast, G. R., da Silva, L., et al. 2006, A&A, 460, 695
Torres, C. A. O., Quast, G. R., Melo, C. H. F., & Sterzik, M. F. 2008, in Young Nearby Loose Associations, Vol. I ed. B. Reipurth (The Southern Sky ASP Monograph Publications; San Francisco, CA: ASP), 757
Torres, G., Guenther, E. W., Marschall, L. A., et al. 2003, AJ, 125, 825
van Altena, W. F., Lee, J. T., & Hoffleit, E. D. 1995, The General Catalogue of Trigonometric [Stellar] Parallaxes (New Haven, CT: Yale University Observatory)
van Leeuwen, F. (ed.) 2007, A&A, 474, 653
Voges, W., Aschenbach, B., Boller, T., et al. 1999, A&A, 349, 389
Vrba, F. J., Henden, A. A., Luginbuhl, C. B., et al. 2004, AJ, 127, 2948
Weinberger, A. J., Anglada-Escude, G., & Boss, A. P. 2013, ApJ, 762, 118
Weinberger, A. J., Becklin, E. E., Zuckerman, B., & Song, I. 2004, AJ, 127, 2246
West, A. A., Hawley, S. L., Bochanski, J. J., et al. 2008, AJ, 135, 785
Wilson, J. C., Miller, N. A., Gizis, J. E., et al. 2003, in IAU Symp. 211, Brown Dwarfs, ed. E. Martín (Cambridge: Cambridge Univ. Press), 197
Witte, S., Helling, C., Barman, T. S., Heidrich, N., & Hauschildt, P. H. 2011, A&A, 529, 44
Wright, E. L., Eisenhardt, P. R. M., Mainzer, A. K., et al. 2010, AJ, 140, 1868
Zacharias, N., Finch, C. T., Girard, T. M., et al. 2012, yCat, 1322, 0
Zacharias, N., Finch, C., Girard, T., et al. 2009, yCat, 1315, 0
Zapatero Osorio, M. R., Béjar, V. J. S., Miles-Páez, P. A., et al. 2014, A&A, 568, 6
Zuckerman, B., Bessell, M. S., Song, I., & Kim, S. 2006, ApJL, 649, L115
Zuckerman, B., & Song, I. 2004, ARA&A, 42, 685
Zuckerman, B., Song, I., & Bessell, M. S. 2004, ApJL, 613, L65
Zuckerman, B., Song, I., Bessell, M. S., & Webb, R. A. 2001, ApJL, 562, L87
Zuckerman, B., Vican, L., Song, I., & Schneider, A. C. 2013, ApJ, 778, 5
Zuckerman, B., & Webb, R. A. 2000, ApJ, 535, 959
Zwitter, T., Siebert, A., Munari, U., et al. 2008, AJ, 136, 421